hexagon:2611.00497v1

Towards a conformal field theory
of critical percolation. I.

The bulk stress tensor and Ward identities

Alberto Gandolfi[1,2]

[1]Division of Science, New York University Abu Dhabi,
PO Box 129188, Abu Dhabi, United Arab Emirates.

[2]NYUAD Center for Interdisciplinary Data Science & AI (CIDSAI),
NYUAD Research Institute, New York University Abu Dhabi,
PO Box 129188, Abu Dhabi, UAE.

Email: ag189@nyu.edu

Abstract

We construct joint correlations of the bulk holomorphic stress tensor and the density field for critical site percolation on the triangular lattice, allowing any fixed finite numbers of insertions at separated points in the plane. Density correlations encode open-cluster connections; their two-point function is the renormalized probability that an open path joins two marked sites. Each stress insertion probes the directional response of these connections by closing and rotating a small ellipse and extracting the second angular component. To justify this construction, we extend Camia's existence and conformal covariance results for density correlations from simply connected domains to the domains with finitely many analytic holes created by the ellipses, and prove uniform bounds for combining these correlations with the local ellipse responses. The main estimate controls the complete frontier record: the second angular coefficient has a comparable-scale defect of order $(r/d)^{9/4}$, giving a Cauchy exponent $1/4$ after quadratic normalization. The limits require no radius averaging, are distributions in the density coordinates, and are independent of the fixed ellipse shape parameters. They satisfy the conformal Ward identities with central charge zero and yield sequential stress-collision and contour identities.

Status of this version. This is a preliminary preprint. The detailed verification of the mathematical arguments and their dependencies is ongoing and is not yet complete. The manuscript is being made public to make the arguments available for scrutiny and discussion while this verification continues. Its mathematical claims should therefore be regarded as provisional.

2020 Mathematics Subject Classification. Primary 60K35; Secondary 81T40, 60J67, 82B43.

Key words and phrases. Critical planar percolation, conformal field theory, bulk stress-energy tensor, conformal Ward identities, Schramm–Loewner evolution, scaling limits, density correlations, conformal covariance.

Contents

1 Introduction **1**

2 Previous results and conventions **2**
2.1 Percolation records and arm estimates . . . 2
2.2 Density correlations and logarithmic observables . . . 3
2.3 Continuum interfaces and two-curve estimates . . . 4
2.4 Related stress constructions . . . 5
2.5 The bulk stress tensor and its logarithmic partner . . . 5

3 Local sources and main results **6**
3.1 The source is a finite probability experiment . . . 6
3.2 Two geometric estimates . . . 7
3.3 Main results . . . 7
3.4 Proof dependencies . . . 7

I The signed angular response **8**

4 The local boundary-strip argument **8**
4.1 Configurations, records, and separating paths . . . 8
4.2 From the witness to the measure estimate . . . 12
4.3 Ellipses and angular source rows . . . 14

5 An angular average for two random angles **15**
5.1 The defining equations . . . 15
5.2 Reduction to one variable . . . 17
5.3 Computing the eigenvalues . . . 20
5.4 The limiting measure and a uniform bound . . . 22
5.5 The angular average with V . . . 24

6 Crossing probabilities with an elliptical hole **25**
6.1 A crossing removed by a closed set . . . 25
6.2 The two-curve exploration and the angular integral . . . 26
6.3 Comparison of the normalized maps . . . 28
6.4 An integral bound . . . 29
6.5 Iteration and the angular limit . . . 30
6.6 Four arbitrary boundary points . . . 33

7 Connections between finitely many boundary arcs **38**
7.1 Effect of closing a connected set . . . 38
7.2 Conditioning on all but two interfaces . . . 40
7.3 Counting interfaces near the target . . . 47
7.4 Summing over distance scales . . . 48

8 An estimate for the complete frontier record **49**
8.1 Exploring outside a fixed disk . . . 50
8.2 Number and separation of the remaining tips . . . 54
8.3 Separation after conformal mapping . . . 56
8.4 A uniform estimate for the remaining domains . . . 58
8.5 Passing to the complete frontier record . . . 60

9 Limits as the ellipse radii tend to zero **61**
9.1 Comparing arbitrary small radii . . . 61
9.2 A space for the limits . . . 62
9.3 Joint limits for several ellipses . . . 63
9.4 Dependence on the centers . . . 64

II Density correlations **65**

10 Finite-hole density correlations **65**

11 Published inputs and normalization at the marks **67**
11.1 Configurations and events at fixed positive scales 67
11.2 Cluster signs and local arms 69

12 Small boundary changes at fixed hole size **71**

13 Closed circuits and finite-hole correlations **73**
13.1 Existence of the finite-hole correlations 76

14 Conformal covariance without filling the holes **76**

15 Exact conditioning and the uniform completion bound **79**

16 Infinity and angular averages at fixed radii **80**
16.1 Truncation and changes of chart 80
16.2 Density observations averaged over orientations 81

III The finite stress hierarchy **83**

17 Arbitrary finite stress insertions with density spectators **83**
17.1 Ellipse variables and joint limits 83
17.2 Ward recursion and transport of tests 84
17.3 Mapping the first ellipse to a disk 86
17.4 Removing the additional disk 88
17.5 Ward identification by induction 89

18 Conclusion and further questions **90**

A Examples and consequences of the Ward identities **91**
A.1 The first three stress responses 91
A.2 A connection observed through one, two, and three rotating ellipses 91
A.3 Sequential stress collisions and local contour operations 93

B Checks on normalization and on the order of limits **95**
B.1 Exact conditioning in an adaptive exploration 95
B.2 Why a bounded random clock error is not enough 95
B.3 A positive normalization test for the one-stress response 96

C Close inner approximations on prescribed lattices **96**

D Geometry of an inner-cell disk **100**

E Use of generative AI **100**

1 Introduction

The stress tensor expresses local conformal symmetry through its action on correlation functions. The conformal Ward identities relate this action to the response of those correlations to changes of geometry [25, Section 1.1, (1.5) and (1.8)]. We construct this action for critical site percolation on the triangular lattice. Explicit local lattice sources yield joint correlations of any fixed finite collection of holomorphic stress insertions and density insertions at separated points. These correlations satisfy the Ward recursion with central charge $c = 0$.

The density observations have a simple cluster interpretation. Each lattice site is independently open or closed with probability $1/2$. Give each open cluster an independent random sign, equally likely to be $+1$ or -1, and give closed sites the value zero. Divide each site value by the plane probability of an open connection from a site to distance one. The limits of correlations of these variables define the density insertion Φ [1, Theorem 1.5, (1.8)–(1.11)]. For two marked sites, the correlation is the normalized probability that an open path joins them. Section 2 recalls this normalization.

Now force all sites in a small ellipse away from the two marked sites to be closed. Some configurations lose their connection; others still contain an open path around the obstacle. Turning the ellipse changes which paths it blocks. We retain the cosine and sine components at twice its orientation angle ϕ, combined through the Fourier weight $e^{-2i\phi}$. The local lattice source (4.8) uses this Fourier weight, divided by the squared ellipse size and the prescribed shape factor. Equation (A.4) gives its exact relation to the normalized connection probability. This angular extraction has a precedent in conformal restriction [19, Section 2, (2.1)–(2.4)].

Several disjoint ellipses can be rotated independently, as in Figure 1. Their normalized joint second angular Fourier coefficient measures how these local obstacles act together on the same connection question. Its continuum limit realizes repeated insertions of the same stress field at different locations. The examples in Appendix A.2 make the responses to one, two, and three ellipses explicit.

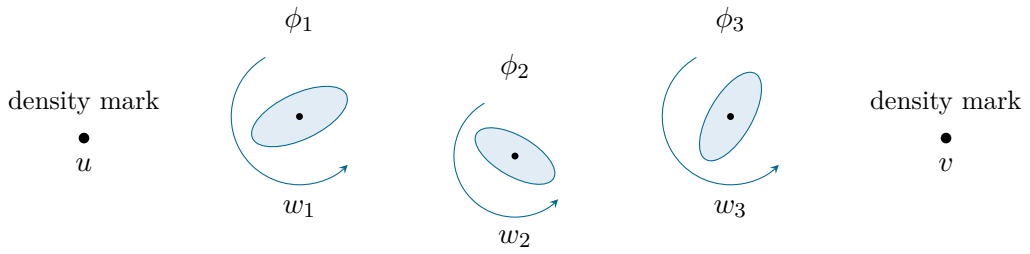


Figure 1: Several closed elliptical obstacles for one connection question between the density marks u and v. The centers w_j are fixed, and the orientation angles ϕ_j vary independently. The normalized second Fourier coefficient in each angle is the lattice response in (A.4); its limit gives repeated stress insertions in the sense of Theorem 17.1. The theorem allows any fixed finite number of obstacles.

The lattice mesh tends to zero at fixed positive ellipse radii r_j, which then vanish jointly at arbitrary relative rates; see subsection 8.5. All marked points remain separated. The correlations converge as distributions in the density coordinates, that is, after integration against smooth compactly supported functions of those coordinates. After each such test, convergence is locally uniform in the stress centers. The limits are symmetric in the stress insertions and independent of the fixed ellipse shape parameters. For a fixed test and fixed separation, the radius error is bounded by $C \sum_j r_j^{1/4}$; see (17.4). Theorem 17.1 gives the precise statement.

To combine sources, we must retain the local information that determines how each small obstacle affects the exterior. Our local estimate retains the color of every frontier cell of a surrounding disk and records which open frontier cells are joined by paths inside that disk. It controls every bounded observation of this record and gives the Cauchy estimate (9.3). The local sources are represented by finite complex measures, called rows, on record spaces; they are defined in subsection 4.1. A separate construction proves existence and conformal covariance of density correlations in domains with finitely many holes whose analytic boundaries satisfy the bounds in Theorem 10.1. The bound (10.5) controls the result of joining local records to exterior density observations. Together, these estimates allow several sources to shrink independently while their joint effect remains controlled.

The one-stress Ward identity admits a shorter proof. For a fixed smooth density test, the construction and covariance in Part II, the elementary four-arm hole-influence bound (4.6), and the Joukowski change of variables already give the limit and its Ward identity; see the direct argument at the start of subsection 17.5. Part I supplies the stronger estimates uniform in the L^1 norm of the density test and, in the present proof, the bounds needed to shrink two or more stress sources jointly.

Within these correlations, the Ward recursion (17.7) also gives sequential collisions of two stress insertions, the normal-ordered square, and local contour identities with central charge zero. These consequences are established in Appendix A. The stress response with two density insertions is nonzero, although correlations containing only separated stress insertions vanish. Thus the directional probes have a nontrivial action on connection statistics even when the stress field has vanishing vacuum correlations. The spin-two four-leg field of dimension two and its logarithmic mixing with the stress tensor were identified at the CFT level in [27]. Subsection 2.5 relates this description to the present construction and explains the role of the exact lattice zero.

Section 2 discusses the earlier constructions and inputs, and Section 3 introduces the local sources and summarizes the main results. Sections 4–9 prove the local angular estimate and define its completion. Sections 10–16 construct the density correlations in domains with finitely many holes. Section 17 combines these results and identifies the stress action. Appendix A gives explicit stress responses, sequential collisions, and contour identities. Further questions concerning simultaneous collisions, compatible subtraction rules, and other percolation observables are discussed in Section 18.

2 Previous results and conventions

We review the probabilistic inputs and earlier constructions related to the results in Section 3.

Unless stated otherwise, theorem, equation, and page numbers in citations refer to the arXiv version linked in the bibliography when one is given, and otherwise to the listed publication.

2.1 Percolation records and arm estimates

Critical site percolation on $a\mathbb{T}$, the triangular lattice of mesh $a > 0$, assigns independent fair open or closed colors to the hexagonal cells. We use the inner-cell approximation and forced-closed convention of subsection 4.1. The two banks of an explored slit are kept separate. A frontier occupation word $\mathcal{B}$ assigns an open or closed color to every labelled frontier cell. Its maximal consecutive runs of one color are the boundary arcs. The precise frontier, word, and conditional law $\mathbb{P}^{a,\mathcal{B}}$ are defined in subsection 4.1; connections between distinct open arcs

are recorded separately. The standard interface representation is described in [1, Section 1.2] and [14, Section 6.1.2].

For a disk D, the *complete frontier record* consists of the frontier colors and the partition of the open frontier cells according to open connectivity inside D. With a prescribed word, this reduces to a partition of its open arcs. An exterior completion attaches exterior colors and connections to this record, as in subsection 4.1. Distinct open arcs are identified only when an interior or exterior connection joins them.

For a complex measure m on a finite record space S, our variation norm is

$$\|m\|_{\mathrm{var}} = \sum_{s\in S} |m(s)| = \sup_{|F|\le 1} \left| \sum_{s\in S} F(s)m(s) \right|. \tag{2.1}$$

A completion kernel C is a Markov kernel and satisfies $\|mC\|_{\mathrm{var}} \le \|m\|_{\mathrm{var}}$. A coupling bounds the variation distance between two laws by twice their disagreement probability.

For $j = 4, 6$, let $\alpha_j^a(s,t)$ be the probability of j disjoint alternating-color arms across the annulus of radii $s < t$. Write $\alpha_j(s,t)$ for the limit at fixed positive radii. Let $\alpha_3^+(s,t)$ be the corresponding half-plane probability for two open arms and one closed arm. Fixed numerical changes of radii are absorbed into constants. We use

$$\alpha_4(s,t) \le C_p(s/t)^p, \qquad 0 < p < 5/4, \tag{2.2}$$

$$\alpha_6(s,t) \le C_\eta(s/t)^{35/12-\eta}, \qquad \eta > 0, \tag{2.3}$$

$$\alpha_3^+(s,t) \le C(s/t)^2.$$

The bulk bounds follow from the arm exponents in [7, Theorem 4 and (9)]. The constant-times-square half-plane bound follows from [8, Proposition 17, Section 4.6, and Theorem 24(2)]. Fixed-scale convergence, buffered approximations, and prescribed landing arcs are treated in [9, Section 2.4, Lemma 2.9, Corollary 2.10, and Remark 2.11]; see also subsection 4.2 below.

Russo–Seymour–Welsh (RSW) estimates and the van den Berg–Kesten (BK) inequality give an exponential tail for the number of disjoint open crossings of a fixed-ratio annulus. A closed circuit has uniformly positive probability, so the probability of an open radial crossing is at most $1 - c$. BK then bounds the probability of k disjoint such crossings by $(1-c)^k$. These bounds apply to ordinary product occupations in the annulus; see [8, Section 2.3 and (4.12)].

2.2 Density correlations and logarithmic observables

Give each open cluster an independent symmetric sign, and let S_v be its sign at an open site v, and zero at a closed site. Conditional on the colors, a product of signs has mean one exactly when all marked sites are open and each cluster contains an even number of marks. Otherwise its mean is zero [1, (1.8)–(1.9)].

Use the density variables $\Phi_a(v) = \pi_a^{-1} S_v$, where $\pi_a = \mathbb{P}_a(0 \leftrightarrow \partial B(0,1))$ under the unmodified full-plane law. Camia proves that, in a simply connected domain U, including the plane,

$$G_{U,n}(\mathbf{z}) = \lim_{a\downarrow 0} \mathbb{E}_U^a \prod_{j=1}^n \Phi_a(z_j^a) \tag{2.4}$$

exists at distinct points and satisfies

$$G_{f(U),n}(f\mathbf{z}) = \prod_{j=1}^n |f'(z_j)|^{-5/48} G_{U,n}(\mathbf{z}) \tag{2.5}$$

for conformal bijections f [1, Theorem 1.5, (1.10)–(1.11)]. Here z_j^a approximates z_j and $\mathbb{E}_U^a$ averages colors and signs. The limiting density insertion Φ has weights $h_\Phi = \bar{h}_\Phi = 5/96$. The associated full-plane random distribution is constructed in [1, Theorem 1.7]. A fixed rescaling to unit plane two-point coefficient is used only in Appendix B.3.

The rooted one-arm normalization satisfies

$$\lim_{a\downarrow 0} \frac{\mathbb{P}_a(0 \leftrightarrow \partial B(0,d))}{\pi_a} = d^{-5/48}, \qquad d > 0, \tag{2.6}$$

by [1, (2.1)]. This normalization lets us retain the small probability that a mark reaches a fixed local distance before estimating its exterior completion. Theorem 10.1 extends the density limits and covariance to the finite-hole domains of Section 10. It also supplies the L^1 completion bound (10.5), uniform over holes inside fixed separated source regions.

Camia and Feng prove logarithmic collision asymptotics for the density four-point function [4, Theorem 1.1, (1.9)], refined in [3, Theorem 1.1, (1.7)]. They construct an energy observable and, at distinct points in the plane, prove Möbius-covariant mixed correlation limits for $k \geq 1$ energy insertions and even $n \geq 2$ density insertions [3, (1.8), (1.15), and Theorem 1.4]. They also define its logarithmic partner and compute the two- and three-point limits specified in [3, (1.23) and Theorem 1.6, (1.24)–(1.26)]. Our Ward theorem, Theorem 17.1, concerns density insertions; extensions to other observables are discussed in Section 18.

2.3 Continuum interfaces and two-curve estimates

Camia and Newman establish the full interface scaling limit and its conformal invariance [2, Theorems 1 and 7]. The quad-crossing topology has continuous restriction to subdomains [10, Theorem 1.13(4)]. We use these curve and quad-crossing descriptions for fixed-scale events. The complete-record angular limits of Theorem 9.1 use the rows defined in subsection 4.1 and their completion across meshes in subsection 9.2.

For fixed finite alternating boundary data, Karrila proves joint percolation-interface convergence in disk coordinates, including under marked Carathéodory approximation [14, Section 5.1.1, Theorem 5.8, and the proof of Proposition 6.2]. Karrila's Proposition 5.9 and Theorem 5.10 give the conditional Markov property, positive link-pattern probabilities, and conditional convergence. Uniqueness after uniformization [12, Theorem 4.2] identifies the fixed-pattern limits as global multiple SLE_6. Proposition 1.4 of Beffara–Peltola–Wu concerns FK-Ising; their Remark 1.5 states the percolation extension [13]. Theorem 7.2 states this criterion with numbered hypotheses; Lemma 7.3 verifies them for percolation and relates the conclusion to their proof. Proposition 8.5 applies this criterion to the domains left by our exploration, after verifying that they belong to the required model class and converge in the marked sense conditional on the complete transcript. Only disk-coordinate convergence and observables in a compact interior region are used. The stronger convergence of full curves in the physical plane is covered by Karrila's rough-domain theorem [15, Theorem 4.2], under the additional endpoint hypotheses stated there.

Condition on all but two curves of a global multiple-SLE law. When the remaining four endpoints lie on one complementary component, the conditional pair has the two-SLE law there. The retained curves have their marginal law, which includes the remaining pair's partition weight. Lemma 7.3 derives this weight from Zhan's cascade and normalization identities [12, (2.4)–(2.5), (3.4), and Lemma 3.6]. Lemma 7.4 then proves the selected-pair decomposition and its continuum passage.

Let (γ_1, γ_2) have a two-SLE_6 law in a simply connected domain U, with four distinct marked boundary prime ends and a fixed admissible connectivity pattern. Write $\mathfrak{g}_U(w)$ for

its two-curve Green function, normalized as in [11, Theorem 1.1 and Definition 1.3]. For $w \in U$, the joint approach probability has exponent $5/4$. As $r \downarrow 0$,

$$\mathbb{P}_U\{\gamma_1, \gamma_2 \text{ both meet } B_r(w)\} = c\mathfrak{g}_U(w) r^{5/4} \left[1 + O\left((r/\operatorname{dist}(w, \partial U))^{11/15}\right)\right]. \tag{2.7}$$

The error constant is uniform in the four boundary endpoints [11, Theorem 1.1, (1.1)–(1.3)]. We use this positive scalar estimate in the argument below. The weighted second-angular kernel and complete-record angular stabilization are established separately in Theorems 5.4 and 9.1.

2.4 Related stress constructions

Doyon, Riva and Cardy extract spin two from small elliptical perturbations and obtain Ward recursions under conformal restriction and stated regularity assumptions [19, Assumptions 2.1, Theorem 2.1, and (4.11)]. Doyon's construction for dilute CLE, $8/3 < \kappa \leq 4$, gives Ward identities and the stress transformation law under explicit continuity and differentiability hypotheses [20, Hypotheses 3.1–3.3 and 5.1; Theorems 5.4–5.5].

Chelkak, Glazman and Smirnov construct a discrete stress observable for the loop $O(n)$ model. In its critical Ising specialization, they prove convergence of one- and two-stress correlations and mixed stress–energy/spin correlations [21, Theorems 1–3]. Baverez and Jego construct two commuting Virasoro representations for simple SLE loop measures, with $0 < \kappa \leq 4$ [22, Theorem 1.5].

Camia and Feng identify, up to normalization, a boundary stress tensor and its logarithmic partner in the collision expansion of boundary density correlations [26, Section 2.2, (2.14)–(2.17)]. Their comparison of crossing events before and after removing a small boundary-attached region relates the response to a boundary three-arm event [26, Section 3.3, Figure 2 and pp. 14–16]. This gives a percolation antecedent for relating stress insertions to domain perturbations. Their boundary field identification uses the formal limits in (2.16) and (3.35) of that paper.

Camia, Foit, Gandolfi and Kleban identify the Brownian loop soup bulk stress tensor through the second angular mode of an edge-field product. They compute its two-point function and Ward correlations with two edge fields or two layering fields [6, (2.4), (2.10), (2.14), and (2.16)].

Kupiainen and Oikarinen construct correlations with arbitrary finite numbers of stress insertions in probabilistic Liouville theory on the sphere, with vertex charges satisfying the Seiberg bounds [25, Theorem 1.1]. These correlations are defined by differentiation with respect to the metric. Smoothness in the metric, diffeomorphism covariance, and Weyl covariance then give Ward identities [25, (1.5), (1.8), and Proposition 3.3].

Here the local source is a shrinking, rotating closed ellipse. Complete-record estimates construct the completed local rows of Theorem 9.1. Together with the fixed-radius density mesh limits and the L^1 completion bound, these yield the density-tested stress correlations of Theorem 17.1. Their Ward action follows from conformal changes of variables. We use T for the insertion defined through these correlation limits, a convention also used in [5, Theorem 2.3 and (2.10)]. The Ward hierarchy, sequential collision identities, and contour relations hold within the tested correlations specified in Section 17.

2.5 The bulk stress tensor and its logarithmic partner

The spin-two scaling dimension underlying our angular estimate is already present in the logarithmic CFT description of percolation. Vasseur, Gainutdinov, Jacobsen and Saleur

identify a bulk spin-two four-leg field X_κ whose weights in the dense-loop Coulomb-gas continuation, written with their parameter $g = 16/\kappa$, are

$$h_X(\kappa) = \frac{3}{2} + \frac{3}{\kappa}, \qquad \bar{h}_X(\kappa) = -\frac{1}{2} + \frac{3}{\kappa}, \qquad x_X(\kappa) = h_X + \bar{h}_X = 1 + \frac{6}{\kappa};$$

see [27, p. 4, Coulomb-gas discussion and (8a)]. At $\kappa = 6$ these weights become $(2, 0)$, the collision point with the holomorphic stress tensor. Thus the exponent $5/4 + 3/4 = 2$ in Proposition 6.3 agrees with a known CFT dimension. Away from $\kappa = 6$, this continuation follows the four-leg field, whose dimension differs from the constant stress dimension two. Our construction and estimates concern $\kappa = 6$. The new input is the uniform angular control of complete frontier records, its completion against density observations, and the resulting joint limits and Ward identities.

In the normalization in which the zeroth Virasoro modes act by $L_0 t = 2t + T$ and $\bar{L}_0 t = T$, the bulk logarithmic pair has two-point functions

$$\langle T(z)T(0)\rangle = 0, \qquad \langle T(z)t(0)\rangle = \frac{b}{z^4}, \qquad \langle t(z,\bar{z})t(0)\rangle = \frac{\theta - 2b\log|z|^2}{z^4}.$$

Here θ is a normalization-dependent constant. Vasseur et al. obtain $b_{\mathrm{bulk}} = -5$ from periodic lattice calculations and a Coulomb-gas/OPE argument [27, (1)–(3) and (8a), pp. 2–4]. The shift $t \mapsto t + \lambda T$ changes θ by $2\lambda b$ and preserves the logarithmic coefficient. These statements concern the bulk stress partner; the boundary construction recalled above has its own logarithmic coupling.

Our local ellipse variables have exactly zero vacuum two-point function at every mesh whenever their supports are disjoint; see subsection 17.1. Hence their limiting stress insertion satisfies $\langle TT\rangle = 0$ before any comparison with logarithmic CFT. Within a pair with the displayed two-point functions and $b \neq 0$, a fixed linear combination $A = \alpha T + \beta t$ satisfies

$$z^4\langle A(z)A(0)\rangle = 2\alpha\beta b + \beta^2(\theta - 2b\log|z|^2).$$

Vanishing at all separated points forces $\beta = 0$. The nonzero Ward action on densities, exemplified by (A.6), fixes the remaining stress normalization. Thus the lattice identity excludes a nonzero logarithmic-partner component within this standard pair, while the Ward identities identify the stress action in the correlation sector constructed here. The zero alone is not a uniqueness statement about fields in a full logarithmic CFT. It remains to construct t and its mixed correlation with T, and to determine b from percolation limits.

3 Local sources and main results

We introduce the local sources and summarize the geometric estimates, using the definitions and precise hypotheses at the later locations indicated below. The spectral, density, and stress results are stated in Sections 5, 10, and 17; this section gives an overview and the proof dependencies.

3.1 The source is a finite probability experiment

At each stress center, rotate a small ellipse with semiaxes $r(1 + e)$ and $r(1 - e)$ and force its inner-cell approximation closed. The second angular Fourier coefficient defines the local variable $\tau_{a,r,e}$ and the signed complete-record rows $V_{r,e}$ and $Q_{r,e} = r^{-2}V_{r,e}$. Subsection 4.3 gives the formal definitions, the comparison defect $\Delta_{r,b,e}$, and the exact forcing identity. The identity turns correlations with τ into angular averages of observations in the domains with closed holes. It also gives zero expectation for every nonempty product of local sources with disjoint supports. The angular prescription has a precedent in [19, Section 2, (2.1)–(2.4)].

3.2 Two geometric estimates

Strip regularity. Theorem 4.3, stated and proved in subsection 4.2, controls the variation of the complete frontier-record law under a small normal displacement of a closed analytic hole. Its hypotheses use the shape bounds and record conventions of subsection 4.1; its estimate is preserved by exterior completion.

Protected exploration. Theorem 8.4, stated and proved in subsection 8.3, reduces arbitrary frontier words to controlled finite interface problems while retaining the original record. The exploration leaves a protected disk unqueried and has a common transcript for every allowed ellipse, in the precise sense of Lemma 8.1. The theorem combines the completion identities, an exponential bound on the number of surviving tips, a separation estimate, and marked compact exhaustion. Proposition 8.5 then applies the interface-convergence criterion to the conditional residual laws.

3.3 Main results

Complete-record angular stabilization. Theorem 9.1, stated and proved in subsection 9.2, gives the uniform 9/4 defect estimate and arbitrary-radius Cauchy bound for the angular rows. It constructs the completed local limit $T_{D,e}(w)$, including the version uniform over prescribed frontier words. The shape parameter remains part of this local limit. Scalar limits obtained by applying exterior observations also require the fixed-radius mesh limits in subsection 9.3.

Angular spectrum and kernel. Proposition 5.3 gives the spectrum of the second-angular generator, and Theorem 5.4 gives the uniform kernel estimate. The operator realization and its identification with the probabilistic semigroup are proved in Propositions 5.1 and 5.2. The angular kernel with V follows from (5.35).

Density correlations. The density variables are the normalized cluster-sign variables Φ_a of (10.2); their limiting insertion has weights $h_\Phi = \bar{h}_\Phi = 5/96$. Theorem 10.1 extends Camia's density correlations to the finite-hole domains of Section 10, with covariance (10.4) and the uniform completion bound (10.5). Subsection 16.2 proves the mesh limits (9.10) for geometric angular sources at fixed positive radii. These are the inputs used in subsection 9.3.

Stress correlations and Ward identities. Theorem 17.1 constructs every fixed finite number of stress insertions against density observations and identifies their limits with the Ward recursion (17.7). The quantitative bounds are (17.4) and (17.5).

Appendix A records consequences of the recursion, including the sequential stress collision formula (A.11). Within the limiting correlations, subtracting its double and simple poles and then merging the two centers defines $:TT:$ in Proposition A.1. Within the same tested correlations, the contour modes (A.13) satisfy $[L_p, L_q] = (p-q)L_{p+q}$, as proved in (A.14). The stress response with two densities is nonzero by (A.6), while separated stress-only correlations vanish by (A.10). Complex conjugation gives the purely antiholomorphic hierarchy. Section 18 discusses simultaneous collisions, mixed Ward identities, and further observables.

3.4 Proof dependencies

Part I proves the complete-record estimate of Theorem 9.1. Section 4 controls shape changes, and the operator and angular analysis in Sections 5–6 gives the two-curve estimate. Section 7 justifies the conditional-pair reduction using percolation convergence and Zhan's cascade law. Proposition 8.5 verifies the convergence hypotheses for the explored residual domains. Protected exploration and Section 9 then give the uniform Cauchy bounds.

Part II proves Theorem 10.1. It extends Camia's density correlations to finite-hole domains

and supplies the completion bound for arbitrary rows and the mesh limits at fixed radii for geometric angular sources. Sections 11–14 distinguish the simply connected cluster theorem of Camia–Conijn–Kiss from their restricted-configuration theorem for arbitrary domains, and supply the shielding and transport needed for the holes.

For $m \geq 2$, Part III combines these inputs to establish the joint stress limits. Conformal transport and induction identify the limits with the Ward recursion in Theorem 17.1. Shape independence holds for these density-tested correlations; the complete-record limit (9.8) retains its shape parameter.

For $m = 1$, the direct argument in subsection 17.5 uses Part II, the elementary four-arm hole-influence bound (4.6), and smooth test transport to obtain the limit and Ward identity. Its error involves derivatives of the test. The stronger bounds (17.4) and (17.5), proportional to $\|\psi\|_{L^1}$, use Part I for every $m \geq 1$, including $m = 1$.

Part I
The signed angular response

4 The local boundary-strip argument

We compare the boundary connections obtained when two nearby holes are forced closed. We first specify the common probability space and the information recorded at the outer boundary.

Conventions. We use standard terminology from measure-theoretic probability, percolation, complex analysis, and operator theory. Our stochastic-calculus and Markov-process conventions follow Le Gall.[1] Spectral terminology follows [18, Section IV.1, pp. 239–248]. Smooth means C^∞, and C_c^∞ denotes smooth functions of compact support. A conformal map between domains means a holomorphic bijection. All L^2 spaces are complex, with $\langle f, g\rangle_{L^2(\mu)} = \int \overline{f} g \, d\mu$; operator products mean composition. Write $\mathbf{1}_A$ for the indicator of A, $\|\cdot\|_\infty$ for the pointwise supremum norm, $\lceil x \rceil$ for the ceiling, and Γ for Euler's gamma function. We use O and o on the stated ranges; subscripts on O record allowed constant dependencies.

Notation. We use U, D for planar domains, K for closed holes, and Q for normalized angular rows. We reserve Δ for the comparable-radius defect (4.11); the signed surgery row is $\mathsf{J}_{\alpha,ij}$, defined in (7.1). Geometric boxes are B, and compact sets of insertion coordinates are $\mathscr{C}$. Angular kernels are K_t, the unitary identification is $\mathscr{I}$, and generic distributions are $\mathscr{F}$. The crossing event is Cross, with probability p_{cr}; p_α denotes a link-pattern probability, and P a conditional probability in Section 14. We write $h_\Phi = 5/96$ for the density weight, use δ_w for center displacements, and write $\|\cdot\|_{C^k}$ for derivative norms of tests. Other local symbols are defined where they occur.

4.1 Configurations, records, and separating paths

Consider critical site percolation on the triangular lattice $a\mathbb{T}$ of mesh $a > 0$. We identify each site with its hexagonal cell; adjacent cells share an edge. Each random cell is independently

[1] J.-F. Le Gall, *Brownian Motion, Martingales, and Stochastic Calculus*, Graduate Texts in Mathematics 274, Springer, 2016, DOI: 10.1007/978-3-319-31089-3. See Sections 2.1–2.2 (Brownian motion), 4.3–4.5 (quadratic variation and covariation), 5.1–5.2 (stochastic integration and Itô's formula), and 6.1, 8.1, 8.3 (Markov processes and stochastic differential equations).

open (occupied) or closed with probability 1/2. A path is a sequence of adjacent cells. It is open or closed when all its cells have that color, and simple when it visits each cell at most once. For a planar set H, its inner-cell approximation H^a consists of the cells contained in H. *Forcing H closed* sets every cell of H^a to closed. All other cells keep their random colors.

A Jordan body is the closure of the region enclosed by a simple closed curve. Let K, K' be strictly convex Jordan bodies with real-analytic boundaries. Fix a size $\rho > 0$ and uniform constants $\eta \in (0,1)$ and $M > 1$. Each body contains a disk of radius $\eta\rho$ and is contained in a disk of radius $M\rho$. For either body H, let $n_H(x)$ be the outward unit normal at $x \in \partial H$. Require the normal map $(x,t) \mapsto x + tn_H(x)$ to be injective for $x \in \partial H$ and $|t| < \eta\rho$. Its image is the *tubular neighborhood*. At each boundary point, require an injective analytic map f on the disk of radius $\eta\rho$ centered there. It maps the boundary portion to the real axis, the exterior side to the upper half-plane, and satisfies $M^{-1} \le |f'| \le M$. These maps are the *boundary charts*. These bounds define the shape class used below.

Normal displacement at most δ means that $\partial K'$ is obtained from ∂K by moving each point along its normal by at most δ. Assume $0 < \delta \le c\rho$, with c sufficiently small in terms of η, M.

Write $B(w,r) = \{z \in \mathbb{C} : |z - w| < r\}$. Choose $D = B(w, d_0)$ with $K \cup K' \subset B(w, C_0\rho)$ and $d_0 \ge 2C_1\rho$, where $C_1 > C_0$ is fixed sufficiently large in terms of η, M to enclose the local witness regions used below. Its lattice frontier Γ_a consists of cells of D^a adjacent to a cell outside D^a. This frontier is the *remote cut*. The geometric constants C_0, C_1 and the constants c, C depend only on η, M; c, C may change between estimates. The mesh limit is always taken with ρ, δ, d_0 fixed.

A *frontier occupation word* is a map

$$\mathcal{B} : \Gamma_a \longrightarrow \{\text{open}, \text{closed}\}.$$

Every entry retains its frontier-cell label. Each boundary edge inherits the label and color of its incident frontier cell. Read these labelled boundary edges in cyclic order; maximal consecutive runs of one color are the boundary arcs. The two banks of a later explored slit are kept as separate boundary sides. The conditional law $\mathbb{P}^{a,\mathcal{B}}$ fixes the colors on Γ_a to this word and leaves every other sampled cell independent and fair. The containing domain is understood from the notation. Open connections between different boundary arcs are determined by paths and are recorded separately.

For a sampled configuration ω and a hole $H \subset D$, let ω^H be the configuration after forcing H^a closed. Its *complete frontier record* is the random variable

$$S^H(\omega) = (\mathcal{B}^H(\omega), \mathcal{P}^H(\omega)).$$

Here $\mathcal{B}^H(\omega)$ lists the colors of all cells of Γ_a in ω^H, and $\mathcal{P}^H(\omega)$ partitions its open frontier cells: two belong to the same block exactly when an open path in D^a joins them in ω^H. Write ν_H^{a,d_0} for the law of S^H under the unconditioned product law and $\mathcal{S}_a$ for the common finite set of color-and-partition records for this mesh and frontier.

A *row* on $\mathcal{S}_a$ is a finite complex measure, represented by the vector of its masses $(m(s))_{s \in \mathcal{S}_a}$. Thus

$$m = \sum_{s \in \mathcal{S}_a} m(s)\delta_s, \qquad m(F) = \sum_{s \in \mathcal{S}_a} m(s)F(s),$$

where δ_s is unit mass at s and F is any function on the record space. The law ν_H^{a,d_0} is a probability row. Angular averages and differences of these laws are complex rows. The *variation norm* of a row is

$$\|m\|_{\text{var}} = \sum_{s \in \mathcal{S}_a} |m(s)| = \sup_{|F| \le 1} |m(F)|.$$

The same terminology applies to rows on the finite arc-partition spaces used below.

Attaching a fixed exterior configuration joins the corresponding frontier classes; this operation is an *exterior completion*. If c is its map from local records to completed records, its action on a row is the pushforward

$$(mc)(t) = \sum_{s:c(s)=t} m(s).$$

The triangle inequality gives $\|mc\|_{\mathrm{var}} \le \|m\|_{\mathrm{var}}$. Random exterior data give the completion kernels defined in subsection 9.2.

Choose inward and outward parallel offsets of K, obtained by constant normal displacements and denoted by K^- and K^+. Choose them so that $K^- \subset K, K' \subset K^+$ and their normal separation is at most $C\delta$. The region $K^+ \setminus K^-$ is the *boundary strip*. Sample the cells outside K^- once, and use those same colors for all four holes, closing the cells of the chosen hole. This construction is the *coupling*; $\mathbb{P}$ denotes its probability law. The variables $S^{K^-}(\omega)$ and $S^{K^+}(\omega)$ are the records just defined with $H = K^-$ and $H = K^+$, evaluated using this same sample ω. A *discrepancy* means that these two records differ. The frontier colors agree, and closing cells can only split open connectivity classes. Equality of the two extreme records therefore implies equality of the intermediate records. One-cell adjustments, of size $O(a)$, make the lattice envelopes nested. Summing the differences of the record indicators gives the coupling bound

$$\|\nu^{a,d_0}_{K'} - \nu^{a,d_0}_{K}\|_{\mathrm{var}} \le 2\mathbb{P}(S^{K'} \ne S^{K}) \le 2\mathbb{P}(S^{K^-} \ne S^{K^+}).$$

An *arm* is a path joining the inner and outer boundaries of a specified annular region. Multiple arms are pairwise disjoint; alternating arms have alternating colors in cyclic order. A *sampled* arm uses the independent random colors in the coupling. A *crosscut* is a simple curve with distinct endpoints on the outer boundary and interior in the domain. Lattice paths are drawn through their cells, with one-cell endpoint adjustments. A *port* is a specified open cell of Γ_a, used as an endpoint of a connection inside D^a. For two distinct ports, choose disjoint short boundary contacts within the incident cells. Their *complementary outer arcs* are the two intervening boundary portions. A closed crosscut separating the ports has one endpoint on each complementary arc; the cell-level endpoint adjustments are described in the proof below. We use the planar crossing alternative: for four successive boundary arcs, failure of an open crossing between one pair of opposite arcs gives a closed crossing between the other pair.

Lemma 4.1 (Sampled exterior tails)**.** *If the extreme records differ, there are occupied frontier ports u, v, a simple open path γ joining them in the smaller-hole configuration, and a closed crosscut λ separating them in the larger-hole configuration. The portions of λ before its first and after its last visit to K^+ are disjoint paths of sampled closed sites from the hole to the two complementary outer arcs.*

Proof. The frontier colors agree under the coupling. A discrepancy therefore implies that two open frontier cells are connected only in the smaller-hole configuration. Erasing loops from a connecting path gives γ. Apply the crossing alternative with the ports as one pair of opposite boundary arcs. The other pair consists of the complementary frontier arcs. A single-cell port can be thickened within its own open cell or extended through a short exterior strip. These extensions are disjoint and add no interior connection. The larger-hole configuration therefore has a closed separator; erase loops to obtain λ.

If λ avoided the changed region, it would already separate u and v in the smaller-hole configuration, a contradiction. Trim at its first and last visits to K^+. Simplicity makes the

retained tails disjoint, and their interior sites lie outside K^+; these sites were sampled, not forced. Endpoint adjustments of one lattice cell do not affect this statement.

□

Lemma 4.2 (Deterministic-box witness)**.** *If the records differ as in Lemma 4.1, at least one of at most $C\rho/\delta$ fixed square boxes near ∂K^- has the following property. Two sampled open arms and one sampled closed arm join the box to distance $c\rho$, outside K^-. Each box has diameter $C'\delta$; a box with these arms is called a* witness*. In addition, four alternating sampled arms cross an outer annulus centered at w, from radius $C_1\rho$ to a radius comparable to d_0. This annulus is disjoint from all the local three-arm regions.*

The witness boxes in the next proof are selected before the paths are observed.

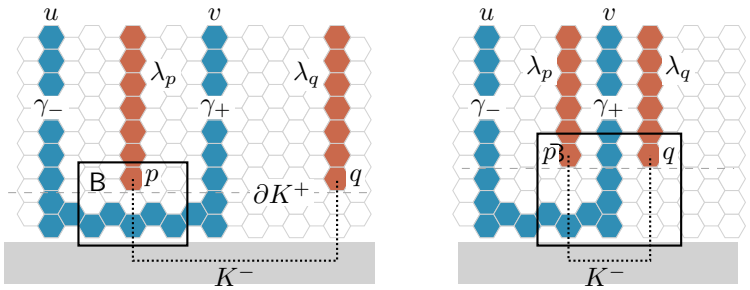
Proof. Cover ∂K^- by squares of diameter a fixed multiple of δ, chosen before sampling. Choose them with bounded overlap: each point belongs to at most a fixed number of squares. The boundary length is $O(\rho)$, so at most $C\rho/\delta$ squares are needed. Take a/δ sufficiently small. Draw paths through cell centers and, when necessary, move their terminal pieces within one cell to separate corner contacts. Let p, q be the attachment points of the two sampled closed tails from Lemma 4.1, and denote those tails by λ_p, λ_q.

The tails have their interiors outside K^+. Connect p and q to K^- by inward normal segments and join their inner ends inside K^-. The tubular-neighborhood bounds give segment lengths $O(\delta)$. If the attachment cells are within $O(\delta)$ of each other, use their distinct entrance edges. Two short, disjoint connector arcs then fit in one enlarged boundary neighborhood. Join their inner ends inside K^-. Erase redundant portions and adjust the curve within one cell to obtain a simple crosscut with the same outer endpoints as λ. These endpoints separate u from v along the frontier. The replacement crosscut therefore separates the two ports. Figure 2 shows both cases. The connectors are auxiliary geometric curves without a percolation color.

The simple open path γ cannot cross either sampled closed tail or enter the forced-closed cells of K^-. It must meet a short connector arc. Enlarge the fixed cover so that one box B contains this arc and its adjacent closed-tail attachment. A uniform enlargement suffices and preserves the bound on the number of boxes. Orient γ from u to v. Retain its portion before its first visit to B and its portion after its last visit to B. Reverse the first portion and remove the parts in B. The resulting branches, denoted by γ_- and γ_+, are disjoint sampled open paths from B to the frontier. For the selected closed tail, retain the portion after its last visit to B. This gives a sampled closed branch to the frontier. Simplicity makes the open branches disjoint, and their color separates them from the closed branch.

Choose a point of ∂K^- within $O(\delta)$ of B and a ball of radius $c\rho$ contained in its boundary chart. All three frontier endpoints lie outside this ball because $d_0 \geq 2C_1\rho$. Stop each branch at its first exit from the ball. This gives the three required arms between B and that circle, outside K^-. The construction using first and last visits excludes further visits to B. Returns elsewhere in the strip preserve the exit paths and their disjointness. Every retained cell outside B has its sampled color.

For the outer event, take $B(w, C_1\rho)$ enclosing the hole and every local stopping ball. On each open branch and each closed tail, retain the portion after its last departure from this disk. These four disjoint paths cross the outer annulus. Their endpoints alternate in color because the crosscut ends on the two complementary frontier arcs between u and v. Planarity preserves this order through the annulus. Choosing C_1 sufficiently large makes the local three-arm regions and the outer four-arm annulus disjoint, with their locations fixed before sampling. □



(a) Separated attachments (b) Close attachments

Figure 2: Cell-level witnesses for Lemma 4.2. Blue cells form the open path γ; red cells form the sampled closed tails λ_p, λ_q; gray denotes the forced hole. Smooth envelopes are shown in local boundary coordinates. The dotted geometric connector joins the two tails through K^-. The deterministic box B contains an intersection of γ with a short connector and the adjacent tail attachment. The open portions before the first visit to B and after the last visit to B, together with the closed tail after its last visit to B, are the three sampled arms. In panel (b), both attachments lie in the same enlarged box. Each displayed branch continues to the remote frontier; the proof stops it upon its first exit from the fixed local chart.

4.2 From the witness to the measure estimate

For fixed $0 < s < t$, let $\alpha_4^a(s,t)$ be the probability, in unmodified full-plane percolation, of four disjoint alternating sampled arms across $B(0,t) \setminus \overline{B(0,s)}$. Define

$$\alpha_4(s,t) = \lim_{a \downarrow 0} \alpha_4^a(s,t).$$

This limit exists by [9, Lemma 2.9]. It is unchanged by translating the annulus. Fixed multiplicative changes of the radii affect the comparison only by a constant factor; see [9, Sections 2.1 and 2.3].

Theorem 4.3 (Completed-record strip regularity)**.** *Let K, K' have size ρ in the strictly convex analytic shape class of subsection 4.1, with its size, tubular-neighborhood, and boundary-chart bounds fixed. Use the normal-displacement convention there, with displacement at most $0 < \delta \le c\rho$, and assume $K \cup K' \subset B(w, C_0\rho)$. Choose a fixed $C_1 > C_0$ sufficiently large in terms of these bounds and take the common frontier in $D = B(w, d_0)$ with $d_0 \ge 2C_1\rho$. For $H = K, K'$, let ν_H^{a,d_0} be the unconditioned complete frontier-record law after forcing the inner-cell approximation H^a closed. Then*

$$\limsup_{a \downarrow 0} \|\nu_{K'}^{a,d_0} - \nu_K^{a,d_0}\|_{\mathrm{var}} \le C\alpha_4(C_1\rho, d_0)\frac{\delta}{\rho}. \tag{4.1}$$

The constants depend only on the fixed shape bounds. The mesh limit keeps ρ, δ, d_0 fixed. Applying the same exterior-completion map of subsection 4.1 to both laws preserves the estimate.

Proof. Let $\mathsf{B}_1, \dots, \mathsf{B}_N$, with $N \le C\rho/\delta$, be the fixed boxes of Lemma 4.2. For $1 \le j \le N$, let A_j be the event that three disjoint sampled arms join B_j to its local circle of radius $c\rho$, outside K^-. Two arms are open and one is closed. Let A_4^{out} be the event of four alternating sampled arms across the disjoint outer annulus of that lemma. These are existence events in

the fixed regions chosen there; their dependence on the mesh a is suppressed. Lemma 4.2 gives

$$\{S^{K^-} \neq S^{K^+}\} \subset A_4^{\mathrm{out}} \cap \bigcup_j A_j. \tag{4.2}$$

Each A_j depends on cells disjoint from those determining A_4^{out}. Independence and the union bound therefore give

$$\mathbb{P}(S^{K^-} \neq S^{K^+}) \leq \sum_j \mathbb{P}(A_j)\mathbb{P}(A_4^{\mathrm{out}}). \tag{4.3}$$

For fixed $0 < s < t$, let $\alpha_3^+(s,t)$ be the mesh-limit probability of three disjoint arms, two open and one closed, joining the two semicircles of the upper half-annulus

$$\{z \in \mathbb{C} : s < |z| < t,\ \operatorname{Im} z > 0\}.$$

The half-plane estimate of [8, Proposition 17, Section 4.6, and Theorem 24(2)] gives

$$\alpha_3^+(s,t) \leq C(s/t)^2. \tag{4.4}$$

Keep δ, ρ fixed and take the mesh limit before applying the boundary chart from subsection 4.1. The chart's derivative bounds compare the image scales with δ, ρ, and the chart sends the exterior side to the upper half-plane. Conformal invariance and approximation of arm events by crossings with slightly displaced boundaries justify this passage; see [9, Sections 2.3–2.4]. The half-plane estimate gives

$$\limsup_{a \downarrow 0} \mathbb{P}(A_j) \leq C(\delta/\rho)^2. \tag{4.5}$$

Fix C_1 from subsection 4.1 large enough that $B(w, C_1\rho)$ contains every local witness region. Since $d_0 \geq 2C_1\rho$, the inner and outer annular radii are distinct. Consequently,

$$\limsup_{a \downarrow 0} \mathbb{P}(A_4^{\mathrm{out}}) \leq C\alpha_4(C_1\rho, d_0).$$

There are at most $C\rho/\delta$ boxes. Combining these bounds with (4.3) and the coupling inequality of subsection 4.1 bounds the mesh upper limit of the variation distance by

$$C\frac{\rho}{\delta}\left(\frac{\delta}{\rho}\right)^2 \alpha_4(C_1\rho, d_0) = C\alpha_4(C_1\rho, d_0)\frac{\delta}{\rho},$$

which proves (4.1). All constants depend only on the fixed shape bounds. The exterior-completion assertion follows from contraction of the variation norm. □

Let $\nu_{\varnothing}^{a,d_0}$ be the law of the same frontier record with no cells forced closed. We also have

$$\limsup_{a \downarrow 0} \|\nu_K^{a,d_0} - \nu_{\varnothing}^{a,d_0}\|_{\mathrm{var}} \leq C\alpha_4(C_1\rho, d_0). \tag{4.6}$$

To see this, use one common sample for the configurations with and without the hole. A lost connection between two open frontier cells supplies two open branches and two separating closed branches outside a disk enclosing K. They form four alternating arms. The coupling inequality gives (4.6), using the outer part of the proof of Lemma 4.2; compare [1, (2.55)].

4.3 Ellipses and angular source rows

For $w \in \mathbb{C}$, $r > 0$, $0 < e < 1$, and $\phi \in [0, 2\pi)$, let

$$K_{r,e,\phi}(w) = \left\{ w + e^{i\phi}(x + iy) : \frac{x^2}{r^2(1+e)^2} + \frac{y^2}{r^2(1-e)^2} \le 1 \right\}. \tag{4.7}$$

The parameter e specifies the semiaxes. For e in a fixed compact subinterval of $(0, 1)$, these ellipses satisfy the shape bounds of subsection 4.1 uniformly in the center and angle. Write $K^a_{r,e,\phi}(w)$ for the cells contained in this ellipse, as in subsection 4.1, and $N_a(r, e, \phi, w)$ for their number. Define

$$\tau_{a,r,e}(w) = \frac{1}{2\pi e r^2} \int_0^{2\pi} e^{-2i\phi} 2^{N_a(r,e,\phi,w)} \mathbf{1}_{\{K^a_{r,e,\phi}(w) \text{ closed}\}}\, d\phi. \tag{4.8}$$

At fixed mesh the forced set changes only finitely many times with ϕ. The variable depends only on colors in $B(w, 2r)$. This is the source used in (17.1). The angular prescription has a precedent in [19, Section 2, (2.1)–(2.4)].

For any deterministic finite set of sampled cells K and any integrable observable Y, independence gives

$$\mathbb{E}[2^{|K|} \mathbf{1}_{\{K \text{ closed}\}} Y] = \mathbb{E}[Y \mid K \text{ closed}]. \tag{4.9}$$

Consequently $\mathbb{E}\tau_{a,r,e} = 0$, and every nonempty product of these variables at pairwise disjoint supports has expectation zero. For density observations, the conditional law assigns independent signs to the resulting open clusters; see (15.1).

Fix $D = B(z_0, d)$, $w \in B(z_0, d/4)$, and $e \in [e_-, e_+] \Subset (0, 1)$. Take $0 < r \le r_0 = c_* d$, with $c_* > 0$ sufficiently small. Let $\nu^{a,D}_{r,e,\phi,w}$ be the complete frontier-record law in this fixed disk after forcing $K^a_{r,e,\phi}(w)$ closed, with the record conventions of subsection 4.1. Define the complex rows

$$V^{a,D}_{r,e}(w) = \frac{1}{2\pi e} \int_0^{2\pi} e^{-2i\phi} \nu^{a,D}_{r,e,\phi,w}\, d\phi, \qquad Q^{a,D}_{r,e}(w) = r^{-2} V^{a,D}_{r,e}(w), \tag{4.10}$$

$$\Delta^{a,D}_{r,b,e}(w) = V^{a,D}_{r,e}(w) - b^{-2} V^{a,D}_{br,e}(w), \qquad \tfrac{1}{2} \le b \le 1. \tag{4.11}$$

The integrals are taken separately for each record in the finite state space $\mathcal{S}_a$. Each difference uses the same mesh and record space. Limits follow the convention of subsection 8.5. For a prescribed frontier occupation word $\mathcal{B}$, let $\nu^{a,D,\mathcal{B}}_{r,e,\phi,w}$ be the corresponding law under $\mathbb{P}^{a,\mathcal{B}}$ from subsection 4.1; the same formulas define $V^{a,D,\mathcal{B}}_{r,e}$, $Q^{a,D,\mathcal{B}}_{r,e}$, and $\Delta^{a,D,\mathcal{B}}_{r,b,e}$. The exploration in subsection 8.1 uses these fixed-color laws.

Since the laws have mass one,

$$V^{a,D}_{r,e}(\mathbf{1}) = 0, \qquad \|V^{a,D}_{r,e}\|_{\mathrm{var}} \le e_-^{-1}, \qquad \|\Delta^{a,D}_{r,b,e}\|_{\mathrm{var}} \le 5/e_-. \tag{4.12}$$

These mass and variation bounds also hold for the conditional rows, since their underlying laws are probability measures. Lemma 8.1 gives the analogous bounds after conditioning on the common exploration transcript defined there.

For the translation comparison, fix $D = B(z_0, d_0)$ and write ρ for the ellipse radius, with $0 < \rho \le c d_0$ and $e \in [e_-, e_+] \Subset (0, 1)$. Use the rows of (4.10) in this fixed disk.

Let $\delta_w \in \mathbb{C}$ satisfy $|\delta_w| \le c\rho$. In the supremum below, w ranges over centers with $w, w + \delta_w \in B(z_0, d_0/4)$. At fixed positive scales, slightly displaced boundaries give fixed arm events containing those for all sufficiently close centers, angles, and shape parameters. A finite cover of the compact closure of this parameter range makes the preceding estimates uniform as $a \downarrow 0$.

Translation by δ_w changes the ellipse boundary by normal displacement at most $C|\delta_w|$. Apply (4.1) in $B(w, d_0/2) \subset D$, then complete with the independently sampled exterior inside D. Contraction and fixed-factor comparison of α_4 give the same bound with outer scale d_0. Integrating in angle and using $e \geq e_- > 0$ therefore gives

$$\limsup_{a\downarrow 0} \sup_{w} \|Q^{a,D}_{\rho,e}(w+\delta_w) - Q^{a,D}_{\rho,e}(w)\|_{\mathrm{var}} \leq C \frac{\alpha_4(C_1\rho, d_0)}{\rho^2} \frac{|\delta_w|}{\rho}. \tag{4.13}$$

The disk and its frontier remain fixed throughout this comparison. The constants are uniform over the stated ranges of centers and shape parameters.

5 An angular average for two random angles

We define two random angles and estimate an expectation with a complex angular weight. Section 6 connects this calculation with the ellipse of subsection 4.3.

5.1 The defining equations

Fix $(Z_1(0), Z_2(0)) \in (0,\pi)^2$ and independent standard real Brownian motions B_1, B_2. Time is $t \geq 0$; omitted time subscripts in differential equations mean evaluation at t. Solve

$$dZ_j = \sqrt{\frac{6\sin Z_j}{\sin Z_1 + \sin Z_2}}\, dB_j + \frac{4\cos Z_j}{\sin Z_1 + \sin Z_2}\, dt, \qquad j = 1, 2. \tag{5.1}$$

Zhan proves that the solution stays in $(0,\pi)^2$ for all time [11, Lemma 4.1, (4.2), p. 26]. Write $\mathbb{P}_{c4}$ for its law and $\mathbb{E}$ for expectation under that law. We call it the reference diffusion.

For the continuous processes below, $\langle M, N\rangle_t$ denotes quadratic covariation as defined in Le Gall, Sections 4.3–4.5. The case $M = N$ is quadratic variation. Put $q = (Z_1 + Z_2)/2$ and $v = (Z_1 - Z_2)/2$. Define B_+, B_-, starting at zero, by

$$dB_\pm = \frac{\sqrt{\sin Z_1}\, dB_1 \pm \sqrt{\sin Z_2}\, dB_2}{\sqrt{\sin Z_1 + \sin Z_2}}.$$

Each is standard Brownian motion by Lévy's characterization (Le Gall, Section 5.3.1): its quadratic variation is t. Their joint equations are

$$dq = \frac{\sqrt{6}}{2}\, dB_+ + 2\cot q\, dt, \qquad dv = \frac{\sqrt{6}}{2}\, dB_- - 2\tan v\, dt, \tag{5.2}$$

$$d\langle B_+, B_-\rangle_t = \cot q \tan v\, dt. \tag{5.3}$$

Thus B_+ and B_- need not be independent. These formulas specialize [11, (5.1) and the following equations, p. 31] to Zhan's parameter $\kappa = 6$.

Define a further real process V, starting at $V_0 = 0$, by

$$dV = -\frac{\cos Z_1 + \cos Z_2}{\sin Z_1 + \sin Z_2}\, dt = -\cot q\, dt. \tag{5.4}$$

This is the variable in [11, (4.3), p. 27, and the proof of Lemma 4.1, p. 31]. Define the angle Θ by

$$\Theta = V + \frac{q}{2}, \qquad d\Theta = \frac{\sqrt{6}}{4}\, dB_+, \qquad d\langle \Theta, q\rangle_t = \frac{3}{4}\, dt. \tag{5.5}$$

This gives $\mathbb{E}e^{2i(\Theta_t-\Theta_0)} = e^{-3t/4}$. The nonzero quadratic covariation records the dependence between Θ and q.

Set $z = \sin v/\sin q$, $\mathsf{X} = (0,\pi)\times(-1,1)$, and $X_t = (q_t, z_t)$. The inverse coordinates are $v = \arcsin(z\sin q)$, using values in $(-\pi/2,\pi/2)$, and $Z_1 = q+v$, $Z_2 = q-v$. For $x = (q,z) \in \mathsf{X}$, write $\mathbb{P}_{c4,x}$ for the law with $X_0 = x$, and $\mathbb{E}_{c4,x} = \mathbb{E}_{c4,q,z} = \mathbb{E}_{q,z}$ for its expectation.

Unless specified otherwise, $f : \mathsf{X} \to \mathbb{C}$ is bounded and Borel measurable.

The transition probabilities and their action on functions are

$$P_t(x,A) = \mathbb{P}_{c4,x}\{X_t \in A\}, \qquad P_t f(x) = \mathbb{E}_{c4,x} f(X_t) = \int f(y) P_t(x,dy).$$

Because the coefficients do not depend on time, the Markov property gives $P_0 f = f$ and $P_{s+t} f = P_s(P_t f)$ for $s,t \geq 0$.

For $f \in C_c^\infty(\mathsf{X})$, define the pointwise generator by $\mathcal{A}f(x) = \lim_{s\downarrow 0}(P_s f(x) - f(x))/s$. Itô's formula gives

$$\mathcal{A} = \frac{3}{4}\partial_q^2 + 2\cot q\,\partial_q + \frac{3}{4\sin^2 q}\left[(1-z^2)\partial_z^2 - \frac{8}{3}z\partial_z\right]. \tag{5.6}$$

Indeed $d\langle q,z\rangle = d\langle\Theta,z\rangle = 0$, the coefficient of dt in dz is $-2z/\sin^2 q$, and $d\langle z,z\rangle_t = 3(1-z^2)(2\sin^2 q)^{-1}dt$.

Let $dq\,dz$ be Lebesgue area measure and put $Z_0 = \int_{\mathsf{X}} \sin^{8/3} q(1-z^2)^{1/3}\,dq\,dz$. The probability measure

$$\pi_0(dq\,dz) = Z_0^{-1}\sin^{8/3} q(1-z^2)^{1/3}\,dq\,dz \tag{5.7}$$

is invariant: $\int P_t f\,d\pi_0 = \int f\,d\pi_0$ for every bounded Borel f and $t \geq 0$. This follows from [11, (5.12) and Lemma 5.2, pp. 33–34] under the coordinate change $(q,z) \mapsto (\cos q, z\sin q)$, whose area factor is $\sin^2 q$.

Define the second-angular kernel by

$$\mathsf{K}_t f(q,z) = \mathbb{E}_{c4,q,z}\left[e^{2i(\Theta_t-\Theta_0)} f(q_t,z_t)\right]. \tag{5.8}$$

For Borel A, put $\mathsf{K}_t(x,A) = \mathsf{K}_t \mathbf{1}_A(x)$. Then P_t and K_t are probability and finite complex Borel kernels, respectively.

For $s,t \geq 0$, conditioning at time s gives $\mathsf{K}_{s+t} = \mathsf{K}_s\mathsf{K}_t$. Its pointwise generator on the smooth compactly supported functions above is

$$\mathcal{A}_2 = \mathcal{A} + \frac{3i}{2}\partial_q - \frac{3}{4}. \tag{5.9}$$

The last term comes from the quadratic variation of Θ; the imaginary derivative comes from the quadratic covariation in (5.5). Equation (5.9) specifies a differential expression; its closed $L^2(\pi_0)$ realization and its identification with the semigroup generator are proved in subsection 5.2. Substituting $V_t = -\int_0^t \cot q_s\,ds$ into $\Theta = V + q/2$ gives

$$\mathsf{K}_t f(q,z) = e^{-iq}\mathbb{E}_{q,z}\left[e^{-2i\int_0^t \cot q_s\,ds} e^{iq_t} f(q_t,z_t)\right]. \tag{5.10}$$

In particular, $|\mathsf{K}_t f| \leq P_t|f|$. For $f(q,z) = \cos q$ and $q = \pi/2$, a direct Itô calculation gives $\mathsf{K}_t f = -3it/2 + o(t)$. In contrast, $P_t f = 0$, since the equation for q is unchanged by reflection $q \mapsto \pi - q$. Thus K_t is not $e^{-3t/4}P_t$.

5.2 Reduction to one variable

The bound $|\mathsf{K}_t f|^2 \le P_t|f|^2$ and invariance of π_0 give $\|\mathsf{K}_t f\|_{L^2(\pi_0)} \le \|f\|_{L^2(\pi_0)}$. Approximation by bounded functions therefore extends K_t uniquely to a contraction on $L^2(\pi_0)$. For bounded continuous f, path continuity gives $\mathsf{K}_t f(x) \to f(x)$ at every x, and dominated convergence gives convergence in $L^2(\pi_0)$. Such functions are dense in this space, so the contraction bound gives strong continuity for every $f \in L^2(\pi_0)$. Write $\mathcal{B}_2$ for this semigroup's generator: its domain consists of those f for which $(\mathsf{K}_t f - f)/t$ has an L^2 limit as $t \downarrow 0$, and $\mathcal{B}_2 f$ is that limit; see [18, Definition II.1.2, p. 49]. We construct its operator domain below.

Let $C_n^{5/6}$ be the degree-n Gegenbauer polynomial, $n = 0, 1, \ldots$, as in NIST DLMF, Table 18.3.1. These polynomials form an orthogonal basis of $L^2((-1,1),(1-z^2)^{1/3}dz)$; completeness follows from DLMF, Section 18.2(viii). By Table 18.8.1, the bracketed z-operator in (5.6) sends $C_n^{5/6}$ to $-n(n+5/3)C_n^{5/6}$. The nth Gegenbauer sector is the subspace of functions $f_n(q)C_n^{5/6}(z)$ with $f_n \in L^2((0,\pi), \sin^{8/3} q\, dq)$. Completeness and the product form of π_0 give the orthogonal decomposition into these sectors.

Set $\ell = 4/3$, $b = -i\ell$, and $L = \ell + n$. Define the multiplication operator $\mathscr{I}$ by

$$(\mathscr{I}\psi)(q) = e^{-iq} \sin^{-\ell} q\, \psi(q). \tag{5.11}$$

It is unitary from $L^2((0,\pi), dq)$ to the weighted q-space. Direct differentiation on the nth sector gives the identity of differential expressions

$$\mathscr{I}^{-1}(-\mathcal{A}_2)\mathscr{I} = \frac{3}{4}(H_{\ell+n} - \ell^2), \qquad H_L = -\partial_q^2 + L(L-1)\csc^2 q - 2b\cot q. \tag{5.12}$$

The displayed H_L is the trigonometric Rosen–Morse expression: [17, (28), p. 7] gives $H_L/2$ with parameter $a = L - 1$. In particular, (5.12) has not yet specified a boundary condition.

Let $\mathcal{V} = H_0^1(0,\pi)$ be the closure of $C_c^\infty(0,\pi)$ under the norm $(\int_0^\pi (|\psi|^2 + |\psi'|^2)\, dq)^{1/2}$. Here ψ' is the weak derivative, defined by $\int \psi\phi' = -\int \psi'\phi$ for every $\phi \in C_c^\infty(0,\pi)$. Inner products and norms without a measure subscript in the one-dimensional calculation use $L^2((0,\pi), dq)$. Put $c_L = L(L-1)$ and define

$$a_L(\psi) = \int_0^\pi (|\psi'|^2 + c_L \csc^2 q\, |\psi|^2)\, dq, \qquad \|\psi\|_{\mathcal{V}_L}^2 = a_L(\psi) + \|\psi\|_2^2,$$
$$\mathfrak{q}_L(\phi,\psi) = \int_0^\pi (\overline{\phi'}\psi' + c_L \csc^2 q\, \overline{\phi}\psi - 2b\cot q\, \overline{\phi}\psi)\, dq.$$

A form is closed when its domain is complete in its form norm. It is sectorial with vertex zero if its diagonal values lie in a sector $|\operatorname{Im} w| \le C \operatorname{Re} w$, with $\operatorname{Re} w \ge 0$; see [28, Chapter VI, Sections 1.2–1.3, pp. 310–314].

Proposition 5.1 (The closed sector operators)**.** *For every $L = \ell + n$, the form $\mathfrak{q}_L$ on $\mathcal{V}$ is densely defined, closed, and sectorial. Its associated operator, also denoted by H_L, has domain*

$$\operatorname{Dom}(H_L) = \left\{\psi \in \mathcal{V} : -\psi'' + c_L \csc^2 q\, \psi - 2b\cot q\, \psi \in L^2(0,\pi)\right\}, \tag{5.13}$$

where the complete differential expression is interpreted distributionally. It is characterized by $\mathfrak{q}_L(\phi,\psi) = \langle \phi, H_L\psi\rangle$ for every $\phi \in \mathcal{V}$ and $\psi \in \operatorname{Dom}(H_L)$. The operator is closed and maximal accretive, has compact resolvent, and satisfies

$$\|(H_L + 1)^{-1}\|_{2\to 2} \le \frac{1}{L^2 + 1}.$$

Here maximal accretivity means accretivity, $\operatorname{Re}\langle\psi, H_L\psi\rangle \ge 0$, together with surjectivity of $H_L + 1$. The numerical range lies in the common sector $|\operatorname{Im} w| \le 3 \operatorname{Re} w$; thus these are m-sectorial operators in the terminology of [28, Chapter V, Section 3.10]. The adjoint H_L^* is the realization (5.13) with b replaced by $\overline{b}$.

Proof. The form norm and coercivity. With $d(q) = \min(q, \pi - q)$, the Hardy inequality for convex domains [29, Theorem 2, p. 3], applied to $(0, \pi)$, and $\sin q \geq 2d(q)/\pi$ give

$$\int_0^\pi \frac{|\psi|^2}{d(q)^2}\, dq \leq 4\|\psi'\|_2^2, \qquad \|\psi'\|_2^2 \leq a_L(\psi) \leq (1 + \pi^2 c_L)\|\psi'\|_2^2.$$

Thus $\|\cdot\|_{\mathcal{V}_L}$ is equivalent to the H_0^1 norm for fixed L, and C_c^∞ is dense in this form norm.

For $\psi \in C_c^\infty$, integration by parts gives

$$a_L(\psi) = \|\psi' - L\cot q\, \psi\|_2^2 + L^2\|\psi\|_2^2 \geq L^2\|\psi\|_2^2. \tag{5.14}$$

Hardy's inequality makes multiplication by $\cot q$ continuous from $\mathcal{V}$ to L^2, so the identity extends to all of $\mathcal{V}$. Since $b = -i\ell$, $\operatorname{Re}\mathfrak{q}_L(\psi, \psi) = a_L(\psi)$. Also, for every $\eta > 0$,

$$2\ell|\cot q| \leq \eta c_L \csc^2 q + \frac{4}{\eta}, \qquad c_L \geq 4/9. \tag{5.15}$$

Indeed, use $|\cot q| \leq \csc q$ and $2xy \leq \eta x^2 + \eta^{-1}y^2$ with $x = \sqrt{c_L}\csc q$ and $y = \ell/\sqrt{c_L}$. The off-diagonal estimate needed below is

$$\left|2b\int_0^\pi \cot q\, \overline{\phi}\psi\, dq\right| \leq \frac{2\ell}{L\sqrt{c_L}} a_L(\phi)^{1/2} a_L(\psi)^{1/2} \leq 3a_L(\phi)^{1/2} a_L(\psi)^{1/2}.$$

It follows by Cauchy–Schwarz, $\|\cot q\, \phi\|_2 \leq a_L(\phi)^{1/2}/\sqrt{c_L}$, and (5.14). Consequently

$$\begin{aligned} &|\mathfrak{q}_L(\phi, \psi) + \langle\phi, \psi\rangle| \leq 4\|\phi\|_{\mathcal{V}_L}\|\psi\|_{\mathcal{V}_L}, \\ &\operatorname{Re}(\mathfrak{q}_L(\psi, \psi) + \|\psi\|_2^2) = \|\psi\|_{\mathcal{V}_L}^2, \qquad |\operatorname{Im}\mathfrak{q}_L(\psi, \psi)| \leq 3a_L(\psi). \end{aligned} \tag{5.16}$$

These estimates prove closedness and sectoriality with constants uniform in L.

The operator and its domain. The first representation theorem [28, Theorem VI.2.1, p. 322] supplies the associated closed m-sectorial operator. Its form characterization gives (5.13): testing against C_c^∞ gives the displayed distributional expression; conversely, if that expression is an L^2 function, integration against compactly supported test functions, followed by density in the form norm, gives the characterization for every $\phi \in \mathcal{V}$. Only the sum in (5.13) is required to be in L^2. For example, at $L = 4/3$ the second derivative and inverse-square term of a regular eigenfunction need not be individually in L^2.

The shifted weak equation

$$\mathfrak{q}_L(\phi, u) + \langle\phi, u\rangle = \langle\phi, g\rangle, \qquad \phi \in \mathcal{V},$$

has a unique solution for every $g \in L^2$, by the bounded coercive form in (5.16). Taking $\phi = u$ and real parts gives

$$(L^2 + 1)\|u\|_2^2 \leq \|u\|_{\mathcal{V}_L}^2 = \operatorname{Re}\langle u, g\rangle \leq \|u\|_2\|g\|_2.$$

This proves the resolvent estimate and gives a bound on u in $\mathcal{V}$ for bounded sets of data. The compact embedding $H_0^1(0, \pi) \hookrightarrow L^2(0, \pi)$ follows from [30, Theorem 8.8, (6), pp. 212–213], applied to real and imaginary parts. Thus $(H_L + 1)^{-1}$ is compact.

Finally, the adjoint form is obtained by replacing b by $\overline{b}$. The adjoint assertion follows from [28, Theorem VI.2.5, p. 323], including equality of the stated domains. □

On the nth sector define $\mathcal{A}_2^{(n)}$ by (5.12), with inputs $(\mathscr{I}\psi)C_n^{5/6}$ for $\psi \in \mathrm{Dom}(H_{\ell+n})$. Define the candidate full operator by the orthogonal sum

$$\mathrm{Dom}(\mathcal{A}_2) = \Big\{ f = \sum_{n\ge 0} f^{(n)} : f^{(n)} \in \mathrm{Dom}(\mathcal{A}_2^{(n)}), \quad \sum_{n\ge 0} \|\mathcal{A}_2^{(n)} f^{(n)}\|^2_{L^2(\pi_0)} < \infty \Big\}, \qquad \mathcal{A}_2 f = \sum_{n\ge 0} \mathcal{A}_2^{(n)} f^{(n)}. \tag{5.17}$$

The notation $f = \sum f^{(n)}$ here presupposes $f \in L^2(\pi_0)$. Each sector operator is closed, so componentwise passage to a graph limit proves that this sum is closed. Finite sums of sector functions for which $\mathscr{I}^{-1} f_n$ is smooth and compactly supported show that its domain is dense.

Proposition 5.2 (Identification with the angular expectation)**.** *The generator $\mathcal{B}_2$ of the probabilistic semigroup (5.8), equivalently the Feynman–Kac expectation (5.10), is exactly $\mathcal{A}_2$ with domain (5.17). This operator has compact resolvent.*

Proof. A fixed resolvent of the candidate operator. Put $\lambda_* = \frac{3}{4}(\ell^2+1) = 25/12$. On the nth sector,

$$(\lambda_* - \mathcal{A}_2^{(n)})^{-1} = \frac{4}{3}\mathscr{I}(H_{\ell+n}+1)^{-1}\mathscr{I}^{-1}, \qquad \|(\lambda_* - \mathcal{A}_2^{(n)})^{-1}\| \le \frac{4/3}{(\ell+n)^2+1} \le \lambda_*^{-1}. \tag{5.18}$$

These blocks therefore define a bounded operator on the orthogonal sum. If $u^{(n)}$ is the image of $f^{(n)}$ under the corresponding block, then $\mathcal{A}_2^{(n)} u^{(n)} = \lambda_* u^{(n)} - f^{(n)}$. Both terms on the right are square summable, so $u \in \mathrm{Dom}(\mathcal{A}_2)$ and $(\lambda_* - \mathcal{A}_2)u = f$. The same identity proves injectivity. Thus the block sum is the resolvent of the operator with the stated domain.

Cutoff resolvents converge in the form norm. For $0 < \varepsilon < \pi/2$, put $I_\varepsilon = (\varepsilon, \pi-\varepsilon)$ and identify $\mathcal{V}_\varepsilon = H_0^1(I_\varepsilon)$ with its zero extension in $\mathcal{V}$. Let H_L^ε be the operator of $\mathfrak{q}_L$ restricted to this space. For $g \in L^2(0,\pi)$ set

$$u = (H_L+1)^{-1} g, \qquad u_\varepsilon = (H_L^\varepsilon + 1)^{-1}(g|_{I_\varepsilon}),$$

extending u_ε by zero. Write $B_L(\phi,\psi) = \mathfrak{q}_L(\phi,\psi) + \langle \phi, \psi\rangle$. The two weak equations give $B_L(v, u-u_\varepsilon) = 0$ for every $v \in \mathcal{V}_\varepsilon$. For $e = u - u_\varepsilon$ and any such v, (5.16) therefore gives

$$\|e\|^2_{\mathcal{V}_L} = \mathrm{Re}\, B_L(e,e) = \mathrm{Re}\, B_L(u-v, e) \le 4\|u-v\|_{\mathcal{V}_L}\|e\|_{\mathcal{V}_L}.$$

Consequently

$$\|u - u_\varepsilon\|_{\mathcal{V}_L} \le 4 \inf_{v\in\mathcal{V}_\varepsilon} \|u-v\|_{\mathcal{V}_L} \longrightarrow 0. \tag{5.19}$$

The limit holds because every compactly supported smooth approximation to u belongs to all sufficiently large cutoff intervals, and such approximations are dense in the form norm by the Hardy estimate. The cutoff resolvents satisfy the same bound $(L^2+1)^{-1}$ as the full resolvent.

Stopped Itô identity on the cutoff interval. Let $\tau_\varepsilon = \inf\{t \ge 0 : q_t \notin I_\varepsilon\}$, with $\tau_\varepsilon = 0$ when the initial point is outside the interval. Define the killed family

$$\mathsf{K}_t^\varepsilon f(x) = \mathbb{E}_x\left[e^{2i(\Theta_t - \Theta_0)} f(X_t) \mathbf{1}_{\{t<\tau_\varepsilon\}} \right], \qquad \mathsf{R}_\varepsilon f = \int_0^\infty e^{-\lambda_* t} \mathsf{K}_t^\varepsilon f \, dt.$$

Its time-zero operator on the full space is the strip projection. The bounds $|\mathsf{K}_t^\varepsilon f|^2 \le P_t |f|^2$ imply $\|\mathsf{K}_t^\varepsilon\|_{2\to 2} \le 1$ and $\|\mathsf{R}_\varepsilon\|_{2\to 2} \le \lambda_*^{-1}$.

Fix n and first take $g \in C_c^\infty(I_\varepsilon)$. The weak Dirichlet solution u_ε above is smooth up to both ends of I_ε: its equation expresses u_ε'' in terms of smooth bounded coefficients, u_ε, and g, and one-dimensional regularity can be iterated. Put

$$F(q,z) = (Uu_\varepsilon)(q)C_n^{5/6}(z), \qquad \widehat{g}(q,z) = (Ug)(q)C_n^{5/6}(z)$$

on the strip, extending them by zero outside. On its interior, the differential identity (5.12) gives $(\lambda_* - \mathcal{A}_2)F = \frac{3}{4}\widehat{g}$. Use a C^2 continuation of the strip formula for F past the cutoff endpoints to apply Itô's product rule to $e^{-\lambda_* s + 2i(\Theta_s - \Theta_0)}F(X_s)$ up to $s = t \wedge \tau_\varepsilon$. Only values in the closed strip enter this calculation; the zero extension is used in the Hilbert-space formulas. All q coefficients and derivatives of Uu_ε are bounded on the closed cutoff interval, and the Gegenbauer polynomial and its derivatives are bounded on $[-1,1]$. The covariance coefficients from (5.2), (5.5), and (5.6) are bounded there as well. Thus the stopped stochastic integral is square integrable on each bounded time interval and has mean zero. The reference process stays in X, so the cutoff in q suffices.

At τ_ε the function F is zero by the Dirichlet condition. Taking expectations yields, for x in the strip,

$$F(x) = e^{-\lambda_* t}\mathsf{K}_t^\varepsilon F(x) + \frac{3}{4}\int_0^t e^{-\lambda_* s}\mathsf{K}_s^\varepsilon \widehat{g}(x)\, ds.$$

The first term tends to zero as $t \to \infty$ because F is bounded and $\lambda_* > 0$. Hence

$$\mathsf{R}_\varepsilon\big((Ug)C_n^{5/6}\big) = \frac{4}{3}\mathscr{I}(H_L^\varepsilon + 1)^{-1}(g|_{I_\varepsilon})\, C_n^{5/6}, \qquad L = \ell + n, \tag{5.20}$$

with the zero-extension convention. The L^2 bounds on both sides extend this identity to every $g \in L^2(0,\pi)$, by first approximating its restriction to the strip by $C_c^\infty(I_\varepsilon)$. This establishes the sector resolvent identity directly from the stochastic law.

Removal of the cutoffs and equality of domains. Every continuous path q_s, $0 \le s \le t$, stays in a compact subinterval of $(0,\pi)$, because the reference diffusion never reaches the endpoints. Thus $\tau_\varepsilon \to \infty$ almost surely as $\varepsilon \downarrow 0$. For bounded f, dominated convergence gives $\mathsf{K}_t^\varepsilon f \to \mathsf{K}_t f$ pointwise and in $L^2(\pi_0)$. The uniform contraction bounds extend this convergence to every $f \in L^2(\pi_0)$. Dominated convergence for the norm-valued Laplace integrals then gives

$$\mathsf{R}_\varepsilon f \longrightarrow \int_0^\infty e^{-\lambda_* t}\mathsf{K}_t f\, dt = (\lambda_* - \mathcal{B}_2)^{-1} f;$$

the last identity is [18, Theorem II.1.10, p. 55]. On a single sector, (5.19) and (5.20) identify this limit with (5.18). The two bounded resolvents therefore agree on finite sector sums, a dense subspace, and hence on all of $L^2(\pi_0)$. Their ranges are their respective operator domains. Equality of the resolvents gives equality of these domains and, on their common range, equality of the operators $\mathcal{B}_2 = \mathcal{A}_2$.

Finally, each resolvent block in (5.18) is compact, and its norm tends to zero as $n \to \infty$. The full resolvent is a norm limit of finite sums of these compact blocks, and is therefore compact. □

5.3 Computing the eigenvalues

We now use the boundary condition determined by the form to justify the first-order factorization. Define the differential expressions

$$A_L^- = \partial_q - L\cot q + b/L, \qquad A_L^+ = -\partial_q - L\cot q + b/L. \tag{5.21}$$

The superscripts distinguish the two expressions; with imaginary b they do not denote a Hilbert-space adjoint pair. Multiplication on the interior gives

$$H_L = A_L^+ A_L^- + E_0(L), \qquad H_{L+1} = A_L^- A_L^+ + E_0(L), \tag{5.22}$$

$$E_0(L) = L^2 - \frac{b^2}{L^2} = L^2 + \frac{\ell^2}{L^2}, \qquad \psi_{L,0}(q) = \sin^L q\, e^{-bq/L}. \tag{5.23}$$

Every solution of $A_L^-\psi = 0$ is a constant multiple of $\psi_{L,0}$. This function belongs to $\mathcal{V}$, satisfies $H_L\psi_{L,0} = E_0(L)\psi_{L,0}$ in the interior, and therefore belongs to $\mathrm{Dom}(H_L)$ by (5.13). The factorization method is described in [17, (7)–(8), p. 3]; the domain arguments needed for the present imaginary parameter follow next.

Proposition 5.3 (Spectrum of the angular generator)**.** *The spectrum of the closed operator $-\mathcal{A}_2$ from Proposition 5.2 consists exactly of*

$$\lambda_N = \frac{3}{4}\left[(N+4/3)^2 - \frac{16}{9} + \frac{16}{9(N+4/3)^2}\right], \qquad N = 0, 1, \dots. \tag{5.24}$$

In particular,

$$\lambda_0 = \frac{3}{4}, \qquad \lambda_1 = \frac{587}{196}, \qquad \lambda_1 - \lambda_0 = \frac{110}{49}. \tag{5.25}$$

Proof. Endpoint behavior and preservation of the domains. Let $H_L\psi = E\psi$ with $\psi \in \mathrm{Dom}(H_L)$ nonzero. Interior regularity makes ψ a classical solution. At zero the indicial exponents are L and $1-L$. Their difference $2L-1 = 5/3 + 2n$ is nonintegral. The Frobenius theorem therefore gives two independent convergent power series with these leading powers; see DLMF, Section 2.7(i), (2.7.3)–(2.7.5). The branch q^{1-L} has infinite form energy, since its derivative squared has order q^{-2L}. Its coefficient must vanish. At $L = 4/3$ this excluded branch is nevertheless in L^2, which is why the form boundary condition in (5.13) is essential. The same argument holds at π.

We call the surviving behaviors q^L and $(\pi - q)^L$ regular. At zero the regular expansion is

$$\psi(q) = q^L(c_0 + c_1 q + c_2 q^2 + O(q^3)), \qquad c_1 = -\frac{b}{L}c_0, \qquad c_2 = \frac{L(L-1)/3 + 2b^2/L - E}{2(2L+1)}c_0, \tag{5.26}$$

with $c_0 \neq 0$. The coefficient equations follow by substituting $\csc^2 q = q^{-2} + 1/3 + O(q^2)$ and $\cot q = q^{-1} - q/3 + O(q^3)$ into the differential equation. Convergence of the Frobenius series also justifies differentiation of the remainder. At π, use $s = \pi - q$ and replace b by $-b$ in these coefficients.

It follows that

$$A_L^-\psi(q) = \frac{E_0(L) - E}{2L+1}c_0 q^{L+1} + O(q^{L+2}), \qquad (A_L^-\psi)'(q) = O(q^L).$$

The analogous bounds hold at π. Thus $A_L^-\psi \in \mathcal{V}$. The differential identities (5.22) imply $H_{L+1}(A_L^-\psi) = E(A_L^-\psi)$ in the interior, so its complete differential expression is in L^2. By (5.13), a nonzero image lies in $\mathrm{Dom}(H_{L+1})$ and is an eigenfunction with the same eigenvalue.

Conversely, if $\eta \in \mathrm{Dom}(H_{L+1})$ is an eigenfunction, its regular expansion gives

$$A_L^+\eta(q) = -(2L+1)d_0 q^L + O(q^{L+1}), \qquad d_0 \neq 0.$$

At π the leading coefficient has the opposite sign and is again nonzero. The derivatives have order q^{L-1} and $(\pi - q)^{L-1}$, so $A_L^+\eta \in \mathcal{V}$ and is nonzero. The partner equation gives its L^2

differential expression; hence it belongs to $\mathrm{Dom}(H_L)$. These checks justify the factorizations as mappings of eigenfunctions with the stated domains.

Exhaustion of the sector spectrum. Apply A_L^- successively to a nonzero eigenfunction. If the chain never terminates, (5.14) forces its unchanged eigenvalue to satisfy $\operatorname{Re} E \geq (L+j)^2$ for every $j \geq 0$, a contradiction. At its terminal stage, the function is a multiple of $\psi_{L+j,0}$, and

$$E = E_j(L) = (L+j)^2 + \frac{\ell^2}{(L+j)^2}, \qquad j = 0, 1, \dots. \tag{5.27}$$

Conversely, applying $A_L^+ \cdots A_{L+j-1}^+$ to $\psi_{L+j,0}$ produces a nonzero regular eigenfunction in $\mathrm{Dom}(H_L)$ at this value; the empty product is used when $j = 0$. Compact resolvent implies that every finite spectral value is an eigenvalue of finite algebraic multiplicity [18, Corollary IV.1.19, p. 248]. Thus (5.27) is the full sector spectrum. For real b, its classical counterpart is [17, (41), p. 9]; the argument above proves the formula for $b = -4i/3$ with the required realization.

The full spectrum. The full operator has compact resolvent by Proposition 5.2. Each of its eigenfunctions has a nonzero component in some Gegenbauer sector, which is an eigenfunction of that sector operator. Conversely, a sector eigenfunction is in the full domain. Applying (5.12) to (5.27) and putting $N = n + j$ gives exactly (5.24). The function $x \mapsto x^2 + \ell^2/x^2$ is strictly increasing for $x \geq \ell$, since $\ell > 1$. This orders the values and gives (5.25). □

5.4 The limiting measure and a uniform bound

For a finite complex Borel measure μ on X, write $\mu(f) = \int f \, d\mu$ and

$$\|\mu\|_{\mathrm{var}} = \sup_{\|f\|_\infty \leq 1} |\mu(f)|,$$

with the supremum over bounded Borel functions. Let $\mathbf{1}$ be the constant function one. If $I_p = \int_0^\pi \sin^p q \, dq$, integration by parts gives $I_{p+2}/I_p = (p+1)/(p+2)$. Symmetry makes the integral of $\sin(2q)\sin^p q$ zero. Since $\cos(2q) = 1 - 2\sin^2 q$, taking $p = 8/3$ gives

$$\frac{\int_0^\pi e^{2iq} \sin^{8/3} q \, dq}{\int_0^\pi \sin^{8/3} q \, dq} = -\frac{4}{7}. \tag{5.28}$$

Define

$$\pi_2(dq\, dz) = -\frac{7}{4} e^{2iq} \pi_0(dq\, dz), \qquad \pi_2(1) = 1, \qquad \pi_2(\mathcal{A}_2 f) = -\frac{3}{4}\pi_2(f) \quad (f \in \mathrm{Dom}(\mathcal{A}_2)). \tag{5.29}$$

To prove the last assertion on the stated operator domain, observe that the function $\chi(q) = \sin^\ell q \, e^{-iq}$ is the regular ground eigenfunction for the adjoint realization H_ℓ^*, with eigenvalue $\ell^2 + 1$, by Proposition 5.1 and (5.23) with b replaced by $\bar{b}$. It belongs to the adjoint domain because it is in $\mathcal{V}$ and its differential expression equals $(\ell^2+1)\chi \in L^2$. Under $\mathscr{I}$ it becomes e^{-2iq}. Consequently

$$g_* = -\frac{7}{4} e^{-2iq} \in \mathrm{Dom}(\mathcal{A}_2^*), \qquad \mathcal{A}_2^* g_* = -\frac{3}{4} g_*, \qquad \pi_2(f) = \langle g_*, f \rangle_{L^2(\pi_0)}.$$

Only its zeroth sector is nonzero, so the adjoint identity holds on the entire domain (5.17), including infinite sector sums. It also gives $\pi_2(\mathsf{K}_t f) = e^{-3t/4}\pi_2(f)$ by differentiating first for $f \in \mathrm{Dom}(\mathcal{A}_2)$ and then using density.

The principal spectral projection. For $n = j = 0$, $\mathscr{I}\psi_{\ell,0} = \mathbf{1}$, so $\mathbf{1} \in \mathrm{Dom}(\mathcal{A}_2)$ and $\mathcal{A}_2\mathbf{1} = -\frac{3}{4}\mathbf{1}$. The ordering in Proposition 5.3 and uniqueness, up to scale, of the regular

Frobenius solution at one endpoint show that its eigenspace is exactly $\mathbb{C}\mathbf{1}$. There is no $g \in \mathrm{Dom}(\mathcal{A}_2)$ with $(\mathcal{A}_2 + 3/4)g = \mathbf{1}$, because applying π_2 would give $0 = 1$. Every longer nontrivial generalized-eigenvector chain would produce this equation at its penultimate step after rescaling. Thus $-3/4$ is algebraically simple; see [18, Section IV.1.17, pp. 246–247] for these notions.

Put $\Pi f = \pi_2(f)\mathbf{1}$. The identities just proved show that $\Pi^2 = \Pi$ and that it commutes with K_t and its generator on the generator domain. It is the Riesz spectral projection for $-3/4$: the spectral projection has range $\mathbb{C}\mathbf{1}$ by algebraic simplicity, while the left eigenfunctional π_2, normalized by $\pi_2(1) = 1$, annihilates its invariant spectral complement. More explicitly, applying (5.29) to $u = (\zeta - \mathcal{A}_2)^{-1} f$ gives

$$\pi_2((\zeta - \mathcal{A}_2)^{-1} f) = (\zeta + 3/4)^{-1} \pi_2(f).$$

If P is the Riesz projection, integrating around $-3/4$ gives $\pi_2(Pf) = \pi_2(f)$. Since $\operatorname{ran} P = \mathbb{C}\mathbf{1}$ and $\pi_2(1) = 1$, this proves $P = \Pi$; see [18, formula (1.7), p. 244, and Proposition IV.1.16, p. 245]. Finally, $\|\pi_2\|_{\mathrm{var}} = 7/4$ directly from its density in (5.29).

Analyticity on the full orthogonal sum. The argument must be uniform over the sectors to obtain analyticity on their orthogonal sum. Let $\widehat{C}_n$ be $C_n^{5/6}$ normalized to have norm one in $L^2((-1,1),(1-z^2)^{1/3}dz)$. The unitary identification of $\mathscr{H} = \bigoplus_{n\geq 0} L^2(0,\pi)$ with $L^2(\pi_0)$ is

$$(\mathscr{I}_{\oplus}\psi)(q,z) = Z_0^{1/2} \sum_{n\geq 0} (\mathscr{I}\psi_n)(q)\widehat{C}_n(z).$$

Orthogonality and (5.7) show that $\|\mathscr{I}_{\oplus}\psi\|^2_{L^2(\pi_0)} = \sum_n \|\psi_n\|_2^2$. On this sum define

$$\mathscr{V} = \left\{ \psi = (\psi_n) : \psi_n \in \mathcal{V}, \quad \sum_{n\geq 0} \|\psi_n\|^2_{\mathcal{V}_{\ell+n}} < \infty \right\}, \qquad \mathfrak{q}(\phi,\psi) = \sum_{n\geq 0} \mathfrak{q}_{\ell+n}(\phi_n,\psi_n).$$

The bound (5.16) makes the series absolutely convergent. The form domain is complete in the summed form norm, and finite sector sums show that it is dense. Moreover, $|\operatorname{Im}\mathfrak{q}(\psi,\psi)| \leq 3\operatorname{Re}\mathfrak{q}(\psi,\psi)$. Thus $\mathfrak{q}$ is a densely defined closed sectorial form with vertex zero.

Its associated operator is exactly $H = \bigoplus H_{\ell+n}$ with square-summable component actions. Indeed, tests supported in one sector give the component domains and actions for any vector in the associated operator domain. Conversely, for a vector in the direct-sum graph domain,

$$\sum_{n\geq 0} a_{\ell+n}(\psi_n) = \operatorname{Re}\sum_{n\geq 0}\langle \psi_n, H_{\ell+n}\psi_n\rangle \leq \left(\sum_n \|\psi_n\|_2^2\right)^{1/2} \left(\sum_n \|H_{\ell+n}\psi_n\|_2^2\right)^{1/2} < \infty.$$

This places it in $\mathscr{V}$, and passage from finite-sector tests to all of $\mathscr{V}$ proves the form identity. Under the same unitary identification, $\mathcal{A}_2 = \frac{3}{4}(\ell^2 - H)$, with equality of domains.

Kato's holomorphic-semigroup theorem for m-sectorial operators [28, Theorem IX.1.24, p. 492] gives

$$\|e^{-\zeta H}\| \leq 1 \quad (\zeta \neq 0,\ |\arg\zeta| < \arctan(1/3)).$$

After the fixed shift and scaling, this is an analytic extension of K_t, with bound $\|\mathsf{K}_\zeta\| \leq \exp(\frac{3}{4}\ell^2 \operatorname{Re}\zeta)$ in that sector. Here analytic means holomorphic in operator norm away from zero, with the semigroup property and strong continuity at zero in each smaller sector, as in [18, Definition II.4.5, p. 101]. Its generator agrees with the probabilistic generator by Proposition 5.2, so uniqueness of the generated semigroup identifies this extension on positive real times. Analyticity implies norm continuity for positive times, and the compact resolvent proved above then gives compactness of K_t for every $t > 0$ by [18, Theorem II.4.29, p. 119].

From the spectral gap to an operator-norm bound. Let $Y = \ker \pi_2$, the closed invariant complement of $\mathbb{C}\mathbf{1}$. The restricted generator has spectrum $\{-\lambda_N : N \geq 1\}$. Spectral mapping for analytic semigroups [18, Corollary IV.3.12, p. 281] therefore gives

$$r(e^{3/4}\mathsf{K}_1|_Y) = e^{-110/49},$$

where r is the spectral radius. For any $0 < \gamma < 110/49$, the spectral-radius formula $r(T) = \lim_{k\to\infty} \|T^k\|^{1/k}$ gives a constant M_γ with $\|(e^{3/4}\mathsf{K}_1|_Y)^k\| \leq M_\gamma e^{-\gamma k}$ for all integers $k \geq 0$. Write $t = k + s$ with $0 \leq s < 1$. Since $\|\mathsf{K}_s\| \leq 1$, multiplication by $e^{3s/4}\mathsf{K}_s$ and by $I - \Pi$ gives

$$\|e^{3t/4}\mathsf{K}_t - \mathbf{1}\pi_2\|_{L^2(\pi_0)\to L^2(\pi_0)} \leq C_\gamma e^{-\gamma t}, \qquad t \geq 0. \tag{5.30}$$

This is also the remainder estimate of [18, Corollary V.3.2(iii), pp. 330–331], with loss $110/49 - \gamma$. The strict inequality on γ absorbs polynomial factors from higher generalized eigenspaces.

Zhan's bound [11, Lemmas 5.1–5.2, pp. 33–34] gives $P_1(x, A) \leq C\pi_0(A)$ for every Borel $A \subset \mathsf{X}$ and every $x \in \mathsf{X}$. Consequently,

$$|\mathsf{K}_1 f(x)| \leq P_1|f|(x) \leq C\|f\|_{L^2(\pi_0)}. \tag{5.31}$$

This defines $\mathsf{K}_1 f(x)$ for every $f \in L^2(\pi_0)$, independently of its values on sets of π_0-measure zero.

Theorem 5.4 (Uniform angular-kernel convergence)**.** *For the probabilistic kernel K_t of (5.8) and the measure π_2 of (5.29), every $0 < \gamma < 110/49$ admits $C_\gamma < \infty$ such that*

$$\sup_{x\in\mathsf{X}} \|e^{3t/4}\mathsf{K}_t(x,\cdot) - \pi_2\|_{\mathrm{var}} \leq C_\gamma e^{-\gamma t}, \qquad t \geq 1. \tag{5.32}$$

Proof. For a bounded Borel f and $t \geq 1$, write

$$(e^{3t/4}\mathsf{K}_t - \Pi)f = e^{3/4}\mathsf{K}_1(e^{3(t-1)/4}\mathsf{K}_{t-1} - \Pi)f.$$

The identity uses $\mathsf{K}_1\mathbf{1} = e^{-3/4}\mathbf{1}$, which follows from (5.5) at every starting point. The smoothing estimate (5.31) turns the L^2 estimate (5.30) into a bound uniform over all $x \in \mathsf{X}$. Since $\|f\|_{L^2(\pi_0)} \leq \|f\|_\infty$, taking the supremum over $\|f\|_\infty \leq 1$ proves (5.32). □

5.5 The angular average with V

For V from (5.4), define

$$\mathsf{K}_t^V f(x) = \mathbb{E}_{c4,x}[e^{2i(V_t - V_0)} f(X_t)], \qquad X_t = (q_t, z_t). \tag{5.33}$$

Its measure notation is $\mathsf{K}_t^V(x, A) = \mathsf{K}_t^V \mathbf{1}_A(x)$. Define φ_0 and a complex measure ν by

$$\varphi_0(q, z) = e^{iq}, \qquad \nu(f) = -\frac{7}{4}\int_{\mathsf{X}} e^{iq} f(q, z)\, \pi_0(dq\, dz), \qquad \nu(\varphi_0) = 1. \tag{5.34}$$

Write $(\varphi_0\nu)f = \varphi_0\nu(f)$ for the resulting rank-one projection. Since $\Theta = V + q/2$, for every $0 < \gamma < 110/49$ there is $C_\gamma < \infty$ such that

$$\begin{aligned} \mathsf{K}_t^V f(q, z) &= e^{iq}\mathsf{K}_t(e^{-iq} f)(q, z), \\ \sup_{x\in\mathsf{X}} \|e^{3t/4}\mathsf{K}_t^V(x,\cdot) - \varphi_0(x)\nu\|_{\mathrm{var}} &\leq C_\gamma e^{-\gamma t}, \qquad t \geq 1. \end{aligned} \tag{5.35}$$

The estimate follows from (5.32), since multiplication by $e^{\pm iq}$ preserves absolute values. The same identity gives $\mathsf{K}_t^V \varphi_0 = e^{-3t/4}\varphi_0$, and the defining expectation gives $\|\mathsf{K}_t^V f\|_\infty \leq \|f\|_\infty$.

6 Crossing probabilities with an elliptical hole

We study the change in a crossing probability when the ellipse of subsection 4.3 is forced closed.

6.1 A crossing removed by a closed set

Use the lattice model of subsection 4.1. A lattice Jordan domain is a finite union of cells whose boundary is a simple closed curve. Divide its boundary into four successive arcs A, B, C, D. Fix the boundary cells on A, C to be open and those on B, D to be closed. An open crossing from A to C is an open path between these arcs inside the domain. Let Cross be the event that such a crossing exists.

Let W_B, W_D be the closed clusters containing the cells on B, D. For a connected set K of interior cells, write $W \rightsquigarrow K$ if the cluster W contains or is adjacent to a cell of K. Let Cross^K be the crossing event after forcing K closed in the same sample. Write $\mathbb{P}$ for the law of the random cell colors, and put $p_{\mathrm{cr}} = \mathbb{P}(\mathsf{Cross}) > 0$, $p_{\mathrm{cr}}^K = \mathbb{P}(\mathsf{Cross}^K)$.

Lemma 6.1 (Lost crossing)**.** *With these definitions,*

$$\mathbf{1}_{\mathsf{Cross}\setminus\mathsf{Cross}^K} = \mathbf{1}_{\mathsf{Cross}}\mathbf{1}_{\{W_B \rightsquigarrow K\}}\mathbf{1}_{\{W_D \rightsquigarrow K\}}. \tag{6.1}$$

Define the conditional contact probability by

$$H(K) = \frac{\mathbb{P}(\mathsf{Cross} \cap \{W_B \rightsquigarrow K,\ W_D \rightsquigarrow K\})}{p_{\mathrm{cr}}}.$$

Then

$$p_{\mathrm{cr}}^K = p_{\mathrm{cr}}[1 - H(K)]. \tag{6.2}$$

Proof. On Cross, the two closed boundary clusters are distinct. If closing K removes the open crossing, the crossing alternative of subsection 4.1 gives a closed B–D path. This path must visit K. Its portions before the first and after the last visit give the two original closed-cluster contacts. Conversely, forcing the connected set K closed joins these contacts into a closed B–D path, which prevents Cross^K. This proves (6.1). Since $\mathsf{Cross}^K \subset \mathsf{Cross}$, taking expectations gives (6.2). □

An interface follows cell edges separating open and closed cells. On Cross, the two interfaces starting at boundary color changes pair the endpoints of B and the endpoints of D.

A *quad* consists of a domain Ω conformally equivalent to $\mathbb{D} = B(0, 1)$ and four distinct marked boundary points in cyclic order. Denote the successive arcs by A, B, C, D, with A, C open and B, D closed. If the boundary is not a simple closed curve, the marks and arcs mean points and arcs of the unit circle in a conformal disk coordinate. These are the boundary prime ends used in [11, Section 2.1, pp. 6–8].

Use chordal SLE_6 as defined in [11, Section 2.1, pp. 6–8]. A global two-SLE_6 pair (γ_1, γ_2) with a prescribed pairing satisfies the following conditional law: given either curve, the other is chordal SLE_6 in the component of Ω minus that curve whose boundary contains its assigned endpoints. For the lattice limits, first take a bounded quad whose boundary is a simple closed curve. Use the marked lattice approximations of [13, Definition 4.1] as $a \downarrow 0$. Conditional on Cross, the two interfaces converge in law to this pair, with the pairing specified above. This is the $m = 2$ case of Lemma 7.3, whose percolation convergence proof uses [14, Proposition 6.2 and Theorems 5.8 and 5.10]. Curves are compared uniformly after increasing changes of their parameters, as in [13, Section 1.2].

Write $\mathbb{P}_\Omega$ for the law of this pair and $p_{\mathrm{cr},\Omega} > 0$ for the limit of the unconditioned crossing probabilities. The latter is given by Cardy's formula [16, preprint (1.1)–(1.2), p. 2]. For a general quad, define $\mathbb{P}_\Omega$ by conformal transport of the corresponding disk curves, with boundary points interpreted in the prime-end closure, and define $p_{\mathrm{cr},\Omega}$ by the disk crossing probability. A *target* is a compact set $K \subset \Omega$. A curve hits K when the corresponding disk curve hits its image under the disk map; this agrees with intersection of the physical trace with K. Only the map on the interior is needed for this definition. Define

$$H_\Omega(K) = \mathbb{P}_\Omega\{\gamma_1 \cap K \neq \varnothing, \gamma_2 \cap K \neq \varnothing\}.$$

Continue the lattice-limit argument in a bounded quad with simple closed boundary. Fix $\epsilon > 0$. For the targets below, impose all the geometric assumptions of subsection 4.1, with fixed constants η, M and scale $\rho = \epsilon$. In particular, the targets are strictly convex Jordan bodies with the stated size, tubular-neighborhood, and analytic-boundary-chart bounds. For sufficiently small real s, let $K^{(s)}$ be the body enclosed by

$$\partial K^{(s)} = \{y + s n_K(y) : y \in \partial K\},$$

where n_K is the outward unit normal from subsection 4.1. Positive s moves the boundary outward; negative s moves it inward. A *continuity offset* is a value s for which

$$\lim_{\varepsilon \to 0} H_\Omega(K^{(s+\varepsilon)}) = H_\Omega(K^{(s)}).$$

The function of s is nondecreasing and bounded by one, so its discontinuities are at most countable.

At mesh a, apply the lattice identity to the inner-cell approximation K^a of subsection 4.1. There is a constant $c_{\mathrm{lat}} > 0$, depending only on the cell geometry, with the following property. On Cross, the two-contact event contains the event that both interfaces hit $K^{(-c_{\mathrm{lat}}a)}$ and is contained in the event that both hit $K^{(c_{\mathrm{lat}}a)}$. Conditional interface convergence therefore gives (6.2) at each fixed continuity offset as $a \downarrow 0$.

To remove this restriction, let K' be a second target in the same class. Choose a disk as in subsection 4.1 around K, K', with its closure inside Ω, and fix the colors outside it. The crossing indicator is a function of the frontier record and these exterior colors. Apply (4.1), average over the exterior colors, and divide by $p_{\mathrm{cr},\Omega}$. For normal displacement at most $\delta \le c\epsilon$, this gives a finite constant C_ϵ such that

$$|H_\Omega(K') - H_\Omega(K)| \le C_\epsilon \frac{\delta}{p_{\mathrm{cr},\Omega}}. \tag{6.3}$$

The bound first holds at continuity offsets. Approximating from both sides by such offsets makes the two limits agree. Thus it holds for all targets in the specified class. The constant depends on the fixed disk, ϵ, and the bounds in subsection 4.1, uniformly in the four boundary marks. The forced-crossing probabilities consequently converge. Writing $p_{\mathrm{cr}}^K = \lim_{a\downarrow 0} \mathbb{P}(\mathsf{Cross}^{K^a})$, equation (6.2) holds in the continuum with $p_{\mathrm{cr}} = p_{\mathrm{cr},\Omega}$ and $H = H_\Omega$.

6.2 The two-curve exploration and the angular integral

Orient each curve from its initial point a_j to its terminal point b_j. First take $b_1 = 1$ and $b_2 = -1$ in $\mathbb{D}$. The oriented pairs are

$$(a_1 \longrightarrow b_1;\ a_2 \longrightarrow b_2) = (e^{iZ_1} \longrightarrow 1;\ -e^{iZ_2} \longrightarrow -1), \qquad 0 < Z_1, Z_2 < \pi.$$

The counterclockwise arcs from b_j to a_j are closed; the remaining two arcs are open. Put $q = (Z_1 + Z_2)/2$, $v = (Z_1 - Z_2)/2$, and $z = \sin v / \sin q$, as in Section 5. Write $x = (q, z) \in \mathsf{X}$, and let $p_{\mathrm{cr}}(x), H_x, \mathbb{P}_{2,x}, \mathbb{E}_{2,x}$ denote the crossing probability, target-hitting function, two-curve law, and its expectation in this quad.

An exposed initial segment runs from a curve's initial point to its last revealed point, called its *tip*. Its *filled hull* is the closure of the segment together with all components of $\mathbb{D}$ minus that segment which do not contain 0. This includes its initial boundary point. Two exposed segments are admissible when their filled hulls are disjoint, avoid 0, and contain neither terminal point. Let D be the component containing 0 after these hulls are removed. Its radial conformal map is the map $g : D \to \mathbb{D}$ with $g(0) = 0$ and $g'(0) > 0$.

The *balanced parametrization* grows both initial segments continuously and increasingly, writing D_t, g_t for the resulting domain and map, so that

$$g_t'(0) = e^t, \qquad g_t(b_2) = -g_t(b_1).$$

Thus $t = \log g_t'(0)$ is the radial capacity, and the terminal images remain opposite. Define T, the *lifetime of this exploration*, by taking $[0, T)$ to be the maximal interval on which an admissible choice satisfying these conditions exists. The admissibility definition and the construction of this clock are in [11, Section 3.1, p. 14, and Section 4, pp. 25–26].

Write $g_t(b_1) = e^{iV_t}$, with V_t continuous and $V_0 = 0$. The two tip images have arguments $W_1(t), W_2(t)$, chosen so that

$$Z_1(t) = W_1(t) - V_t \in (0, \pi), \qquad Z_2(t) = W_2(t) - (V_t - \pi) \in (0, \pi).$$

Apply the same formulas for q, v, z to obtain $X_t = (q_t, z_t)$.

On the reference probability space $\mathbb{P}_{c4,x}$ of Section 5, use the diffusion (5.1) and V_t from (5.4). Set

$$W_1 = V + Z_1, \qquad W_2 = V - \pi + Z_2, \qquad \lambda_j = \frac{\sin Z_j}{\sin Z_1 + \sin Z_2}, \quad j = 1, 2.$$

Define its maps by the radial Loewner equation

$$\partial_t g_t(\zeta) = g_t(\zeta) \sum_{j=1}^{2} \lambda_j(t) \frac{e^{iW_j(t)} + g_t(\zeta)}{e^{iW_j(t)} - g_t(\zeta)}, \qquad g_0(\zeta) = \zeta.$$

The domain D_t consists of points whose solutions remain in $\mathbb{D}$ up to time t. The weights λ_j are the two contributions to the joint capacity rate, and their sum is one. This constructs the reference maps for every $t \geq 0$. It is Zhan's reference evolution in the balanced clock; see [11, p. 6, (3.7), p. 15, and (4.2)–(4.3), pp. 26–27].

Let ${}_2F_1$ denote the Gauss hypergeometric function defined in NIST DLMF, (15.2.1). Put

$$R = \frac{\cos(Z_1/2)\cos(Z_2/2)}{\cos v} \in (0, 1),$$

and define

$$\mathfrak{g}(x) = \mathfrak{g}(Z_1, Z_2) = \frac{[\sin(Z_1/2)\sin(Z_2/2)]^{1/3}\cos^{2/3} v}{{}_2F_1(1/3, 2/3; 4/3; R)}. \tag{6.4}$$

For every bounded measurable function Ψ of the maps and angles up to a fixed time t,

$$\mathbb{E}_{2,x}[\mathbf{1}_{\{t<T\}}\Psi] = e^{-5t/4}\mathfrak{g}(x)\mathbb{E}_{c4,x}\left[\frac{\Psi}{\mathfrak{g}(X_t)}\right]. \tag{6.5}$$

This identity specifies the change from the reference law to the two-curve law before T. It is the expectation form of the formula preceding Zhan's Lemma 5.4 [11, p. 35].

A holomorphic map is *normalized* at 0 when it fixes 0 and has derivative one there. Write $B_s = B(0,s)$ and define

$$F_t(\zeta) = e^{-iV_t} g_t(e^{-t+iV_t}\zeta), \qquad F_t(0) = 0, \quad F_t'(0) = 1. \tag{6.6}$$

Koebe's quarter theorem says that a univalent map f on $\mathbb{D}$, with $f(0) = 0$, has $B(0, |f'(0)|/4)$ in its image. Applied to g_t^{-1}, it gives $B_{e^{-t}/4} \subset D_t$; hence F_t is univalent on $B_{1/4}$. This is the use of that theorem in [11, proof of Theorem 1.1, p. 38]. Normalized univalent maps have uniform bounds on each smaller disk.[2] In particular, every derivative of F_t is uniformly bounded on each fixed B_s with $s < 1/4$.

Fix $e \in [e_-, e_+] \subset (0,1)$ as in subsection 4.3 and choose a sufficiently small $\epsilon > 0$. For any injective holomorphic map F on a neighborhood of $\overline{B}_{(1+e_+)\epsilon}$ that maps this disk into $\mathbb{D}$, define

$$\mathfrak{h}_{\epsilon,e}(x, F) = \frac{1}{2\pi e} \int_0^{2\pi} e^{2i\theta} H_x(F(K_{\epsilon,e,\theta}(0)))\, d\theta. \tag{6.7}$$

The ellipses $K_{r,e,\phi}(w)$ are those defined in subsection 4.3. The bound $0 \le H_x \le 1$ gives $|\mathfrak{h}_{\epsilon,e}| \le e_-^{-1}$. For $0 < r \le \epsilon$, define the positive second angular coefficient to mean

$$\mathcal{H}^+_{r,e}(x) = \frac{1}{2\pi e} \int_0^{2\pi} e^{2i\phi} H_x(K_{r,e,\phi}(0))\, d\phi.$$

Replacing $e^{2i\phi}$ by $e^{-2i\phi}$ gives its complex conjugate, called the negative coefficient.

Set $t = \log(\epsilon/r)$ and require $(1+e_+)\epsilon < 1/4$. If both curves eventually hit the ellipse, then $t < T$ and their exposed segments avoid it. The containing disk has radius $(1+e_+)r < e^{-t}/4$; see [11, proof of Theorem 1.1, p. 38]. Conditional on the exposed segments, the remaining curves have the two-SLE$_6$ law in D_t, from their respective current tips to b_1, b_2. This is the domain Markov property in [11, Lemma 6.1, pp. 36–37]. Mapping by $e^{-iV_t} g_t$ and setting $\theta = \phi - V_t$ therefore gives

$$\mathcal{H}^+_{r,e}(x) = \mathbb{E}_{2,x}\left[\mathbf{1}_{\{t<T\}} e^{2iV_t} \mathfrak{h}_{\epsilon,e}(X_t, F_t)\right], \tag{6.8}$$

because $e^{-iV_t} g_t(K_{r,e,\phi}(0)) = F_t(K_{\epsilon,e,\phi-V_t}(0))$.

6.3 Comparison of the normalized maps

Let $\mathrm{id}(\zeta) = \zeta$ be the identity map. For f analytic on a neighborhood of the closed disk $\overline{B}_s$, define

$$\|f\|_{C^k(\overline{B}_s)} = \max_{0\le j\le k} \sup_{\zeta\in\overline{B}_s} |f^{(j)}(\zeta)|, \qquad k = 0, 1, \ldots,$$

where $f^{(j)}$ is its jth derivative and $f^{(0)} = f$. For $s, u \ge 0$ under the reference law, the map $g_{s,s+u} = g_{s+u} \circ g_s^{-1} : g_s(D_{s+u}) \to \mathbb{D}$ describes the additional growth after time s. Define

$$F^{\mathrm{new}}_u(\zeta) = e^{-iV_{s+u}} g_{s,s+u}(e^{-u+iV_{s+u}}\zeta).$$

Thus F^{new}_u uses the same future angles and capacity weights as F_{s+u}, but starts with the identity map at time s.

[2] See C. T. McMullen, *Complex Dynamics and Renormalization*, Section 2.4, Theorem 2.7, pp. 15–16; author's text. Bounds on derivatives follow from Cauchy's integral formula for derivatives, NIST DLMF, (1.9.31).

Lemma 6.2 (Comparison of normalized maps)**.** *There is a fixed $r_* \in (0,1/4)$ and, for every integer $k \geq 0$, a finite constant C_k such that, for every $s, u \geq 0$,*

$$\|F_{s+u} - F_u^{\mathrm{new}}\|_{C^k(\overline{B}_{r_*})} \leq C_k e^{-u}. \tag{6.9}$$

The constants are independent of s, the initial angles, and the reference path.

Proof. Substitution in $g_{s+u} = g_{s,s+u} \circ g_s$ gives

$$F_{s+u}(\zeta) = F_u^{\mathrm{new}}\left(e^{u-i(V_{s+u}-V_s)} F_s(e^{-u+i(V_{s+u}-V_s)}\zeta)\right). \tag{6.10}$$

Set $a_n = F_s^{(n)}(0)/n!$ for $n \geq 2$. The Taylor expansion is $F_s(\zeta) = \zeta + \sum_{n\geq 2} a_n \zeta^n$. The inner argument becomes

$$\zeta + \sum_{n\geq 2} a_n e^{-(n-1)u+i(n-1)(V_{s+u}-V_s)}\zeta^n. \tag{6.11}$$

For fixed $R \in (0,1/4)$, Cauchy's formula and the uniform bounds above give $|a_n| \leq C_R R^{-n}$. On a sufficiently small fixed disk, the last sum is therefore at most $C|\zeta|^2 e^{-u}$. Choose a slightly larger disk where the derivatives of F_u^{new} remain bounded. Integrating its first derivative along the segment between the two arguments proves (6.9) for $k = 0$. Cauchy's derivative formula on this larger disk proves the claim for each k. □

Decrease ϵ so that $(1+e_+)\epsilon < r_*$. For the normalized univalent maps just considered, $F(\epsilon\zeta)/\epsilon = \zeta + O(\epsilon)$ with uniform derivative bounds. Hence their images of the ellipses satisfy the geometric assumptions of subsection 4.1 with common constants. In particular, the bounds on the tubular neighborhoods and boundary charts remain uniform. Lemma 6.2 changes these image boundaries by normal displacement at most $C\epsilon e^{-u}$.

6.4 An integral bound

Put $c_C = \Gamma(2/3)/[\Gamma(1/3)\Gamma(4/3)]$. Cardy's formula gives

$$p_{\mathrm{cr}}(x) = c_C R^{1/3} {}_2F_1(1/3, 2/3; 4/3; R). \tag{6.12}$$

This follows by substituting the cyclic endpoints $(e^{iZ_1}, -1, -e^{iZ_2}, 1)$ into [16, preprint (1.1)–(1.2), p. 2]. Multiplication by (6.4) gives

$$p_{\mathrm{cr}}(x)\mathfrak{g}(x) = c_C 2^{-2/3}[\sin Z_1 \sin Z_2 \cos v]^{1/3}. \tag{6.13}$$

The invariant probability measure π_0 and its normalization Z_0 were defined in (5.7). Put $c_\pi = (2Z_0)^{-1}$. Changing variables from (q,z) to (Z_1, Z_2) gives

$$\pi_0(dZ_1\, dZ_2) = c_\pi \sin q \cos v (\sin Z_1 \sin Z_2)^{1/3}\, dZ_1\, dZ_2. \tag{6.14}$$

Indeed, $dq\, dz = \cos v\, (2\sin q)^{-1} dZ_1\, dZ_2$. Thus, for a finite positive constant C,

$$\frac{\pi_0(dZ_1\, dZ_2)}{p_{\mathrm{cr}}(x)\mathfrak{g}(x)} = C \sin q \cos^{2/3} v\, dZ_1\, dZ_2, \qquad \int_{\mathsf{X}} \frac{d\pi_0}{p_{\mathrm{cr}}\mathfrak{g}} < \infty. \tag{6.15}$$

The factor $\sin q \cos^{2/3} v$ is bounded on $(0,\pi)^2$.

Define $\varphi(x,F) = \mathfrak{h}_{\epsilon,e}(x,F)/\mathfrak{g}(x)$ and $m(x) = 1/[p_{\mathrm{cr}}(x)\mathfrak{g}(x)]$. Since $p_{\mathrm{cr}} \leq 1$, we have $\mathfrak{g}^{-1} \leq m$. Equation (6.3), the map comparison, and (6.15) give

$$\begin{aligned} |\varphi(x,F)| &\leq Cm(x), \\ |\varphi(x,F_{s+u}) - \varphi(x,F_u^{\mathrm{new}})| &\leq C_\epsilon e^{-u} m(x), \qquad m \in L^1(\pi_0). \end{aligned} \tag{6.16}$$

6.5 Iteration and the angular limit

Define

$$u_t(x) = \mathbb{E}_{c4,x}[e^{2iV_t}\varphi(X_t, F_t)], \qquad F_0 = \mathrm{id}. \tag{6.17}$$

The transition bound $P_1(x, dy) \le C\pi_0(dy)$ proved in Section 5, together with invariance of π_0, gives

$$\sup_x \mathbb{E}_{c4,x} m(X_t) \le C \int_{\mathsf{X}} m \, d\pi_0 < \infty, \qquad t \ge 1.$$

Hence u_t is uniformly bounded for $t \ge 1$. Condition at a time $s \in [0, 1]$. Replace F_{s+t} by F_t^{new} while keeping X_s and the subsequent reference evolution. The expectation with this replacement is $\mathsf{K}_s^V u_t$, where K_s^V is defined in (5.33). Define $d_{s,t} = u_{s+t} - \mathsf{K}_s^V u_t$. Equation (6.16) and the displayed expectation bound give

$$\begin{aligned} u_{s+t} &= \mathsf{K}_s^V u_t + d_{s,t}, \\ \|d_{s,t}\|_\infty &\le C_\epsilon e^{-t}, \qquad t \ge 1, \quad 0 \le s \le 1. \end{aligned} \tag{6.18}$$

The norm is the supremum over $x \in \mathsf{X}$, as in Section 5.

For integers $n \ge 1$, put $f_n = u_n$ and $d_n = d_{1,n}$. Iteration gives

$$f_n = \mathsf{K}_{n-1}^V f_1 + \sum_{j=1}^{n-1} \mathsf{K}_{n-1-j}^V d_j. \tag{6.19}$$

Using $\varphi_0(q, z) = e^{iq}$ and the measure ν from (5.34), define

$$\mathfrak{a}_{\epsilon,e} = e^{3/4}\nu(f_1) + \sum_{j \ge 1} e^{3(j+1)/4}\nu(d_j). \tag{6.20}$$

The Cardy calculation below evaluates $\mathfrak{a}_{\epsilon,e}$ in (6.22). Constants denoted by C, C_ϵ, or C_γ are finite positive bounds and may change between estimates. The series converges absolutely because $\|d_j\|_\infty \le Ce^{-j}$ leaves the summable factor $e^{-j/4}$.

Choose $1/4 < \gamma < 110/49$. Equation (5.35) bounds the difference between $\mathsf{K}_\tau^V f$ and $e^{-3\tau/4}\varphi_0\nu(f)$ by $C_\gamma e^{-(3/4+\gamma)\tau}\|f\|_\infty$ for $\tau \ge 1$. Enlarge the constant to include $\tau = 0$. Apply these bounds in (6.19) and multiply by $e^{3n/4}$. The sum of the errors is at most

$$C \sum_{j=1}^{n-1} e^{-\gamma(n-1-j)} e^{-j/4} \le C' e^{-n/4}. \tag{6.21}$$

The error from the initial term and the tail of (6.20) satisfy the same bound. For $t = n + s$, with $n \ge 1$ an integer and $0 \le s < 1$, use (6.18). Here $\mathsf{K}_s^V \varphi_0 = e^{-3s/4}\varphi_0$ and $\|\mathsf{K}_s^V f\|_\infty \le \|f\|_\infty$ by (5.33)–(5.35).

Proposition 6.3 (Limit and normalization of the angular coefficient)**.** *The amplitude in* (6.20) *is*

$$\mathfrak{a}_{\epsilon,e} = \frac{4}{3}\epsilon^2. \tag{6.22}$$

For $t \ge 1$,

$$\sup_{x \in \mathsf{X}} |e^{3t/4}u_t(x) - e^{iq}\mathfrak{a}_{\epsilon,e}| \le C_\epsilon e^{-t/4}. \tag{6.23}$$

With $L_e(x) = \frac{4}{3}\mathfrak{g}(x)e^{iq}$, independent of e, as $r \downarrow 0$ through arbitrary positive values,

$$\mathcal{H}_{r,e}^+(x) = r^2 L_e(x) + O_\epsilon(\mathfrak{g}(x) r^{9/4}). \tag{6.24}$$

For the ratio $b \in [1/2, 1]$ between two radii and $0 < r \le \epsilon \exp(-1)$,

$$|\mathcal{H}^+_{r,e}(x) - b^{-2}\mathcal{H}^+_{br,e}(x)| \le C\mathfrak{g}(x)r^{9/4}. \tag{6.25}$$

The bounds are uniform in x and $e \in [e_-, e_+]$; constants may depend on the fixed ϵ, e_-, e_+.

Proof. The preceding iteration proves (6.23) for the series (6.20). Initially set $L_e(x) = \epsilon^{-2}\mathfrak{g}(x)e^{iq}\mathfrak{a}_{\epsilon,e}$. Equations (6.5), (6.8), and (6.17) give $\mathcal{H}^+_{r,e} = e^{-5t/4}\mathfrak{g}(x)u_t(x)$. Substitution of $t = \log(\epsilon/r)$ gives (6.24) with this coefficient. The terms proportional to r^2 cancel at the two radii because $b^{-2}(br)^2 = r^2$. The remaining bounds give (6.25). The limit $L_e = \lim_{r\downarrow 0} r^{-2}\mathcal{H}^+_{r,e}$ is independent of the auxiliary ϵ. Equation (6.2) multiplies the angular coefficient by $-p_{\mathrm{cr}}(x)$ for the crossing-probability change $p^K_{\mathrm{cr}} - p_{\mathrm{cr}}$. Its negative coefficient is obtained by complex conjugation.

Cardy calibration. We identify the coefficient by applying conformal maps to the crossing event. Throughout this calculation, $\boldsymbol{Z} = (Z_1, Z_2)$ ranges over a compact subset of $(0, \pi)^2$, enlarged slightly when a change of variables is made.

First, the crossing probability in an analytic annulus, with the two prescribed open outer arcs and the remaining boundary closed, is invariant under a conformal bijection extending across both boundary components with nonzero derivative. We verify the boundary conditions needed to apply Camia–Conijn–Kiss's restricted-configuration theorem [23, Definition 4.4 and Theorem 9.5, pp. 16 and 39–40]. Trim η-neighborhoods of the four marks and use interior boundary collars of width δ. In the remaining region, connections and their dual separators have buffered quad witnesses, as in Camia–Conijn–Kiss's Definition 4.5. A countable dense quad family and finite truncation give finite Boolean approximations; Schramm–Smirnov's Corollary 5.2 [10, p. 37] gives their joint lattice limits.

Passage to the boundary follows from the side and endpoint perturbation estimates in Schramm–Smirnov's Appendix A [10, Lemmas A.1–A.2, pp. 37–43]. More explicitly, away from the marks a discrepancy produces two branches of the crossing and a dual separating branch, or the color-reversed configuration, in a boundary half-annulus. These are three sampled arms. Covering the smooth boundary by $O(\delta^{-1})$ boxes and using (4.4) gives $O_\eta(\delta)$. Near a mark, the discrepancy requires an arm through random cells avoiding the already wired adjacent arc; the endpoint argument in Schramm–Smirnov's Lemma A.1(1), or the corner argument in their Lemma A.2, makes its probability tend to zero with η. Thus the upper and lower crossing approximations agree after the mesh limit, then $\delta \downarrow 0$ and $\eta \downarrow 0$. The map and its inverse are bi-Lipschitz in boundary charts, so their transported collars have the same vanishing errors. Camia–Conijn–Kiss's Theorem 9.5 now gives the asserted fixed-hole invariance.

Put $\xi = er^2e^{2i\phi}$. The inverse Joukowski map

$$\psi_\xi(z) = \frac{z + \sqrt{z^2 - 4\xi}}{2} = z - \frac{\xi}{z} + O(|\xi|^2)$$

uses the square-root branch asymptotic to z at infinity. It maps the exterior of $K_{r,e,\phi}(0)$ onto the exterior of $\overline{B}_r$; the expansion and its derivatives are uniform near $\partial\mathbb{D}$. Let Ω_ξ be the bounded domain enclosed by $\psi_\xi(\partial\mathbb{D})$, and normalize $\chi_\xi : \mathbb{D} \to \Omega_\xi$ by $\chi_\xi(0) = 0$, $\chi'_\xi(0) > 0$. Then

$$\chi_\xi(z) = z - \overline{\xi}z^3 + O(|\xi|^2), \qquad \chi_\xi^{-1}(\zeta) = \zeta + \overline{\xi}\zeta^3 + O(|\xi|^2|\zeta|). \tag{6.26}$$

The first expansion holds in $C^3(\overline{\mathbb{D}})$; the second holds on a fixed interior disk, with the corresponding boundary expansion on $\partial\Omega_\xi$. To verify them, write $\chi_\xi(z) = z(1 + a_\xi(z))$, with

$a_\xi(0)$ real. On $|z|=1$ its boundary equation is

$$\left|1+a_\xi(z)+\frac{\xi z^{-2}}{1+a_\xi(z)}\right|^2=1.$$

At $(a,\xi)=(0,0)$ the linearized equation is $2\operatorname{Re} a+2\operatorname{Re}(\xi z^{-2})=0$. The real-part map is an isomorphism from analytic boundary functions with real constant coefficient to real boundary functions, as seen by comparing Fourier coefficients. The implicit-function theorem in $H^s(\partial\mathbb{D})$, $s>9/2$, therefore gives $a_\xi(z)=-\bar\xi z^2+O(|\xi|^2)$ in C^3. The derivative of $z(1+a_\xi(z))$ is close to one, so this map is univalent; the boundary equation identifies its image with Ω_ξ. Inversion gives (6.26), with the extra factor $|\zeta|$ because the remainder vanishes at zero. Central symmetry and uniqueness make χ_ξ odd.

Let $\beta_\xi=\arg[(\chi_\xi^{-1}\circ\psi_\xi)(1)]$, chosen near zero, and set $\mathcal{F}_\xi=e^{-i\beta_\xi}\chi_\xi^{-1}\circ\psi_\xi$. This maps the outer circle onto itself and fixes $1,-1$. Its image hole is $\widetilde{K}_\xi=e^{-i\beta_\xi}\chi_\xi^{-1}(\overline{B}_r)$. Equation (6.26) bounds the normal displacement of its boundary from ∂B_r by $C(|\xi|r^3+|\xi|^2r)=O(r^5)$, with uniform rescaled C^2 shape bounds. Write $\mathcal{F}_\xi(e^{i\theta})=e^{i\vartheta_\xi(\theta)}$ and $\boldsymbol{Z}_\xi=(\vartheta_\xi(Z_1),\vartheta_\xi(Z_2))$. Since $\beta_\xi=-2\operatorname{Im}\xi+O(|\xi|^2)$,

$$\vartheta_\xi(\theta)=\theta+2er^2\{\sin(2\theta-2\phi)+\sin(2\phi)\}+O(r^4) \tag{6.27}$$

in C^2, uniformly in e,ϕ. Define $p_r^\circ(\boldsymbol{Z})$ as the crossing probability with the closed circular hole $\overline{B}_r$. Fixed-hole invariance and (4.1), completed against the crossing indicator outside a fixed disk $B(0,d)\Subset\mathbb{D}$, give

$$p_{\mathrm{cr}}^{K_{r,e,\phi}}(\boldsymbol{Z})=p_r^\circ(\boldsymbol{Z}_\xi)+O\big(r^4\alpha_4(Cr,d)\big).$$

To remove the circular-hole contribution, put $\mathcal{E}_r=p_r^\circ-p_{\mathrm{cr}}$. Equation (4.6) gives $\|\mathcal{E}_r\|_\infty\le C\alpha_4(Cr,d)$ on the enlarged compact set of marks. For $\zeta\in C_c^\infty((0,\pi)^2)$, transfer $\boldsymbol{Z}\mapsto\boldsymbol{Z}_\xi$ to the test function and its Jacobian. Equation (6.27) implies that the transported test differs from ζ by at most $C|\xi|\|\zeta\|_{C^1}$ in L^1, and hence

$$\left|\int\zeta(\boldsymbol{Z})[\mathcal{E}_r(\boldsymbol{Z}_\xi)-\mathcal{E}_r(\boldsymbol{Z})]\,d\boldsymbol{Z}\right|\le C|\xi|\alpha_4(Cr,d)\|\zeta\|_{C^1}.$$

The unshifted term is independent of ϕ. Its second angular coefficient is zero, and the shifted contribution divided by er^2 tends to zero. This argument differentiates only the test. Taylor expansion of the explicit Cardy function and (6.27) therefore give, in distributions in $\boldsymbol{Z}$,

$$\lim_{r\downarrow0}\frac{1}{2\pi er^2}\int_0^{2\pi}e^{2i\phi}(p_{\mathrm{cr}}^{K_{r,e,\phi}}-p_{\mathrm{cr}})\,d\phi=-i\sum_{j=1}^{2}(e^{2iZ_j}-1)\partial_{Z_j}p_{\mathrm{cr}}.$$

The asymptotic already proved identifies the same limit locally uniformly as $-p_{\mathrm{cr}}L_e$, by (6.2). Thus

$$L_e=\frac{i}{p_{\mathrm{cr}}}\sum_{j=1}^{2}(e^{2iZ_j}-1)\partial_{Z_j}p_{\mathrm{cr}}. \tag{6.28}$$

For the final calculation, write $p_{\mathrm{cr}}=\mathcal{C}(R)$ as in (6.12). The incomplete-beta representation of Cardy's formula gives

$$\mathcal{C}'(R)=\frac{c_C}{3}[R(1-R)]^{-2/3};$$

see DLMF (8.17.1) and (8.17.7). Direct differentiation of $R=(\cos q+\cos v)/(2\cos v)$ gives

$$\partial_{Z_1}R=-\frac{\sin Z_2}{4\cos^2 v},\qquad\partial_{Z_2}R=-\frac{\sin Z_1}{4\cos^2 v},\qquad R(1-R)=\frac{\sin Z_1\sin Z_2}{4\cos^2 v}.$$

Consequently

$$i\sum_{j=1}^{2}(e^{2iZ_j}-1)\partial_{Z_j}p_{\mathrm{cr}}=\mathcal{C}'(R)\frac{\sin Z_1\sin Z_2}{\cos v}e^{iq}=\frac{4}{3}p_{\mathrm{cr}}\mathfrak{g}\,e^{iq},$$

where the last equality uses (6.13). This proves (6.22) and $L_e=(4/3)\mathfrak{g}e^{iq}$ for every allowed e. The estimates above were needed only on compact sets of marks to identify the coefficient; the iteration supplies the stated bounds uniformly on all of X. □

The exponent in (6.24) is the sum of the four-arm exponent 5/4 and the spin-two angular decay 3/4. Its value two agrees with the bulk spin-two four-leg dimension in [27, p. 4]; see subsection 2.5. Proposition 6.3 supplies the uniform asymptotic and the quantitative defect bound needed for completion to arbitrary frontier records.

6.6 Four arbitrary boundary points

Let Ω be a quad as defined in subsection 6.1. Label its marks a_1,b_1,a_2,b_2 clockwise, with curves $\gamma_j:a_j\to b_j$, $j=1,2$. For $w\in\Omega$, let $S=\inf_{y\in\partial\Omega}|w-y|$ be its distance to the boundary. Fix $e\in[e_-,e_+]$ and $b\in[1/2,1]$. Recall that $H_\Omega(K)$ is the probability that both curves of this prescribed two-SLE$_6$ pair hit K, under the law $\mathbb{P}_\Omega$ defined in subsection 6.1. For the ellipses of (4.7), whenever they lie inside Ω, define the *second angular defect* by

$$\mathcal{A}^{\Omega}_{r,b}(w)=\frac{1}{2\pi e}\int_0^{2\pi}e^{-2i\phi}\big[H_\Omega(K_{r,e,\phi}(w))-b^{-2}H_\Omega(K_{br,e,\phi}(w))\big]\,d\phi.$$

The two terms use the same center, shape parameter, orientation, and two-curve law. The parameter e is fixed and suppressed in the notation. The multiplier b^{-2} cancels a contribution proportional to the squared radius; dividing $\mathcal{A}^{\Omega}_{r,b}$ by r^2 gives the difference of the quadratically normalized coefficients. For the corresponding crossing-probability change, (6.2) gives the defect $-p_{\mathrm{cr},\Omega}\mathcal{A}^{\Omega}_{r,b}$.

Choose the conformal map $f:\Omega\to\mathbb{D}$ with $f(w)=0$ and $f'(w)>0$. Define the *conformal radius* by $\mathfrak{r}=1/f'(w)$. Since $|f|<1$ on $B(w,S)$, Cauchy's derivative formula gives $f'(w)\le 1/S$. Koebe's quarter theorem applied to $f^{-1}-w$ gives $\mathfrak{r}/4\le S$. Hence $S\le\mathfrak{r}\le 4S$. Put $\xi_j=f(a_j)$, $\eta_j=f(b_j)$, and

$$\chi=\frac{|\xi_1-\eta_2||\xi_2-\eta_1|}{|\xi_1-\xi_2||\eta_1-\eta_2|}\in(0,1),$$
$$\mathfrak{g}_{\mathbb{D}}=\frac{(|\xi_1-\eta_1||\xi_2-\eta_2|)^{1/3}(|\xi_1-\xi_2||\eta_1-\eta_2|)^{2/3}}{4\,{}_2F_1(1/3,2/3;4/3;\chi)}.$$

Define $\mathfrak{g}_\Omega(w)=\mathfrak{r}^{-5/4}\mathfrak{g}_{\mathbb{D}}$, called the two-curve Green function in this normalization. For the disk with terminal points $1,-1$, $\mathfrak{g}_{\mathbb{D}}$ is exactly (6.4). These formulas are [11, (3.35), p. 25, and Theorem 1.1, p. 2]. That theorem also gives a universal $C_*>0$ such that

$$\mathbb{P}_\Omega\{\gamma_1,\gamma_2\text{ both hit }B(w,\rho)\}=C_*\mathfrak{g}_\Omega(w)\rho^{5/4}[1+O((\rho/S)^{11/15})]$$

as $\rho/S\downarrow 0$, with the error bound independent of the boundary marks.

Lemma 6.4 (Angular difference in a quad)**.** *For the second angular defect of subsection 6.6 and the Green function just defined,*

$$|\mathcal{A}^{\Omega}_{r,b}(w)|\le C\mathfrak{g}_\Omega(w)\frac{r^{9/4}}{S},\qquad 0<r<cS.\tag{6.29}$$

For a length $R > 0$ with $R \le S < 2R$, a fixed small $c_0 > 0$ can be chosen so that

$$|\mathcal{A}^{\Omega}_{r,b}(w)| \le C(r/R)^{9/4}\mathbb{P}_{\Omega}\{\gamma_1, \gamma_2 \text{ both hit } B(w, c_0R)\}, \qquad 0 < r < cR. \tag{6.30}$$

The constants depend only on the fixed interval $[e_-, e_+]$, uniformly in the four boundary marks. The conclusions apply to either noncrossing pairing, with the Green function for that pairing. They also apply almost surely to the conditional two-curve components of Lemma 7.3; neither boundary smoothness nor a positive lower bound on the separation of their prime ends is required.

Proof. 1. Uniformity under a normalized analytic change of the target. First keep the terminal points $1, -1$. Fix $a \in (0, 1/4)$ and let J be univalent on B_a, with $J(0) = 0$ and $J'(0) = 1$. Write

$$\mathcal{H}^{\pm}_{r,e,J}(x) = \frac{1}{2\pi e}\int_0^{2\pi} e^{\pm 2i\phi} H_x(J(K_{r,e,\phi}(0)))\, d\phi.$$

The same J is used for every angle and both radii. We show that, for sufficiently small r,

$$\left|\mathcal{H}^{\pm}_{r,e,J}(x) - b^{-2}\mathcal{H}^{\pm}_{br,e,J}(x)\right| \le C_a\mathfrak{g}(x)r^{9/4}, \tag{6.31}$$

uniformly over this entire class of J, all $x \in \mathsf{X}$, and the specified e, b.

The bounds for normalized univalent maps recalled in subsection 6.2, applied to $J(a\zeta)/a$, and Cauchy's formula give $J(z) = z + O_a(|z|^2)$, $J'(z) = 1 + O_a(|z|)$, and $J''(z) = O_a(1)$ on a fixed smaller disk. They also bound every higher derivative there. Consequently

$$J_{t,V}(\zeta) := e^{t-iV}J(e^{-t+iV}\zeta) = \zeta + O_a(e^{-t}|\zeta|^2)$$

has the corresponding first- and second-derivative errors $O_a(e^{-t}|\zeta|)$ and $O_a(e^{-t})$, uniformly in V and $t \ge 1$. On a smaller fixed disk, $J_{t,V}$ takes values in $B_{1/4}$, so $F_t \circ J_{t,V}$ is defined and univalent. The uniform bounds for F_t apply to this composition as well.

We now check the geometric hypotheses needed to apply (6.3). A boundary parametrization of the ellipse is $z(\alpha) = \epsilon e^{i\phi}(e^{i\alpha} + ee^{-i\alpha})$. It satisfies

$$|z'(\alpha)| \ge \epsilon(1 - e_+), \qquad \operatorname{Im}(\overline{z'(\alpha)}z''(\alpha)) = \epsilon^2(1 - e^2).$$

For either map F_t or $F_t \circ J_{t,V}$, the derivative on this target is $1 + O_a(\epsilon)$ and the second derivative is $O_a(1)$. The curvature numerator of the image boundary is therefore $\epsilon^2(1-e^2)(1+O_a(\epsilon)) + O_a(\epsilon^3) > c\epsilon^2$ when ϵ is sufficiently small. After rescaling by ϵ, these boundaries are uniformly close, with all required analytic-chart derivatives, to the fixed compact family of ellipses. Thus they have the common size, strict-convexity, and tubular-neighborhood bounds of subsection 4.1. Their parametrizations differ in $C^2(\alpha)$ by at most $C_a\epsilon^2e^{-t}$. Projection in the common tubular neighborhood expresses one boundary as a normal graph over the other, with displacement of at most the same order. Equation (6.3) is consequently applicable with constants independent of the angles and boundary marks.

Decrease the fixed ϵ once more so that, when $t = \log(\epsilon/r) \ge 1$,

$$J(K_{r,e,\phi}(0)) \subset B_{e^{-t}/4}$$

for every allowed J, e, ϕ. This follows from $|J(z)| \le C_a|z|$ on the smaller disk and $C_a(1+e_+)\epsilon < 1/4$. The survival and avoidance argument preceding (6.8) now applies to these targets. Substituting $\theta = \phi - V_t$ gives the exact identity

$$\mathcal{H}^{+}_{r,e,J}(x) = \mathbb{E}_{2,x}\left[\mathbf{1}_{\{t<T\}}e^{2iV_t}\mathfrak{h}_{\epsilon,e}(X_t, F_t \circ J_{t,V_t})\right].$$

The exploration is unchanged from the case of the undistorted ellipse. The normal-displacement estimate gives

$$\frac{|\mathfrak{h}_{\epsilon,e}(X_t, F_t \circ J_{t,V_t}) - \mathfrak{h}_{\epsilon,e}(X_t, F_t)|}{\mathfrak{g}(X_t)} \le C_{a,\epsilon} e^{-t} m(X_t), \qquad m = (p_{\mathrm{cr}}\mathfrak{g})^{-1}.$$

Although $p_{\mathrm{cr}}(x)$ can tend to zero, (6.15) and the transition bound used in subsection 6.5 give $\sup_x \mathbb{E}_{c4,x} m(X_t) \le C$ for $t \ge 1$. Apply (6.5) with this integrable weight to obtain

$$|\mathcal{H}^+_{r,e,J}(x) - \mathcal{H}^+_{r,e}(x)| \le C_{a,\epsilon}\mathfrak{g}(x) e^{-9t/4} \le C_a \mathfrak{g}(x) r^{9/4}. \tag{6.32}$$

The chosen ϵ depends only on a, e_-, e_+. Proposition 6.3 therefore yields $\mathcal{H}^+_{r,e,J} = r^2 L_e + O_a(\mathfrak{g} r^{9/4})$ with the same L_e for every J. Since each hitting probability is real, the negative coefficient is the complex conjugate. Applying these estimates at r and br, with the same J, proves (6.31).

2. The bounded preliminary exploration for arbitrary disk marks. Denote the four disk marks by $y = (\xi_1, \eta_1, \xi_2, \eta_2)$ in clockwise order, and choose continuous argument lifts $W_1 > V_1 > W_2 > V_2 > W_1 - 2\pi$. Write $\varpi_s = V_1(s) - V_2(s)$ for the terminal angle gap during the preliminary exploration, with $\varpi_0 = V_1 - V_2$. If $\varpi_0 < \pi$, grow curve 2 alone, with radial capacity s and normalized map $g_s'(0) = e^s$. Its radial lifetime ends when the curve is completed or when 0 is disconnected from any of the required marked prime ends η_2, ξ_1, η_1, whichever occurs first, as in [11, proof of Theorem 1.1, p. 37]. Stop at the first time $\varpi_s = \pi$ before that lifetime, or at the lifetime if no such time exists. Call the resulting time σ, and call the first alternative E. The time σ is a stopping time for the exposed curve, and E belongs to its stopped sigma-field.

Before σ, the radial Loewner equation for the two terminal images gives

$$\frac{d\varpi_s}{ds} = \cot\frac{V_1(s) - W_2(s)}{2} + \cot\frac{W_2(s) - V_2(s)}{2} \ge 2\cot\frac{\varpi_s}{4}.$$

For the inequality, the two positive arguments have sum $\varpi_s/2 < \pi/2$; their sine product is at most $\sin^2(\varpi_s/4)$, and their cotangent sum is the sine of their sum divided by that product. It follows that $\frac{d}{ds}\log\cos(\varpi_s/4) \le -1/2$. Thus the opposite-terminal level is reached, or the lifetime ends, by

$$\sigma \le 2\log\frac{\cos(\varpi_0/4)}{\cos(\pi/4)} \le \log 2. \tag{6.33}$$

If $\varpi_0 > \pi$, grow curve 1 alone and apply the same calculation to $2\pi - \varpi_s$. If $\varpi_0 = \pi$, take $\sigma = 0$ and E certain. This proves the bound used in [11, pp. 39–40], uniformly in all four marks.

By Koebe's quarter theorem, the exposed hull avoids $B_{1/8}$ up to σ, since the remaining domain has conformal radius $e^{-s} \ge 1/2$. On E^c, at least one of the two full curves avoids this ball. Indeed, if the exposed curve finishes, its entire trace is already outside the ball. Otherwise, when the lifetime ends, the component containing the protected ball no longer carries all the required marked prime ends. The two assigned endpoints of the unexposed curve belong to one remaining component, and its trace stays in the closure of that component. If this component does not contain 0, the unexposed curve avoids the ball. If it does, the missing terminal belongs to the exposed curve, whose remaining part stays in its own terminal component and also avoids the ball. These component assignments are those of the two-SLE domain Markov property [11, Lemma 6.1, pp. 36–37]; they give the failure-case conclusion needed from the argument on p. 39. Thus E^c contributes zero to joint hitting of any target contained in $B_{1/8}$.

On E, let $\theta = \arg g_\sigma(\eta_1)$ and rotate by $e^{-i\theta}$. The terminal images become $1, -1$ and the two remaining tip images determine $X_\sigma \in \mathsf{X}$. The stopping vector is $(0, \sigma)$ or $(\sigma, 0)$ and is finite by (6.33). It lies in Zhan's admissible time region exactly on E. His domain Markov lemma therefore gives the conditional law of the remaining pair as $\mathbb{P}_{2,X_\sigma}$.

We also need the following exact Green normalization at the stopping time:

$$\mathbb{E}_{2,y}\Big[\mathbf{1}_E e^{5\sigma/4}\mathfrak{g}(X_\sigma)\Big] = \mathfrak{g}_{\mathbb{D}}(y). \tag{6.34}$$

To prove this identity, let $\mathbb{P}_{c4,y}$ be Zhan's reference law for the same four initial marks. Zhan's Lemma 3.5 [11, p. 25] states that its admissible time region is all of $[0,\infty)^2$. Thus the bounded stopping vector above is admissible almost surely under that law. Equations (3.34) and (3.36) of that paper give the density of the original two-SLE law, restricted to E at this stopping vector, relative to the reference law:

$$e^{-5\sigma/4}\,\frac{\mathfrak{g}_{\mathbb{D}}(y)}{\mathfrak{g}(X_\sigma)}.$$

Here the capacity is σ, the exponent is $5/4$ at $\kappa = 6$, and rotation leaves the Green function unchanged. Multiplying this density by $e^{5\sigma/4}\mathfrak{g}(X_\sigma)$ and integrating proves (6.34). This is precisely [11, (3.37), p. 25]. In particular, it includes the mass lost on E^c and requires no division by $\mathbb{P}_{2,y}(E)$.

3. The Fourier identity at the stopping time. Consider initial targets of the form $J_0(K_{r,e,\phi}(0))$, where J_0 is normalized and univalent on $B_{1/4}$. Normalized-map bounds give a universal $a_0 > 0$ with $J_0(B_{a_0}) \subset B_{1/8}$ for all such J_0. On E, define

$$\widehat{J}(\zeta) = e^{-i\theta} g_\sigma(J_0(e^{-\sigma+i\theta}\zeta)).$$

The protected ball ensures that this map is defined and univalent on B_{a_0}; its value and derivative at 0 are 0 and 1. The constants in Step 1 are therefore uniform over these random maps. Moreover,

$$e^{-i\theta} g_\sigma(J_0(K_{r,e,\phi}(0))) = \widehat{J}(K_{e^\sigma r,e,\phi-\theta}(0)).$$

The exposed segment, the event E, σ, and θ depend only on the initial marked pair and its preliminary exploration; $\widehat{J}$ also depends on the fixed map J_0. None depends on r, b, e, ϕ.

Use $\mathcal{H}^-_{r,e,J_0}(y)$ for the negative coefficient in the original disk quad. Conditional expectation, the preceding target identity, and the substitution $\phi - \theta$ in the angular integral give

$$\begin{aligned}&\mathcal{H}^-_{r,e,J_0}(y) - b^{-2}\mathcal{H}^-_{br,e,J_0}(y)\\ &\quad = \mathbb{E}_{2,y}\left[\mathbf{1}_E e^{-2i\theta}\left\{\mathcal{H}^-_{e^\sigma r,e,\widehat{J}}(X_\sigma) - b^{-2}\mathcal{H}^-_{be^\sigma r,e,\widehat{J}}(X_\sigma)\right\}\right].\end{aligned} \tag{6.35}$$

Fubini's theorem applies because the hitting probabilities are bounded by one and $e \geq e_- > 0$. The angular integrands are periodic, so the random rotation changes only the displayed phase. Choose r below a fixed threshold so that $e^\sigma r \leq 2r$ is in the range of Step 1. The two leading terms proportional to $(e^\sigma r)^2$ then cancel for each exposed segment. Taking absolute values in (6.35), applying (6.31), and using (6.33) gives

$$\begin{aligned}\left|\mathcal{H}^-_{r,e,J_0}(y) - b^{-2}\mathcal{H}^-_{br,e,J_0}(y)\right| &\leq Cr^{9/4}\mathbb{E}_{2,y}[\mathbf{1}_E e^{9\sigma/4}\mathfrak{g}(X_\sigma)]\\ &\leq 2Cr^{9/4}\mathbb{E}_{2,y}[\mathbf{1}_E e^{5\sigma/4}\mathfrak{g}(X_\sigma)]\\ &= 2C\mathfrak{g}_{\mathbb{D}}(y)r^{9/4}.\end{aligned} \tag{6.36}$$

The last equality is (6.34). This proves the disk estimate uniformly even when its distinct marks approach one another.

4. An arbitrary simply connected quad. Use the normalized map f and conformal radius $\mathfrak{r}$ defined before the lemma, and set $J_0(\zeta) = f(w + \mathfrak{r}\zeta)$. The bounds $B(w, S) \subset \Omega$ and $\mathfrak{r} \le 4S$ imply that J_0 is univalent on $B_{1/4}$, with $J_0(0) = 0$ and $J_0'(0) = 1$. Since $f'(w) > 0$, the angle is unchanged in

$$f(K_{r,e,\phi}(w)) = J_0(K_{r/\mathfrak{r},e,\phi}(0)).$$

Conformal transport of the two-curve law and (6.36) now bound the defect by

$$C\mathfrak{g}_{\mathbb{D}}(r/\mathfrak{r})^{9/4} = C\mathfrak{g}_{\Omega}(w)\frac{r^{9/4}}{\mathfrak{r}} \le C\mathfrak{g}_{\Omega}(w)\frac{r^{9/4}}{S}.$$

Taking $r < cS$ ensures the fixed small-radius condition of Step 3 because $S \le \mathfrak{r}$. This proves (6.29). This step uses only interior conformal maps and derivative estimates. Distinct prime ends give distinct disk marks, even if their Euclidean impressions meet.

Either noncrossing pairing can be put in the stated clockwise order by relabelling the curves and, when needed, reversing their orientations. This preserves their hitting events and their two-SLE law; see the reversibility discussion in [11, Section 2.1, p. 8]. The formula for $\mathfrak{g}_{\Omega}$ is always evaluated with that pairing.

5. Conversion to a joint-hitting weight. Choose $c_0 > 0$ so small that the uniform relative error in Zhan's joint-hitting estimate above is at most $1/2$ whenever $\rho/S \le c_0$. For $R \le S < 2R$, take $\rho = c_0 R$. Then

$$\mathbb{P}_{\Omega}\{\gamma_1, \gamma_2 \text{ hit } B(w, c_0 R)\} \ge \tfrac{1}{2} C_* c_0^{5/4} \mathfrak{g}_{\Omega}(w) R^{5/4}.$$

Substitute this lower bound into (6.29), using $S \ge R$, to obtain (6.30). The permissible c_0 is independent of the marks because the relative Green-function error is uniform in them.

6. Conditional quads and averaging. Fix a link pattern and retain all curves except a selected pair. The conditional-law assertion of Lemma 7.3, whose proof uses no estimate from the present lemma, identifies a version of the conditional pair kernel almost surely. The component construction can be performed in a disk coordinate for the original domain, before the retained curves are deleted. For $\kappa = 6 < 8$, the compact retained traces almost surely avoid the remaining assigned boundary marks; the remaining marked components are of the type specified in [12, Section 3, pp. 5–6, especially the remark after Definition 3.1]. Each remaining mark has a neighborhood avoiding the retained traces, so distinct marks remain distinct prime ends. Conformal transport gives the corresponding physical components and their inherited banks without any assumption on the physical outer boundary.

If the two assigned pairs lie in distinct complementary components, or their common component does not contain w, they cannot both hit a connected target contained in the component of w. Their contribution is zero. In the remaining case, that component is simply connected and carries the four assigned, distinct prime ends; with their inherited banks it is a quad in the sense of subsection 6.1. Conditional on the retained data, its kernel is exactly the prescribed global two-SLE law. Steps 1–5 therefore apply to this fixed component, using the same conditional kernel and disk map for both radii and all angles.

This argument allows arbitrary geometry of the retained curves. Only the interior distance $S = \operatorname{dist}(w, \partial\Omega) > 0$ enters the small-radius condition; the analytic target estimates were proved after mapping into the disk. Fix the normalized cascade kernel constructed in Lemma 7.3 on its admissible retained tuples with positive remaining mass. It is a version of the regular conditional law as a probability measure, so the same full-measure set of retained data can be used for all allowed target parameters. Tuples with zero remaining mass have zero actual marginal weight and can be omitted.

For clarity, if $\mathcal{F}_{\mathrm{ret}}$ is the sigma-field of the retained data, (6.30) reads, on $\{R \le S < 2R\}$ and for $r < cR$,

$$|\mathcal{A}^{\Omega}_{r,b}(w)| \le C(r/R)^{9/4}\mathbb{P}\{\gamma_i, \gamma_j \text{ hit } B(w, c_0R) \mid \mathcal{F}_{\mathrm{ret}}\}.$$

Set the contribution to zero in the other-component cases just described. Multiplication by any bounded nonnegative $\mathcal{F}_{\mathrm{ret}}$-measurable weight supported on this shell, followed by the tower property, preserves the bound. In particular, this applies to the actual retained marginal $\mu_{\alpha,ij}$ and then to the pattern weights p_α in Lemma 7.4. Those weights already contain the probability of the selected pairing, so no additional factor $p_{\mathrm{cr},\Omega}$ is inserted. This justifies applying the lemma to the conditional quads in the decomposition and the sum over distance scales. □

7 Connections between finitely many boundary arcs

We apply the two-curve estimate of Lemma 6.4 to the law of the connections between finitely many labelled boundary arcs.

7.1 Effect of closing a connected set

Use the lattice model of subsection 4.1. Let U be a bounded domain conformally equivalent to $\mathbb{D}$, with $2m$ distinct marked boundary prime ends $x_1, \dots, x_{2m}$ in cyclic order, where $m \ge 1$ is an integer. Interpret the boundary in a disk coordinate as in subsection 6.1. Take uniformly bounded lattice approximations U^a with marked points x^a_j, in the model of [14, Section 6.1.2]. Require *marked Carathéodory convergence*: for disk maps $f_a : U^a \to \mathbb{D}$ and $f : U \to \mathbb{D}$ taking a fixed interior reference point to 0 with positive derivative there,

$$f_a^{-1} \longrightarrow f^{-1} \quad \text{uniformly on compact subsets of } \mathbb{D}, \qquad f_a(x^a_j) \longrightarrow f(x_j), \quad j = 1, \dots, 2m.$$

The same convention permits converging interior reference points after translation. See [14, Sections 3.2.3 and 5.1.1]. The maps f_a then converge to f on compact subsets of U. Full-curve convergence below is asserted in disk coordinates under these boundary assumptions.

For $k = 1, \dots, m$, give the successive arcs $A_k = (x_{2k-1}, x_{2k})$ open boundary cells and $C_k = (x_{2k}, x_{2k+1})$ closed boundary cells, with $x_{2m+1} = x_1$. Use the same arc names on the lattice approximations. Here $\mathcal{B}$ denotes the boundary-word data of subsection 4.1 in marked-domain form: the ordered marks, the prescribed colors of their intervening arcs, and the labels $1, \dots, m$ of the open arcs. These data determine the fixed boundary-cell colors on each approximation. The number, cyclic order, and colors of the arcs remain fixed as $a \downarrow 0$.

At finite mesh, the interfaces of subsection 6.1 consist of m disjoint simple paths joining the color-change points, together with interior loops. Call the boundary paths *chords*; they meet the original boundary only at their endpoints. If a cut has two boundary sides, keep those sides separately labelled. The pairing of the endpoint indices is the *link pattern* α. It is noncrossing: its pairs can be joined by disjoint chords. Number the chords $\gamma_1, \dots, \gamma_m$ by increasing smaller endpoint index. The pairing and the prescribed boundary colors form the *colored link diagram*; compare [13, Section 1.1, pp. 2–3].

Let $\mathcal{S}_{\mathcal{B}}$ be the finite set of partitions of the open-arc labels. The original partition s_α puts two labels in the same block exactly when an open path joins their arcs. It is determined by the colored link diagram. For $s \in \mathcal{S}_{\mathcal{B}}$, let δ_s be unit mass at s. For a complex measure μ on this set, use the norm of subsection 4.1:

$$\|\mu\|_{\mathrm{var}} = \sum_{s \in \mathcal{S}_{\mathcal{B}}} |\mu(s)|.$$

Let K be an edge-connected union of interior cells: any two of its cells are joined by a cell path contained in K. Let s^K be the partition after forcing K closed in the original sample. The open and closed cells along the two sides of a chord are its *banks*. A chord contacts K when one of its edges is incident to a cell of K. For the ellipses used below, the inner and outer offsets of width $c_{\mathrm{lat}}a$ from subsection 6.1 compare this contact convention with geometric hitting.

Lemma 7.1 (Effect on the boundary partition)**.** *If K contacts at most one boundary chord, then $s^K = s_\alpha$. If it contacts exactly two, i, j, then s^K is a deterministic partition $s_{\alpha,ij}$ depending only on the colored link diagram and that pair. Define*

$$\mathsf{J}_{\alpha,ij} = \delta_{s_{\alpha,ij}} - \delta_{s_\alpha}, \qquad \|\mathsf{J}_{\alpha,ij}\|_{\mathrm{var}} \le 2. \tag{7.1}$$

Set $\mathsf{J}_{\alpha,ij} = 0$ if no connected interior set can contact exactly that pair. The difference may also be zero otherwise.

Proof. Temporarily fill the outermost interior interface loops with their surrounding color. This preserves the connections between boundary arcs. The components after removing the boundary chords are called faces. Form a graph with one vertex per face and one edge per separating chord. Each new chord divides one face into two. Thus this graph is connected and has no cycles, hence is a tree. Adjacent faces have opposite colors.

Represent cell paths in K joining its contact cells as walks in this tree, recording every contacted chord and its adjacent faces. The contacted edges and intervening faces form a connected part of the tree. Hence two contacted chords share a face: an intervening third edge would require another chord contact. Call their common face the middle face. Repeated visits to a chord retrace its tree edge.

Repeated contacts create no further split of the boundary labels. Indeed, trim a simple cell path between contacts at its first and last visits to the relevant chord banks. Two connections to the same bank, together with the intervening chord segment, enclose only an interior region. After a small thickening, its boundary is a simple closed curve inside the original domain, so its interior contains no original boundary label. The same argument applies to an additional connection after the first connection between two selected chords. Further pieces of K therefore alter only such interior regions unless they contact another boundary chord.

If the middle face is closed, the outside faces are open. The new closed cells extend the same middle closed face; any additional pieces cut off only the interior regions just described. The open boundary partition stays unchanged. If the middle face is open, the outside closed faces are distinct vertices of the tree. Connectivity of K joins their banks, creating a crosscut of the middle face. The cyclic order of the chord endpoints determines the original boundary labels on its two sides. This determines $s_{\alpha,ij}$. With at most one contacted chord, at most one closed boundary face can be extended, so the partition stays unchanged.

For four successive arcs, write $A = A_1$, C_1, $B = A_2$, C_2. In the open-middle case, A, B initially belong to one block. Closing K joins C_1, C_2 and separates A, B. In the closed-middle case, C_1, C_2 are already connected and A, B are separate; their partition stays unchanged. Figure 3 shows both cases.

Restoring an interior interface loop adds a vertex with no original boundary label, joined to its surrounding face by one edge. Nested loops repeat this operation. A path through these new faces cannot join distinct boundary faces without contacting their intervening boundary chord. Thus restoring the loops leaves the conclusion unchanged. Finally, the difference of two unit point masses has variation norm at most two. □

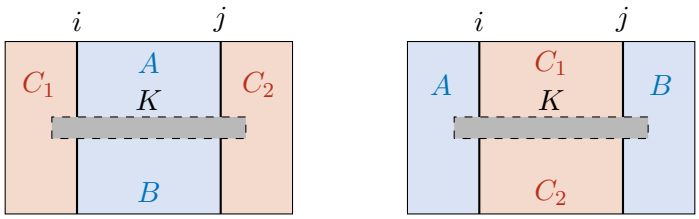


Figure 3: The two four-arc colored link diagrams in Lemma 7.1. Blue regions are open and red regions are closed. The gray connected set K is forced closed. In the left diagram this joins the closed banks and separates A from B; in the right diagram their partition stays unchanged. Interior interface loops enclose no original boundary labels.

7.2 Conditioning on all but two interfaces

The percolation input in this reduction needs a separate statement. Proposition 1.4 of Beffara–Peltola–Wu concerns FK-Ising interfaces; Beffara–Peltola–Wu's Remark 1.5 records the percolation extension. The proof below uses the explicit percolation verification in Karrila and explains how the conditional law needed here follows. This also separates convergence of complete curve tuples from conditioning on a limiting tuple.

Write $\mathbb{P}^a$ for the original color law, before closing a hole, and p^a_α for the probability of the link pattern α. A global multiple SLE_6 law with that pattern is a law under which, conditional on all other curves, each curve is chordal SLE_6 in the component with its assigned endpoints; see [12, Section 2.3, pp. 3–4]. Throughout this subsection, complete curves are compared in the conformal disk coordinates of subsection 7.1, using the uniform metric modulo increasing reparametrizations. Endpoint labels are retained.

The imported convergence criterion. We state the disk-coordinate version of [14, Theorem 5.8, Proposition 5.9, and Theorem 5.10, p. 28] at $\kappa = 6$. The hypotheses below concern either the model family or the particular sequence of domains.

For the crossing conditions, a *boundary annulus* of Ω is $A = A(z; s, t) = B(z, t) \setminus \overline{B(z, s)}$, with $B(z, s) \cap \partial\Omega \neq \varnothing$. A *boundary quadrilateral* $\mathcal{Q} \subset \Omega$ has cyclically ordered sides S_0, S_1, S_2, S_3, with $S_1, S_3 \subset \partial\Omega$ and S_0, S_2 in Ω except at their endpoints. Its modulus mod $\mathcal{Q}$ is the length L of the conformally equivalent rectangle $(0, L) \times (0, 1)$, with S_0 corresponding to the left side. A crossing joins the two circles of A through one component of $A \cap \Omega$, or joins S_0 to S_2 through $\mathcal{Q}$. Boundary sides are understood separately along the two banks of a slit. These are the conventions of [14, Section 4.1.3, pp. 17–18].

Theorem 7.2 (Karrila's convergence criterion in disk coordinates)**.** *Consider a family of laws of disjoint simple lattice chords on simply connected marked subgraphs of lattices whose maximal edge length tends to zero. For every fixed number $k \geq 1$ of curves, assume the following model-family hypotheses.*

(K1) ***Model and domain Markov property.*** *The k paths are vertex-disjoint, pair $2k$ distinct cyclically ordered marked boundary edges, and otherwise use interior edges. The intervening boundary arcs carry alternating conditions; path j starts at edge $2j - 1$ and ends at its even-index partner. Cyclic relabelling by two places preserves the law up to the corresponding permutation of paths. After revealing an initial segment from any marked edge, or a full curve, the remaining curves have the model laws on the resulting marked components, independently between components. These are the discrete domain Markov conventions of [14, Sections 3.1.1–3.1.2].*

(K2) ***One-curve crossing control.*** *Consider the one-curve family, in which both endpoints are specified. At every stopping time τ before its terminal time T, let Ω_τ be the remaining domain. A crossing is* unforced *if its annular component, or its quadrilateral, does not separate the current tip from the target in Ω_τ. Write $E_\tau(A)$ and $E_\tau(\mathcal{Q})$ for the corresponding future-crossing events. For every $\varepsilon > 0$ there are thresholds $M_\varepsilon, L_\varepsilon$, uniform over meshes, admissible graphs, and stopping times, such that*

$$(G) \quad \mathbb{P}^a(E_\tau(A) \mid \mathcal{F}_\tau) \le \varepsilon, \quad t/s \ge M_\varepsilon,$$
$$(C) \quad \mathbb{P}^a(E_\tau(\mathcal{Q}) \mid \mathcal{F}_\tau) \le \varepsilon, \quad \operatorname{mod} \mathcal{Q} \ge L_\varepsilon.$$

Here $\mathcal{F}_\tau$ records the curve up to τ, and the annulus or quadrilateral is a boundary test in Ω_τ. The two conditions are equivalent with adjusted thresholds; either suffices [14, Section 4.1.3].

(K3) ***Collective crossing control.*** *Index the intervening boundary arcs by the parity of their initial marked edge. An annular component $\mathcal{V}$ is unforced for the collection when $\partial\mathcal{V} \cap \partial\Omega$ lies entirely in arcs of one parity. A boundary quadrilateral is unforced for the collection when its sides S_1, S_3 lie entirely in arcs of the same parity. Let $E'(A)$ and $E'(\mathcal{Q})$ be the events that at least one curve makes such a crossing. For every $\varepsilon > 0$, the unconditioned collection law must satisfy (C') below:*

$$(G') \quad \mathbb{P}^a(E'(A)) \le \varepsilon, \quad t/s \ge M_{k,\varepsilon},$$
$$(C') \quad \mathbb{P}^a(E'(\mathcal{Q})) \le \varepsilon, \quad \operatorname{mod} \mathcal{Q} \ge L_{k,\varepsilon}.$$

The thresholds are uniform over all admissible marked graphs and meshes. The displayed annular condition (G') is a sufficient way to verify (C'): one may take $L_{k,\varepsilon} = 4(M_{k,\varepsilon} + 1)^2$ [14, Assumption 5.6 and Lemma 5.7, pp. 27–28].

(K4) ***Local driving limit.*** *Along every uniformly bounded marked Carathéodory convergent sequence with distinct limiting disk marks, the half-plane-capacity driving functions from each marked edge converge weakly, in the topology of uniform convergence on compact time intervals, to the local multiple-SLE_6 driving law with $Z_k \equiv 1$. For every localization neighborhood, both laws are stopped using Karrila's continuous modification of its exit time. Such a neighborhood is closed in $\overline{\mathbb{D}}$, contains a neighborhood of the starting disk mark, avoids the other marks, and has simply connected complement in $\mathbb{D}$. These are the localization and stopping conventions of [14, Section 2.1, especially Section 2.1.5 and Appendix B], as required by Karrila's Assumption 5.1, p. 25.*

(K5) ***Close inner approximations.*** *Along the lattice sequence under consideration, every bounded simply connected auxiliary domain V whose marked prime ends have radial limits admits model domains V^a, with $V^a \subset V$ for all sufficiently fine meshes, converging in the marked Carathéodory sense and closely at the marks. Here close approximation means the following. If p is a mark's radial limit and u the interior reference point, the corresponding Euclidean endpoints satisfy $p^a \to p$. For $0 < r < |p - u|$, let S_r be the innermost component of $V \cap \partial B(p, r)$ separating that prime end from u. For every fixed $w_r \in S_r$ and all sufficiently fine approximations, an access path from p^a to w_r has interior in $V^a \cap B(p, r)$. This is [14, Assumption 5.4, p. 26, and Section 3.2.4, p. 14].*

For the particular sequence with $k = m$, assume in addition:

(K6) ***Marked domain convergence.*** *The domains are uniformly bounded and converge in the marked Carathéodory sense of subsection 7.1, with $2m$ distinct limiting disk marks. Radial limits and close approximation are not required for these marks.*

Then the labelled full-curve tuple converges jointly in disk coordinates, in the uniform curve metric modulo reparametrization. Every admissible link pattern has a positive limiting probability, and the laws conditioned on each pattern also converge. In the limit, the regular conditional law of any one curve given the others is chordal SLE_6 between its assigned prime ends, which almost surely are boundary prime ends of the same simply connected component of the complement of the other curves.

Lemma 7.3 (Percolation convergence and conditional pairs)**.** *Critical site percolation on every prescribed sequence of translated triangular lattices satisfies hypotheses K1–K5 of Theorem 7.2. For the fixed marked data of subsection 7.1, write $p_\alpha > 0$ and $\mathbb{P}_\alpha$ for the limiting pattern probability and conditional curve law furnished by that theorem. Then $\mathbb{P}_\alpha$ is the unique global multiple SLE_6 law with pattern α.*

Fix $i < j$ and let $\boldsymbol{\eta} = (\gamma_k)_{k\neq i,j}$, with its actual marginal law $\mu_{\alpha,ij}$ under $\mathbb{P}_\alpha$. Conditional on this tuple, the remaining curves have the prescribed two-SLE_6 law if their four assigned prime ends belong to one complementary component. If the two assigned pairs belong to different components, their law is the product of the two chordal SLE_6 laws. These assertions hold for $\mu_{\alpha,ij}$-almost every retained tuple. In particular, a connected interior target disjoint from the retained curves can be hit by both remaining curves only in a component containing all four assigned prime ends.

Proof. Verification of K1: the model family. The cells in our triangular-lattice model are the faces of the honeycomb lattice in [14, Section 6.1.2 and Proposition 6.2, pp. 45–46]. Its alternating face colors give exactly our boundary word, and its interfaces are disjoint simple lattice chords. Karrila indexes the curves by their odd starting endpoints. For each fixed link pattern, a deterministic permutation gives our ordering by smaller endpoint index; we keep the odd endpoint as the starting point of each oriented curve. Cyclic relabelling by two places preserves the boundary prescription and product law. Revealing an exploration fixes the colors on its two banks, while all unrevealed cells remain independent fair cells, independently in different remaining components. This proves the required discrete domain Markov property, also on slit domains and translated meshes.

Verification of K2: one-curve crossings. For the one-curve family, the percolation proof of [14, Proposition 6.2, pp. 45–46] verifies (G), hence (C), uniformly over all admissible marked subgraphs. Its RSW blocking argument applies to the family above: in an unforced annular component, a monochromatic connection across a fixed-ratio layer blocks the interface crossing with probability bounded below independently of the graph. Boundary portions can be filled with their prescribed colors, so the bound does not require smoothness of the boundary. After any exploration stopping time, K1 gives the same product law on the remaining marked graph. Reapplying the bound there supplies the conditional estimate required in K2.

Verification of K3: collection crossings. In a component unforced for the collection, every contact with the domain boundary lies on marked arcs of one parity, hence of one fixed color. Fill the complementary pieces with that color. The monochromatic RSW blocking crossings used in [14, proof of Proposition 6.2] then prevent any interface from crossing the component. For mesoscopic annuli, revealing separated fixed-ratio layers successively under the original product law gives, for $a \le cs < R$ and R/s sufficiently large,

$$\begin{aligned}\mathbb{P}^a\{\text{an unforced crossing of the annular component}\} &\le C(1-c_*)^{\lfloor c_1 \log(R/s)\rfloor} \\ &\le C(s/R)^{\zeta}, \qquad \zeta > 0.\end{aligned}$$

The constants may depend on the fixed number of marks. The displayed estimate gives the annular iteration; the proof of Karrila's Proposition 6.2 supplies the crossing condition for all annuli, including tests at the lattice scale. Thus (G') holds on this family, and [14,

Lemma 5.7] gives (C'). These estimates concern the unconditioned collection on each marked graph. By K1 they also apply after an exploration, with the unforced regions recomputed from its induced marks and colors.

Verification of K4: the local driving law. The local multiple-SLE partition function is $Z_m \equiv 1$. It is positive and has the required conformal covariance because the SLE boundary weight at $\kappa = 6$ is zero. Its differential equations and driving drift reduce to

$$\left[3\partial_{x_j}^2 + \sum_{k\neq j} \frac{2}{x_k - x_j}\partial_{x_k}\right] 1 = 0, \qquad 6\partial_{x_j} \log Z_m = 0.$$

Thus the local driver satisfies $dW_t = \sqrt{6}\, dB_t$, starting at its marked real coordinate. Up to the localized stopping used in K4, the discrete exploration is unaffected by the other marks. Single-interface convergence and SLE_6 locality give the local driving convergence along the prescribed marked Carathéodory sequences, exactly as in [14, proof of Proposition 6.2, (6.2), pp. 45–46].

Verification of K5: close inner approximations. Lemma C.1 in Appendix C constructs admissible marked percolation domains inside every bounded simply connected auxiliary domain with radial limits at its marks, along every prescribed sequence of translated lattices. It proves marked Carathéodory convergence and the local access condition in K5, including the case of coincident Euclidean landing points. This verifies Karrila's Assumption 5.4.

Verification of K6 and application. The fixed marked data of subsection 7.1 satisfy K6. Theorem 7.2 therefore gives joint convergence of the full curves in disk coordinates, positive limiting pattern probabilities, convergence after conditioning on each pattern, and the regular conditional one-curve SLE law. Write $\mathbb{P}$ for the unconditioned limit and $\mathbb{E}$ for its expectation. The cited theorem includes the conditional-domain assertion: the last curve's endpoints are prime ends of the same remaining component. These are the issues treated for FK-Ising by tightness, exclusion of pinching, and conditional-law identification in [13, Lemmas 4.5–4.7, pp. 24–26]; here the percolation hypotheses have been verified above.

For a fixed pattern, the crossing estimates can also be conditioned by the elementary bound

$$\mathbb{P}^a(E \mid \alpha) \le \frac{\mathbb{P}^a(E)}{p_\alpha^a} \le \frac{2}{p_\alpha}\mathbb{P}^a(E)$$

for all sufficiently small a, using the positivity just obtained. This gives the required event bound under conditioning on any fixed full pattern.

We now identify the limit for a fixed pattern by conditioning. Let Y consist of all curves except γ_j, and let $k_j(Y; f)$ be the expectation of a bounded Borel function f under chordal SLE_6 in its remaining marked component. Once the endpoint pairs in Y are given, the last pair is forced. The link-pattern event is therefore measurable with respect to Y. For every bounded Borel F, the conditional-law conclusion of Theorem 7.2 gives

$$\mathbb{E}_\alpha[F(Y)f(\gamma_j)] = p_\alpha^{-1}\mathbb{E}\Big[\mathbf{1}_{\{\text{link pattern}=\alpha\}}F(Y)k_j(Y; f)\Big] = \mathbb{E}_\alpha[F(Y)k_j(Y; f)].$$

This is the global multiple-SLE conditional property. Uniqueness in [12, Theorem 4.2, p. 11], applied in the disk, identifies the limit with $\mathbb{P}_\alpha$.

Disintegration of two remaining curves. To make the retained weight explicit, write M_λ^V for Zhan's finite SLE_6 measure with pairing λ, and $\mathsf{Z}_\lambda^V = |\mathsf{M}_\lambda^V|$ for its mass; see [12, Definition 3.1 and Theorem 3.8]. These symbols are distinct from our local rows Q. The empty pairing has unit mass. The measures can be defined first in disk coordinates and then transported conformally; the SLE boundary weight is zero. Write α_k for the assigned endpoint pair of

γ_k. Put $\widehat{\alpha} = \alpha \setminus \{\alpha_i, \alpha_j\}$, $\beta = (\alpha_i, \alpha_j)$, and $U_{\boldsymbol{\eta}} = U \setminus \bigcup_{k \neq i,j} \eta_k$. For a disconnected remaining domain, the measure is the product over components; it is zero if an assigned pair does not belong to one component.

Permute the two selected curves to the last positions. The cascade and permutation identities [12, (3.4) and the proof of Lemma 3.6, pp. 6 and 8] give

$$\mathsf{M}_{\alpha}^{U}(d\boldsymbol{\eta}, d\boldsymbol{\xi}) = \mathsf{M}_{\widehat{\alpha}}^{U}(d\boldsymbol{\eta})\mathsf{M}_{\beta}^{U_{\boldsymbol{\eta}}}(d\boldsymbol{\xi}), \qquad \boldsymbol{\xi} = (\gamma_i, \gamma_j).$$

Taking the first marginal and dividing by Z_{α}^{U} yields

$$\mu_{\alpha,ij}(d\boldsymbol{\eta}) = \frac{\mathsf{Z}_{\beta}^{U_{\boldsymbol{\eta}}}}{\mathsf{Z}_{\alpha}^{U}}\mathsf{M}_{\widehat{\alpha}}^{U}(d\boldsymbol{\eta}), \qquad \mathbb{P}_{\alpha}(d\boldsymbol{\xi} \mid \boldsymbol{\eta}) = \frac{\mathsf{M}_{\beta}^{U_{\boldsymbol{\eta}}}(d\boldsymbol{\xi})}{\mathsf{Z}_{\beta}^{U_{\boldsymbol{\eta}}}}.$$

The conditional identity is the normalization rule [12, (2.4)–(2.5)]; a zero denominator has zero marginal weight. In a component with four assigned prime ends, the normalized kernel is its two-SLE law. In two distinct components it factors into the two chordal laws, as in [12, proof of Lemma 3.5, p. 7]. Components with no assigned endpoint contribute unit probability. Since a connected target avoiding the retained curves lies in one component, both selected curves can hit it only in the four-endpoint case. This proves the lemma and makes explicit the partition weight already present in $\mu_{\alpha,ij}$. □

Remark (Conditioning and marked boundary data). Hypotheses K2 and K3 concern different laws: stopping-time estimates for the one-curve family and estimates over unconditioned marked graphs, respectively. Hypothesis K1 allows both estimates to be used after an exploration. Full link-pattern conditioning is performed after Theorem 7.2; it can force a crossing classified as unforced for the collection, so (C') is imposed before that conditioning. The elementary conditional event bound above is not a stopping-time crossing condition for the conditioned model. Its constants may depend on the positive limiting pattern probability and hence on the fixed marked configuration.

The convergence conclusion uses Karrila's relaxed boundary setup [14, Remark 4.2 and Section 5.1.1]. The conditional laws in Lemma 7.3 follow from the conditional-law conclusion of Theorem 7.2 and Zhan's uniqueness and cascade identities; joint weak convergence alone does not give these conditional laws.

Fix $w \in U$ and $d > 0$ with $B(w, d) \subset U$. Use the ellipses $K_{\rho,e,\phi}(w)$ of subsection 4.3, with $e \in [e_-, e_+]$ and $b \in [1/2, 1]$. For such an ellipse contained in U, let $\nu_{\rho,e,\phi,w}^{a,U,\mathcal{B}}$ be the law on $\mathcal{S}_{\mathcal{B}}$ after closing its inner-cell approximation. For $r > 0$ small enough, define

$$\Delta_{r,b,e}^{a,U,\mathcal{B}}(w) = \frac{1}{2\pi e}\int_0^{2\pi} e^{-2i\phi}\left[\nu_{r,e,\phi,w}^{a,U,\mathcal{B}} - b^{-2}\nu_{br,e,\phi,w}^{a,U,\mathcal{B}}\right] d\phi.$$

The integral is taken at each partition, so this is a row in the sense of subsection 4.1. Define $V^{a,U,\mathcal{B}}$ and $Q^{a,U,\mathcal{B}}$ by (4.10), using this arc-partition law. Then

$$\Delta_{r,b,e}^{a,U,\mathcal{B}}(w) = V_{r,e}^{a,U,\mathcal{B}}(w) - b^{-2}V_{br,e}^{a,U,\mathcal{B}}(w) = r^2(Q_{r,e}^{a,U,\mathcal{B}}(w) - Q_{br,e}^{a,U,\mathcal{B}}(w)).$$

Its variation norm is at most $5/e_-$. Choose a fixed $M_0 > 1 + e_+$ sufficiently large for Lemma 6.4 and the local conformal-map estimate below, and take $2M_0 r < d/64$. Along any mesh sequence choose a subsequence on which every mass of this finite row converges, and write

$$\Delta_{r,b,e}^{U,\mathcal{B}}(w)(s) = \lim_{a \downarrow 0} \Delta_{r,b,e}^{a,U,\mathcal{B}}(w)(s), \qquad s \in \mathcal{S}_{\mathcal{B}},$$

with the limit taken along that subsequence. The estimate below applies to every such subsequential limit. By Lemma 7.3, the original curve law has the limit

$$\mathbb{P} = \sum_{\alpha} p_\alpha \mathbb{P}_\alpha, \qquad \mathbb{E} \text{ denotes expectation under } \mathbb{P}.$$

For a retained tuple $\boldsymbol{\eta}$, let Ω_{ij} be the component containing w. Its boundary data inherit the original arc colors and the two separately labelled banks of each retained curve. Use this component only if $\mathsf{J}_{\alpha,ij} \neq 0$, the retained curves avoid w, and all four assigned endpoints are prime ends of this component. Put $S_{ij} = \operatorname{dist}(w, \partial\Omega_{ij})$ in that case, and put $S_{ij} = 0$ and the pair contribution equal to zero otherwise. The coefficients $\mathsf{J}_{\alpha,ij}$ remain those of the finite colored link diagram in Lemma 7.1. For a contributing pair the inherited colors and pairing give the open-middle case, so its conditional joint-hitting function is $H_{\Omega_{ij}}$.

On each contributing tuple the distance has the representation

$$S_{ij} = \min\left\{ \operatorname{dist}(w, \partial U),\ \inf_{k \neq i,j} \operatorname{dist}(w, \eta_k \cap U) \right\},$$

where the infimum over an empty collection is $+\infty$. Indeed, a disk centered at w lies in its complementary component exactly when it avoids the original boundary and all retained traces. These distances are measurable, for example by the truncated-distance representation below, so the shells $\{R \le S_{ij} < 2R\}$ are measurable with respect to the retained data. If $2R < \operatorname{dist}(w, \partial U)$, such a shell forces a retained curve to enter $B(w, 2R)$.

Let N_R count the original limiting boundary curves meeting $B(w, R)$, and let N_R^a be the lattice count. Choose $R_0 \in [M_0 r, 2M_0 r]$ so that the minimum distance to w of each limiting curve has no atom at R_0. Require the same for every lattice curve along the selected countable mesh sequence. Such a choice exists because a real random variable has at most countably many atoms. The buffer $B(w, R_0)$ contains both ellipse sizes for every angle.

Its avoidance indicators and the count $N_{R_0}^a$ are continuity events even when full curves converge only in disk coordinates. Indeed, choose $R_0 < L < d$, and let $g : U \to \mathbb{D}$ be a normalized disk map. The function

$$\chi(z) = \min\{L, |g^{-1}(z) - w|\}, \qquad z \in \mathbb{D},$$

extends continuously to $\overline{\mathbb{D}}$ by the value L: its nonconstant part lies in the compact set $g(\overline{B(w, L)})$. Under marked Carathéodory convergence, the analogous functions χ_a converge uniformly to χ. This follows from convergence of both maps on the interior compact sets in question; their nonconstant parts remain in a common compact subset of $\mathbb{D}$. Taking the minimum along a curve is continuous in the uniform curve metric. The atom-free choice of R_0 now gives convergence of all the buffer indicators and of $N_{R_0}^a$. This argument also applies to converging centers.

Lemma 7.4 (Buffered pair decomposition)**.** *With these definitions and $\mathcal{A}_{r,b}^{\Omega}$ from subsection 6.6, every subsequential row limit satisfies*

$$\Delta_{r,b,e}^{U,\mathcal{B}}(w) = \sum_{\alpha} p_\alpha \sum_{i<j} \mathsf{J}_{\alpha,ij} \int \mathbf{1}_{\{S_{ij} > R_0\}} \mathcal{A}_{r,b}^{\Omega_{ij}}(w)\, d\mu_{\alpha,ij} + \mathcal{E}_{r,b}, \tag{7.2}$$

$$\|\mathcal{E}_{r,b}\|_{\mathrm{var}} \le \frac{5}{e_-} \mathbb{P}(N_{R_0} \ge 3). \tag{7.3}$$

The error constant is independent of the number and positions of the boundary marks. The same conclusion holds for uniformly bounded marked Carathéodory approximations with a fixed number of distinct limiting marks, convergent interior centers, and parameters $r_a \to r > 0$, $e_a \to e$, $b_a \to b$ in the stated ranges, provided that a common interior disk contains the buffer with the scale separation specified above.

Proof. The identity before taking limits. For a target K in the buffer, write $C_i^a(K)$ for contact by chord i in the convention of Lemma 7.1. Put

$$E_{ij}^a = \{\gamma_k^a \cap B(w, R_0) = \varnothing \text{ for all } k \neq i, j\}, \qquad B^a = \{N_{R_0}^a \geq 3\}.$$

For each sample with pattern α, Lemma 7.1 gives the exact identity of measures on $\mathcal{S}_{\mathcal{B}}$,

$$\delta_{s^K} - \delta_{s_\alpha} = \sum_{i<j} \mathsf{J}_{\alpha,ij} \mathbf{1}_{E_{ij}^a} \mathbf{1}_{C_i^a(K) \cap C_j^a(K)} + \mathbf{1}_{B^a}(\delta_{s^K} - \delta_{s_\alpha}).$$

On B^a every pair leaves a retained curve in the buffer, so all pair terms vanish. On its complement at most two chords contact K. Zero or one contact changes no boundary partition; two contacts select exactly that pair. Conversely, a nonzero pair indicator forces $N_{R_0}^a = 2$. Hence the sum does not overcount.

The normalization can also be checked directly. Prescribe retained paths and their banks, indexed by their endpoint pairs, and let $c^a(\boldsymbol{\eta})$ be the probability of this color cylinder before requiring the remaining pairing. Given this cylinder, all other cells are independent and fair. Let $q^a(\boldsymbol{\eta})$ be the probability of the required remaining pairing under that law. If $\mu_{\alpha,ij}^a$ is the actual retained marginal conditional on α, then

$$p_\alpha^a \mu_{\alpha,ij}^a(\{\boldsymbol{\eta}\}) = c^a(\boldsymbol{\eta}) q^a(\boldsymbol{\eta}).$$

The conditional probability of both contacts is normalized by this same q^a. Thus multiplying it by $p_\alpha^a \, d\mu_{\alpha,ij}^a$ already includes the probability of the remaining pairing. This is the discrete counterpart of the cascade calculation in Lemma 7.3.

Continuity of the target event in the limiting component. We verify this continuity also for components with nonsmooth boundary. Fix a contributing retained tuple with $S = S_{ij} > R_0$ and let $f : \Omega_{ij} \to \mathbb{D}$ satisfy $f(w) = 0$ and $f'(w) > 0$. The normalized map $f(w + S\zeta)/(Sf'(w))$ is univalent on $\mathbb{D}$. The normalized-map bounds and Cauchy estimates recalled in subsection 6.2 therefore give, for r/S small,

$$\sup_{|z-w| \leq 2r} \left| \frac{f'(z)}{f'(w)} - 1 \right| + r \sup_{|z-w| \leq 2r} \frac{|f''(z)|}{f'(w)} + r^2 \sup_{|z-w| \leq 2r} \frac{|f'''(z)|}{f'(w)} \leq C \frac{r}{S}.$$

Take $0 < s < s_* r$, with $s_* > 0$ small enough that the offsets of both ellipse sizes stay in the buffer, in $B(w, 2r)$, and in the specified shape class. Since $e \leq e_+ < 1$, increasing M_0 makes their images strictly convex analytic targets in the shape class of subsection 6.1. The same holomorphic distortion bounds on a fixed neighborhood of the rescaled ellipse control its analytic boundary charts. Their scale is comparable to $f'(w)r$, and the image offset boundaries are normal graphs over $\partial f(K)$ of displacement at most $Cf'(w)s$. Apply (6.3) in the unit disk, where it was proved using the strip estimate, and use conformal transport of the two-SLE law. For each fixed retained tuple,

$$H_{\Omega_{ij}}(K^{(+s)}) - H_{\Omega_{ij}}(K^{(-s)}) \longrightarrow 0 \qquad (s \downarrow 0).$$

Its crossing probability is positive. In particular, monotone convergence for the increasing inner offsets shows that the probability that both curves hit K equals the probability that both hit $\operatorname{int} K$. This proves joint hitting continuity. The displayed difference is bounded by one, so bounded convergence applies after integration over the actual retained marginal.

Passage of joint curve events. It suffices to consider pairs with $\mathsf{J}_{\alpha,ij} \neq 0$. Fix such a pattern and pair, an orientation ϕ, and one of the two radii. Set

$$I_{\alpha,ij}^a(K) = \mathbb{P}^a(E_{ij}^a \cap C_i^a(K) \cap C_j^a(K) \mid \alpha).$$

For each fixed sufficiently small offset $s > 0$, joint curve convergence from Lemma 7.3 brackets this quantity between the corresponding limiting probabilities with targets $K^{(-s)}$ and $K^{(+s)}$. To see this, realize the convergent tuples in an almost surely convergent coupling; the curve space is Polish by [14, Section 3.3.1, p. 14]. A hit of $K^{(-s)}$ has a positive margin inside $K^{(-s/2)}$, so survives a sufficiently small curve perturbation as a hit of that inner offset. Any limit of contacts with K^a is a hit of the larger target. The contact convention contributes an offset of at most $c_{\mathrm{lat}}a$, absorbed by the same margin. The buffer indicator converges by the preceding truncated-distance argument.

Let E_{ij} denote avoidance of the buffer by all retained limiting curves, and write

$$I_{\alpha,ij}(K) = \mathbb{P}_\alpha(E_{ij},\ \gamma_i \cap K \neq \varnothing, \gamma_j \cap K \neq \varnothing).$$

The resulting bounds are

$$I_{\alpha,ij}(K^{(-s)}) \leq \liminf_{a\downarrow 0} I^a_{\alpha,ij}(K) \leq \limsup_{a\downarrow 0} I^a_{\alpha,ij}(K) \leq I_{\alpha,ij}(K^{(+s)}).$$

Disintegrate only these limiting probabilities, using Lemma 7.3. On E_{ij} the connected target is contained in the component of w. If the selected pairs belong to different components, or to a different common component, their simultaneous hitting probability is zero. For a pair with $\mathsf{J}_{\alpha,ij} \neq 0$, the remaining case gives

$$I_{\alpha,ij}(K) = \int \mathbf{1}_{\{S_{ij} > R_0\}} H_{\Omega_{ij}}(K)\, d\mu_{\alpha,ij}.$$

The preceding target continuity makes the outer bounds agree as $s \downarrow 0$. Therefore $I^a_{\alpha,ij}(K) \to I_{\alpha,ij}(K)$. Thus the joint observable converges before we disintegrate its limiting law.

There are finitely many patterns and pairs. Each $I^a_{\alpha,ij}$ lies between zero and one, so bounded convergence also allows passage to the limit in the orientation integral. Taking expectations in the exact lattice identity, multiplying by the angular weights at radii r and br, and using $p^a_\alpha \to p_\alpha$ now gives the pair sum in (7.2). In this calculation every term containing δ_{s_α} has zero angular integral, including its restriction to B^a. The remainder is consequently

$$\mathcal{E}^a_{r,b} = \frac{1}{2\pi e}\int_0^{2\pi} e^{-2i\phi}\mathbb{E}^a\left[\mathbf{1}_{B^a}\left(\delta_{s^{K_{r,e,\phi(w)^a}}} - b^{-2}\delta_{s^{K_{br,e,\phi(w)^a}}}\right)\right] d\phi,$$

and

$$\|\mathcal{E}^a_{r,b}\|_{\mathrm{var}} \leq \frac{1+b^{-2}}{e}\mathbb{P}^a(B^a) \leq \frac{5}{e_-}\mathbb{P}^a(N^a_{R_0} \geq 3).$$

The chosen radius gives $\mathbb{P}^a(N^a_{R_0} \geq 3) \to \mathbb{P}(N_{R_0} \geq 3)$. The full row and its pair part converge along the selected subsequence, so the remainder converges too, proving (7.3). The bound on the bad event was obtained before summing pairs; hence it has no factor depending on their number.

Finally, for varying marked domains use their normalized disk maps. They converge uniformly, with their derivatives, near the fixed compact target region. Ellipses with converging centers and parameters are bracketed there by arbitrarily small offsets of the limiting ellipses. The same joint-event argument applies. This proves the final assertion without requiring uniform convergence of the outer boundaries or convergence of random slit domains. □

7.3 Counting interfaces near the target

An arm event is *polychromatic* when its disjoint arms use both colors. Work first at finite mesh with $0 < R < d/16$. A chord entering $B(w,R)$ supplies two disjoint portions across

$$B(w,d/2) \setminus \overline{B(w,2R)}.$$

Orient each chord with its open bank on the left. Keep its first incoming and last outgoing portions across the annulus. Reorient both from the inner to the outer boundary and take their left banks. These lie in distinct regions between consecutive portions. Reversing the incoming portion exchanges its bank colors, so each chord contributes one open and one closed bank. Thus three chords give six disjoint arms using both colors, after moving the annular boundaries by at most a constant times a.

The six-arm exponent is $(6^2-1)/12 = 35/12$; see [7, Theorem 4 and (9), p. 8, and Remark 6, p. 10]. Convergence of this arm event at fixed scales follows from [9, Lemma 2.9, pp. 22–23]. Consequently, for every $\eta > 0$,

$$\mathbb{P}(N_R \geq 3) \leq C_\eta (R/d)^{35/12-\eta}, \qquad 0 < R < d/16. \tag{7.4}$$

The estimate is taken in the original unconditioned sample. The cells in this annulus have independent random colors, regardless of the prescribed colors outside it.

There is also a bound on the probability of a large count:

$$\mathbb{P}(N_R \geq k) \leq Ce^{-ck}, \qquad k = 1, 2, \ldots, \quad 0 < R \leq d/16. \tag{7.5}$$

Indeed, k chords supply at least a fixed positive fraction of k disjoint open crossings of $B(w, d/2) \setminus \overline{B(w, d/4)}$. A radial crossing joins its inner and outer boundaries. The Russo–Seymour–Welsh (RSW) estimate gives a probability at least $c_* > 0$ of a simple loop of closed cells surrounding the inner disk, hence an open radial crossing has probability at most $1 - c_*$. See [8, Theorem 2 and Corollary 3, p. 1569, and the circuit argument following (4.10), p. 1579]. For integers $h \geq 1$, the van den Berg–Kesten (BK) inequality bounds the probability of h open crossings with disjoint cell sets by the hth power of the one-crossing probability; see [8, Section 2.2, p. 1568]. This proves (7.5); compare the same exponential estimate in [8, (4.12), p. 1580]. These lattice bounds pass to the limiting curves by convergence and arbitrarily small changes of the annular radii.

Lemma 7.5. *For every $\eta > 0$, uniformly over the finite boundary data $\mathcal{B}$,*

$$\mathbb{E}[N_R^2 \mathbf{1}_{\{N_R \geq 3\}}] \leq C_\eta (R/d)^{35/12-\eta}, \qquad 0 < R < d/16. \tag{7.6}$$

Also $\mathbb{E}N_{d/16}^2 \leq C$.

Proof. Use (7.4) with $\eta/2$. Put $L = \lceil C_1 \log(d/R) \rceil$, where C_1 is a sufficiently large fixed constant, so $L \geq 3$. The contribution with $N_R \leq L$ is at most $L^2 \mathbb{P}(N_R \geq 3)$. Summing (7.5) bounds the remaining contribution by $C(L+1)^2 e^{-cL}$. Increasing C_1 if needed makes this tail smaller than the required power. The logarithmic factors are bounded by a constant times $(R/d)^{-\eta/2}$, proving (7.6). Summing (7.5) also gives the final assertion. □

7.4 Summing over distance scales

Fix $R \geq R_0$ and restrict a pair integral to $R \leq S_{ij} < 2R$. Apply Step 6 of the proof of Lemma 6.4 to the limiting conditional kernel of Lemma 7.3, after passing the joint events to the limit in Lemma 7.4. Increase the fixed M_0, if necessary, so that $r < cR_0$. The bound for $|\mathcal{A}_{r,b}^{\Omega_{ij}}(w)|$ is then

$$C(r/R)^{9/4} \mathbb{P}_{\Omega_{ij}}\{\gamma_i, \gamma_j \text{ both meet } B(w, c_0 R)\}, \tag{7.7}$$

where c_0 is the fixed constant in (6.30). If $2R < d$, the original boundary is farther than $2R$ from w. Thus $S_{ij} < 2R$ requires a retained curve to come within $2R$ of the center. When the selected pair also enters $B(w, c_0 R)$, at least three original curves enter $B(w, 2R)$.

The tower property gives

$$\begin{aligned}&\sum_{\alpha:p_\alpha>0} p_\alpha \sum_{i<j} \int \mathbf{1}_{\{R\le S_{ij}<2R\}} \mathbb{P}_{\Omega_{ij}}\{\gamma_i,\gamma_j \text{ meet } B(w,c_0R)\}\, d\mu_{\alpha,ij}\\ &= \mathbb{E}\left[\sum_{i<j} \mathbf{1}_{\{R\le S_{ij}<2R\}} \mathbf{1}_{\{\gamma_i,\gamma_j \text{ meet } B(w,c_0R)\}}\right]\\ &\le \mathbb{E}[N_{2R}^2 \mathbf{1}_{\{N_{2R}\ge 3\}}]. \end{aligned} \tag{7.8}$$

Indeed, the left side is the expected number of pairs with the stated properties. In each sample that number is at most N_{2R}^2, and is zero unless $N_{2R} \ge 3$. The marginal laws and pattern weights in this formula are those of the original sample.

For $R < d/32$, apply Lemma 7.5 and $\|\mathsf{J}_{\alpha,ij}\|_{\mathrm{var}} \le 2$. This part of (7.2) is bounded by

$$C_\eta (r/R)^{9/4} (R/d)^{35/12-\eta} = C_\eta (r/d)^{9/4} (R/d)^{2/3-\eta}. \tag{7.9}$$

Choose $0 < \eta < 2/3$ and sum over $R_k = 2^k R_0$, $k = 0, 1, \ldots$, while $R_k < d/32$. The sum of $(R_k/d)^{2/3-\eta}$ is bounded by a constant, because successive terms have a fixed ratio greater than one and the last radius is at most $d/32$. The total is at most $C(r/d)^{9/4}$.

The remaining pair domains have $S_{ij} \ge d/32$. Choose a fixed $\kappa_0 \in (0, 1/32)$ small enough that the joint-hitting estimate in subsection 6.6 gives

$$\mathbb{P}_{\Omega_{ij}}\{\gamma_i,\gamma_j \text{ meet } B(w,\kappa_0 d)\} \ge c_1 \mathfrak{g}_{\Omega_{ij}}(w) d^{5/4},$$

where $c_1 > 0$ is fixed. This uses the Green function defined there and [11, Theorem 1.1, (1.2), pp. 2–3]. Together with (6.29) and $S_{ij} \ge d/32$, it bounds the angular difference by

$$C(r/d)^{9/4} \mathbb{P}_{\Omega_{ij}}\{\gamma_i,\gamma_j \text{ meet } B(w,\kappa_0 d)\}.$$

Average with $\mu_{\alpha,ij}$ and p_α and count pairs again. The result is at most $C(r/d)^{9/4} \mathbb{E} N_{\kappa_0 d}^2 \le C'(r/d)^{9/4}$. Equation (7.4) also bounds the error in (7.3) by this order, since $R_0 \le 2M_0 r$ and $35/12 - \eta > 9/4$.

Every subsequential limit of the finite vector $\Delta_{r,b,e}^{a,U,\mathcal{B}}(w)$ therefore satisfies this bound. Hence, for sufficiently small r/d,

$$\limsup_{a\downarrow 0} \|\Delta_{r,b,e}^{a,U,\mathcal{B}}(w)\|_{\mathrm{var}} \le C(r/d)^{9/4}. \tag{7.10}$$

The constant is independent of the number and positions of the marked boundary points. The gain that makes the scale sum finite is $35/12 - 9/4 = 2/3$.

A fixed exterior wiring specifies further identifications of the open-arc labels. Combining them with a partition s gives a deterministic map F on $\mathcal{S}_{\mathcal{B}}$. The resulting mass at an output partition t is $\sum_{s:F(s)=t} \mu(s)$, whose absolute values sum to at most $\|\mu\|_{\mathrm{var}}$. Thus (7.10) also holds after this exterior completion, as defined in subsection 4.1.

The boundary data are fixed during this mesh limit. Section 8 treats boundary specifications whose number of arcs may grow as $a \downarrow 0$.

8 An estimate for the complete frontier record

We extend (7.10) to the complete frontier record of subsection 4.1, uniformly over prescribed frontier colors. The number of boundary arcs may now grow as the mesh tends to zero.

8.1 Exploring outside a fixed disk

Fix $z_0 \in \mathbb{C}$, $d > 0$, and $D = B(z_0, d)$. Let $w \in B(z_0, d/4)$. Use the ellipses $K_{\rho,e,\phi}(w)$ of subsection 4.3, with $e \in [e_-, e_+] \subset (0,1)$ and $b \in [1/2, 1]$. Fix $R = \theta d$, where $0 < \theta < 1/64$, and take $r > 0$ sufficiently small that $(1+e_+)r < R/10$. Thus all ellipses of sizes r, br lie in $B(w, R/10)$ and $B(w, 4R) \subset D$. Constants below may depend on θ, e_-, e_+, but not on the prescribed frontier colors.

Give each cell of the frontier Γ_a from subsection 4.1 a distinct label. A *boundary word* $\mathcal{B}$ is the color assignment of subsection 4.1. Read the cells in order along the boundary; maximal consecutive runs of one color are its boundary arcs. Let $\mathbb{P}^{a,\mathcal{B}}$ be the law with this word fixed and all other cells independently open or closed with probability $1/2$. The word may depend on a. Write $\nu^{a,D,\mathcal{B}}_{\rho,e,\phi,w}$ for the resulting complete frontier-record law after forcing $K_{\rho,e,\phi}(w)$ closed. Define

$$\Delta^{a,D,\mathcal{B}}_{r,b,e}(w) = \frac{1}{2\pi e} \int_0^{2\pi} e^{-2i\phi} \left[\nu^{a,D,\mathcal{B}}_{r,e,\phi,w} - b^{-2} \nu^{a,D,\mathcal{B}}_{br,e,\phi,w} \right] d\phi.$$

The integral is taken at each record, and $\|\Delta^{a,D,\mathcal{B}}_{r,b,e}(w)\|_{\mathrm{var}} \le 5/e_-$. Omitting $\mathcal{B}$ means that the frontier colors are also sampled independently. In that case

$$\Delta^{a,D}_{r,b,e}(w) = r^2 (Q^{a,D}_{r,e}(w) - Q^{a,D}_{br,e}(w)),$$

with Q as defined in subsection 4.3.

An exploration reveals cell colors successively, making each decision from the colors already revealed. Work at sufficiently small fixed a/R, and protect every cell whose geometric closure meets $\overline{B(w,R)}$: its color must not be revealed. The component containing these cells is the *target component*. Trace interfaces with their two banks separately labelled, as in subsections 6.1 and 7.1. An *active start* is a boundary color change whose interface has not been completed. A traced initial segment is a *prefix*, and its current endpoint is its *tip*. A tip is *frozen* when the next unknown color needed to continue lies in a protected cell. Figure 4 shows the stopping and boundary-mark conventions.

Exploration algorithm.

Step 1. **Initialize and order.** Start with the prescribed frontier colors and give every initial active start a permanent label. Order oriented boundary edges by the horizontal coordinate of their midpoint, then by its vertical coordinate, and then by their direction; use the bank label to distinguish coincident sides of a cut. Store each prefix's whole path from the original frontier, oriented toward its tip, and carry its original start label along every continuation.

Step 2. **Choose a start and trace.** If every active start is frozen, stop. Otherwise choose the least active start that is not frozen and follow its interface into the unexplored region. Reveal the next incident cell only if its color is unknown and it is unprotected. Use the color of a known bank cell to determine the continuation; contact with it is not a stopping event. Continue until the prefix pairs with another marked start or retained prefix, or until the next required face is protected. In the latter case freeze the current tip. Every possible contact is checked below.

Step 3. **Retain the marked edge.** For every unfinished prefix use the boundary-edge convention of [14, Section 3.1.2(i), p. 12]. If its successive vertices are $\lambda(0), \dots, \lambda(t)$, retain the final edge $\langle \lambda(t-1), \lambda(t) \rangle$ as the new marked boundary edge; put only $\lambda(0), \dots, \lambda(t-1)$ on the cut boundary. The marked prime end is $p = \lambda(t-1)$, approached through the retained edge. At a frozen prefix the unqueried face is

incident to the stopping tip $q = \lambda(t)$, which remains an interior vertex. The faces incident to the newly cut boundary vertices already have their bank colors fixed. This convention preserves the sampled cells and their adjacencies, and p and q are at most one lattice edge apart.

Step 4. Cut and retain the target component. Cut completed segments along their full length, and unfinished prefixes as in Step 3, keeping their two banks separately labelled. Retain the component containing the protected cells.

Step 5. Complete the discarded components. In every other component reveal all remaining cell colors, ordered by the horizontal and then vertical coordinates of their centers, and record the resulting connections. These components are *completed*.

Step 6. Update the starts and repeat. Retire starts whose pairing is determined. Remove every marked edge not incident to the target component, storing its labels and connections with the completed components; a frozen tip removed this way is called *swallowed*. Keep the surviving frozen tips on the active list, relist the color changes on the target boundary, and return to Step 2.

The *transcript* records the ordered sequence of reveals and colors, traced segments, labels, and connections.

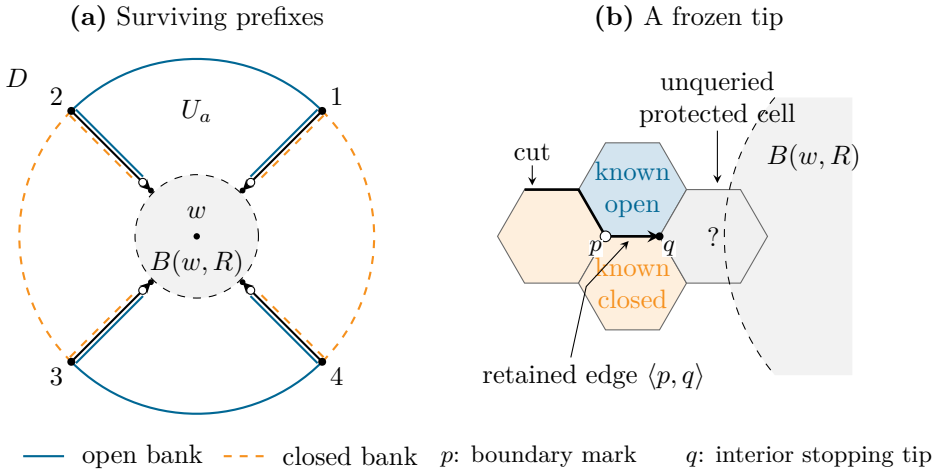


Figure 4: The exploration stops before querying a protected cell. (a) Four surviving prefixes, with their original start labels and separately retained banks; the shaded disk remains in the target component U_a. (b) At a frozen prefix, $p = \lambda(t-1)$ is the boundary mark and $q = \lambda(t)$ remains interior. The edge $\langle p, q\rangle$ is retained, while the next unknown face meets $\overline{B(w,R)}$. The lattice scale and bank separation are exaggerated.

Exploration invariants. We verify after every update that the protected cells lie in one component, that this component is simply connected, that its boundary faces have known colors and all its other faces are unrevealed, and that its boundary color changes are exactly its live marked edges. Here a start label is *live* until it is paired or assigned to a completed component; relisting transports the existing labels and creates no new ones.

First, Lemma D.1 shows that the inner-cell disk is connected, has no holes, and has one simple boundary cycle when a/d is sufficiently small. The initial boundary word supplies precisely its marked color changes, and the protected cells are separated from this frontier.

The induction uses the *three-face rule*: at a honeycomb vertex with specified face colors,

either zero or two incident edges separate opposite colors. An incoming interface edge therefore has a unique outgoing interface edge once the third face is known. In any completion of the unqueried colors, the boundary interfaces are disjoint simple chords as in subsection 7.1; thus every stored prefix is a segment of such a chord. This observation is only a geometric verification: the algorithm uses the recorded colors alone.

Consider the interior endpoint of a retained edge. Its two bank colors are known and opposite. If its third face is unknown and unprotected, reveal it; if known, use its color. The three-face rule chooses the next edge and leaves the unused edge between equal-colored faces. Put the old endpoint on the cut and retain the new edge. All three faces at the newly cut vertex are now known: the two banks keep their opposite colors, and the old color change is transported to the new marked edge without creating any other change. Consecutive cells along either bank are equal or share the unused edge, so each bank is a connected monochromatic cell chain. If the third face is protected, reveal no color and make no further cut; freeze the existing marked edge.

A prefix cannot meet an interior vertex of a previously traced interface, including its own prefix: that would require three interface edges at the contact vertex. Nor can it terminate at an unmarked incoming boundary edge, whose incident boundary faces have the same color. A genuine boundary meeting therefore joins the current prefix to another marked start or retained prefix. Concatenate the known portions and retire their original start labels. At the pairing, the second prefix is read in reverse, so its bank colors match the adjacent boundary arcs. Cutting the completed chord removes exactly the two paired color changes; the other changes are inherited by the resulting components. This also explains why touching a known bank cell is a continuation, rather than a stop followed by relisting.

Every newly cut interior vertex has all three incident face colors known. Hence the cut avoids the closure of every protected cell; the next vertex adjacent to a protected face stays interior by the retained-edge convention. The protected cells form an edge-connected set, because they meet the connected disk and honeycomb faces meeting at a vertex share an edge. They therefore remain in one component. For simple connectedness, adjoin all cuts to the original exterior in the Riemann sphere. This closed set remains connected, since every added segment starts on the existing boundary. A Jordan loop in a complementary component cannot enclose any of this connected exterior, which contains infinity; its entire interior belongs to the same component. Thus every component is simply connected, including those with slit boundaries. Completing a discarded component adjoins its closure to the same exterior and preserves this argument for the target component.

Remove precisely the marked edges not incident to the retained component, recording their labels and connections. Boundary colors agree at every gluing point by the local rule just checked, so no additional color change appears. Every face revealed during a continuation touches a vertex that has become part of the cut; it consequently remains a boundary face if retained. Additional reveals during completion lie in discarded components. This proves all four invariants and preserves the full stored paths of the surviving prefixes. The resulting domain reductions are those of [14, Section 3.1.2, p. 12].

Termination and the remaining domain. The original sets of cells, directed edges, and start labels are finite. The sum of the numbers of unqueried cells, untraced directed edges, live labels, and unfrozen live labels is a nonnegative integer. Every reveal, continuation, freezing, or pairing strictly decreases it: these operations use a new cell or directed edge, remove an unfrozen label, or retire paired labels. A frozen label never becomes unfrozen, since its next required face remains protected and unknown. Each prefix is a segment of a simple chord, so it cannot retrace an edge before a pairing is recorded. Completion only reveals additional cells and retires any labels it contains; every discarded component is processed

once. Completion and relisting cannot increase the potential, and their finite bookkeeping is performed only after a step that decreases the potential. The procedure terminates, and all surviving tips are frozen.

Denote the remaining domain by U_a and its ordered colored arcs, marked boundary edges, and arc labels by $\mathcal{B}_a$. The boundary of U_a consists of honeycomb edges and vertices, including the two sides of each slit. Its corresponding graph is a simply connected lattice subgraph in the precise sense of [14, Section 3.1.1, p. 11]; this definition permits slit boundaries and does not require a Jordan boundary. The verified boundary-face invariant gives exactly the percolation model of [14, Section 6.1.2]. Distinct surviving prefixes are vertex-disjoint paths from their original frontier starts; two may be the disjoint endpoint portions of the same eventual chord.

Represent each remaining mark by the boundary endpoint p of its retained edge. Enlarging a fixed cell-geometry constant C_{lat} to include that edge, we have

$$B(w, R - C_{\mathrm{lat}}a) \subset U_a \subset D, \qquad \big||p - w| - R\big| \le C_{\mathrm{lat}}a$$

for every remaining mark p. Each mark has an access path to $B(w, R - C_{\mathrm{lat}}a)$, starting through its retained edge and lying in U_a except at p, of diameter at most $3C_{\mathrm{lat}}a$. This follows from stopping immediately before the first protected cell. If there are no tips, the remaining boundary has one color. Its arc-partition space is a singleton: the empty partition for a closed boundary, or the one-block partition of the single open boundary arc for an open boundary. Call its unique state s_{triv} the *neutral remaining record*. For every allowed ellipse size, shape, and orientation its law is the unit point mass $\delta_{s_{\mathrm{triv}}}$. Its second angular coefficient and angular defect are therefore zero. The completion below still retains all original frontier colors and connections through the stored transcript.

Let $\mathcal{T}_a$ be the full transcript and Π_a its law under $\mathbb{P}^{a,\mathcal{B}}$. Write τ for a possible value, and $U_a(\tau), \mathcal{B}_a(\tau)$ for its remaining domain and boundary data. In addition to the information above, store all original frontier labels and colors. Store the open-connectivity relation through revealed cells on the union of the original open labels and the remaining open-arc labels. Connections recorded when tips were swallowed are included. The dependence of Π_a on $\mathcal{B}, w$ is suppressed.

Given a remaining arc partition s, combine it with the stored exterior relation by taking the smallest equivalence relation containing both. Restrict to the original open frontier labels and append their stored colors. Call the resulting record $C_a(\tau)(s)$. For a complex measure m on the remaining partitions, its completed measure is

$$(mC_a(\tau))(t) = \sum_{s : C_a(\tau)(s) = t} m(s)$$

for each original record t. The triangle inequality gives $\|mC_a(\tau)\|_{\mathrm{var}} \le \|m\|_{\mathrm{var}}$.

Lemma 8.1 (Exact completion identity)**.** *At fixed $a, \mathcal{B}, w, R$, the common-color coupling gives the same realized transcript $\mathcal{T}_a$ for every allowed ellipse size, shape, and orientation. This is the common transcript; its law Π_a is independent of those ellipse parameters. Before any ellipse is forced closed, conditional on $\mathcal{T}_a$, all unrevealed cells are independent fair cells. With the remaining arc-partition measure defined as in subsection 7.2,*

$$\Delta^{a,D,\mathcal{B}}_{r,b,e}(w) = \int \Delta^{a,U_a(\tau),\mathcal{B}_a(\tau)}_{r,b,e}(w) C_a(\tau)\, \Pi_a(d\tau), \tag{8.1}$$

$$\|\Delta^{a,D,\mathcal{B}}_{r,b,e}(w)\|_{\mathrm{var}} \le \int \|\Delta^{a,U_a(\tau),\mathcal{B}_a(\tau)}_{r,b,e}(w)\|_{\mathrm{var}}\, \Pi_a(d\tau). \tag{8.2}$$

Proof. Use the same sampled colors for every forced ellipse, as in subsection 4.1. All reveals occur outside every ellipse, so the decisions and transcript agree. For a feasible transcript, replay the deterministic exploration with its recorded colors. Every reveal, cut, discarded component, and stopping decision is then the same for every assignment of the unqueried colors. The transcript event therefore fixes exactly the queried colors and imposes no condition on the others. Under the product law, the remaining colors are consequently independent and fair, also after all cells in completed components have been revealed. A related exploration leaving specified cells unobserved appears in [1, proof of Lemma 2.1].

Every known open boundary arc is connected along its bank. The operation $C_a(\tau)$ therefore recovers precisely the original frontier connections, including connections through completed components. Conditional expectation commutes with the angular integrals, since their integrands are bounded and the transcript law is common to both radii and all angles. This proves (8.1). The contraction just proved gives (8.2). □

8.2 Number and separation of the remaining tips

Let k_a be the number of surviving frozen tips, represented by the boundary endpoints $p_1^a, \dots, p_{k_a}^a$ of their retained edges, as above. Put

$$\operatorname{sep}_a = \min_{i<j} |p_i^a - p_j^a|,$$

with $\operatorname{sep}_a = +\infty$ when $k_a < 2$. In this subsection probabilities are under the unforced lattice law $\mathbb{P}^{a,\mathcal{B}}$.

For this estimate, sample the remaining cells without closing an ellipse. Each frozen prefix belongs to a boundary-to-boundary interface reaching $B(w, R + C_{\mathrm{lat}}a)$. Each such full chord supplies at most two prefixes. Distinct chords supply a fixed positive fraction of that many disjoint open crossings of

$$B(w, 4R) \setminus \overline{B(w, 2R)}.$$

Its cells are separated from the prescribed frontier. The finite-mesh RSW and BK argument of subsection 7.3 thus gives, uniformly in $\mathcal{B}, w$ and for sufficiently small a/R,

$$\mathbb{P}^{a,\mathcal{B}}(k_a > M) \le Ce^{-cM}, \qquad M = 1, 2, \dots. \tag{8.3}$$

Fix $0 < \delta < cR$, with $c > 0$ sufficiently small, and take a/δ sufficiently small. Cover the deterministic circle $\partial B(w, R)$ by at most CR/δ square boxes centered on that circle and chosen before sampling. The cover can be enlarged by a fixed factor so that two marks at distance less than δ, together with their terminal retained edges, lie in one covering disk $B(z, s)$, where $z \in \partial B(w, R)$ and $s = C_1\delta$. Put $L = R/4$, with c small enough that $2s < L/2$. The deterministic region

$$A_z(s, L) = \left(B(z, L) \setminus \overline{B(z, s)}\right) \setminus \overline{B(w, R)}$$

is a curvilinear half-annulus, with inner and outer circular arcs and two sides on the protecting circle.

Follow each of the two stored prefixes backwards from its tip to its first hit of $\partial B(z, L)$, and retain the portion after its last hit of $\partial B(z, s)$. The original frontier starts lie outside $B(z, L)$. The exploration invariants give two disjoint simple crosscuts of $A_z(s, L)$, joining its inner and outer arcs; all their bank cells are already revealed and unprotected. Orient these crosscuts from the inner to the outer arc, irrespective of their original exploration directions. Order them from left to right in this quadrilateral, and write L_i, R_i for the left and right

banks of the ith crosscut in this orientation. The two crosscuts separate the region into a left, a middle, and a right component. Other prefixes may lie between the chosen pair.

Write O, C for open and closed. The bank choices are

(L_1, R_1)	(L_2, R_2)	Selected banks	Arm colors
(O, C)	(O, C)	L_1, R_1, L_2	O, C, O
(O, C)	(C, O)	L_1, R_1, R_2	O, C, O
(C, O)	(O, C)	L_1, R_1, R_2	C, O, C
(C, O)	(C, O)	L_1, R_1, L_2	C, O, C

If the left-bank colors are opposite, the outer banks L_1, R_2 have the same color and lie in the two outer components; either middle bank supplies the opposite-colored arm. The middle banks R_1, L_2 may merge, so only R_1 is counted. If the left-bank colors agree, select L_1, R_1, L_2: the equal-colored banks L_1, L_2 lie on opposite sides of the first crosscut, and R_1 has the other color. Figure 5 shows the two cases and their possible bank coalescence.

To obtain disjoint *cell* arms, retain these bank chains between the buffered radii $2s$ and $L/2$ by the same last-departure/first-hit rule, and erase loops in each monochromatic chain. For a/s small, every retained cell lies wholly within the larger region $A_z(s, L)$, so it cannot pass around a crosscut endpoint. Its connected interior is disjoint from the honeycomb edge-path and belongs to one complementary component. The selected same-colored paths therefore cannot share a cell, while paths of opposite colors cannot share a cell in any case. These are three disjoint sampled arms across $A_z(2s, L/2)$; their cells are far from the prescribed frontier, and the protecting circle supplies no colored arm.

Two prefixes of the same eventual chord have opposite outward bank orientations and are covered by the corresponding cases above. Their stored portions are disjoint, since portions that have already joined are paired and removed. Subsequent continuation and pairing, wherever they occur, do not alter the sampled arms already extracted.

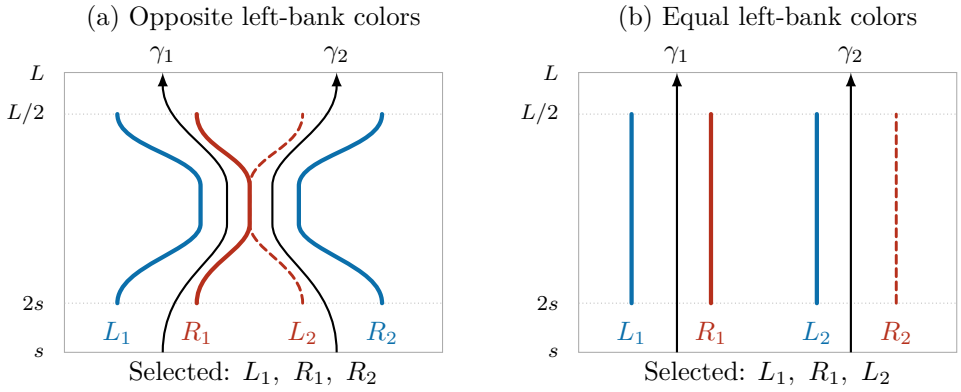


Figure 5: Bank extraction for tip separation, after straightening the exterior half-annulus $A_z(s, L)$. Black arrows orient the retained prefix crosscuts from the inner to the outer boundary. Blue banks are open and red banks closed. Solid colored paths are the selected three arms, restricted to $A_z(2s, L/2)$; dashed banks are not counted. In (a) the middle closed banks may merge, whereas in (b) the middle banks have opposite colors. Color reversal gives the other two cases. Other interfaces can lie between the displayed prefixes.

For each covering disk this is an ordinary arm event in a deterministic region outside the circle. The boundary-chart argument of subsection 4.2, applied to this circle and with colors exchanged when necessary, bounds its mesh-limit probability by $C(\delta/R)^2$; the fixed-factor

buffers change only the constant. The underlying half-plane estimate is [8, Proposition 17, p. 1585, Section 4.6, and Theorem 24(2), p. 1590]. As in subsection 4.2, take the fixed-scale mesh limit before flattening the circle; slightly displaced boundaries and a finite cover of the allowed centers make the bound uniform in w. Summing over the deterministic cover gives

$$\limsup_{a\downarrow 0} \sup_{\mathcal{B},w} \mathbb{P}^{a,\mathcal{B}}(\mathrm{sep}_a < \delta) \le C\frac{R}{\delta}\left(\frac{\delta}{R}\right)^2 = C\frac{\delta}{R}. \tag{8.4}$$

For integers $M \ge 2$, call a transcript *good* when it lies in

$$\mathsf{E}^a_{M,\delta} = \{k_a \le M,\ \mathrm{sep}_a \ge \delta\}.$$

Call its complement bad. Both events are determined by the transcript, and

$$\limsup_{a\downarrow 0} \sup_{\mathcal{B},w} \mathbb{P}^{a,\mathcal{B}}((\mathsf{E}^a_{M,\delta})^c) \le Ce^{-cM} + C\delta/R. \tag{8.5}$$

Conditioning on either event adds no information once the transcript is given. The conditional independence in Lemma 8.1 therefore still holds.

8.3 Separation after conformal mapping

For a bounded simply connected domain U containing 0, let $f_U : U \to \mathbb{D}$ be the conformal map with $f_U(0) = 0$ and $f'_U(0) > 0$. Boundary marks are prime ends, as in subsection 6.1. An approach to a boundary point along a curve in U specifies the boundary side being marked. Radial access to $p \in \partial B(0,R)$ means approach along tp, $0 \le t < 1$.

Planar Brownian motion is $B_1 + iB_2$ for independent real Brownian motions as in subsection 5.1. The *harmonic measure* of a boundary arc from 0 is the probability that this motion, starting at 0, first leaves the domain through that arc. For a prime-end arc, this is its image length under f_U divided by 2π.[3]

Lemma 8.2 (Separation of accessible boundary marks)**.** *Suppose $B(0,R) \subset U \subset B(0,L)$, where $0 < R \le L$, and U is simply connected. Let $p, q \in \partial U \cap \partial B(0,R)$ have radial access and $|p-q| \ge \delta > 0$. Both circular arcs between their images under f_U have lengths bounded below by a positive constant depending only on R, L, δ.*

Proof. The chord joining p, q is a crosscut, in the sense of subsection 4.1, whose interior lies in $B(0,R)$. Put $\delta_{\mathrm{cap}} = \delta^2/(8R)$. The smaller of the two circular caps cut off by its supporting line has depth

$$R - \sqrt{R^2 - |p-q|^2/4} \ge \delta_{\mathrm{cap}}.$$

Consequently, on either side choose a disk of radius $\delta_{\mathrm{cap}}/8$ whose closure lies in $B(0,R)$ and stays a distance at least $\delta_{\mathrm{cap}}/8$ from both the chord and the circle. Brownian motion from 0 has a probability bounded below in terms of R, δ_{cap} of reaching a concentric smaller disk before leaving $B(0,R)$. This initial part of its path may cross the chord, including when the chord passes through 0.

From the chosen disk take a straight outward path, on its side of the supporting line, to a point outside $B(0,L)$. A tube of width depending only on δ_{cap} around this path avoids the chord. By the strong Markov property and the positive probability of Brownian motion

[3] G. Lawler, *Scaling limits and SLE*, PIMS Summer School lecture notes (2010), author's notes. Section 2.4, p. 16, defines harmonic measure and states its conformal invariance. The conformal-map facts used here and below are Lawler's Propositions 4–5 (Section 2.1, p. 12) and his Proposition 6 and Theorem 1 (Section 2.2, p. 13).

staying in such a tube, there is a further lower bound depending only on $R, L, \delta_{\mathrm{cap}}$ for following the tube until leaving $B(0, L)$. If the path leaves U sooner, its first exit is through the boundary arc on the chosen side of the crosscut. Thus the probability of exit through that arc is uniformly positive. The same argument on the other side bounds both harmonic measures below. Their circular images have lengths 2π times those measures. □

For the remaining lattice domains, translate w to 0. The access paths constructed in subsection 8.1 have diameter at most $3C_{\mathrm{lat}}a$. For two δ-separated marks they lie in disjoint neighborhoods when a/δ is small. Take simple subarcs of these paths ending inside $B(0, R - C_{\mathrm{lat}}a)$, join their inner endpoints by a chord there, and erase loops. This gives a crosscut with the specified prime-end banks. It lies within distance Ca of the chord between the radial projections of the marks onto $\partial B(0, R)$. These projections are at least $\delta/2$ apart for small a. Apply the preceding construction with $\delta_{\mathrm{cap}} = \delta^2/(32R)$. Its cap disks lie inside the protected inner disk, and its outward tubes remain a fixed positive distance from the lattice crosscut once a/δ_{cap} is sufficiently small. The same Brownian argument therefore bounds both prime-end arc measures below, uniformly over these domains. The two sides of every cut keep their separate labels.

Use marked Carathéodory convergence as defined in subsection 7.1, translating the interior reference points to 0. Write $p_j^{(n)}, p_j$ for the ordered boundary marks of U_n, U, and normalize $f_n : U_n \to \mathbb{D}$ and $f : U \to \mathbb{D}$ at 0 with positive derivative. The required convergence is that of the inverse maps on compact subsets of $\mathbb{D}$ and of the marked disk coordinates. It also gives $f_n \to f$ uniformly on compact subsets of U.

Lemma 8.3 (Subsequences with separated boundary marks)**.** *For fixed M, δ, every sequence of good remaining domains with mesh tending to zero has a subsequence with a fixed number of marks and marked Carathéodory convergence. Its limiting marks are distinct, and the translated limiting domain contains $B(0, R)$.*

Proof. Let $a_n \downarrow 0$ be the meshes and translate the centers to 0. All domains lie in $B(0, 2d)$. Their inverse maps $f_n^{-1} : \mathbb{D} \to U_n$ are uniformly bounded and hence have a subsequence converging uniformly on compact subsets of $\mathbb{D}$ to an analytic map g. Their derivatives at 0 lie between $R - C_{\mathrm{lat}}a_n$ and $2d$, by the Schwarz lemma. The limit is therefore nonconstant and injective, by the conformal-map facts cited above. Set $U = g(\mathbb{D})$ and $f = g^{-1}$. The domain-convergence equivalence in [14, Section 3.2.3, p. 13] gives $B(0, R) \subset U$.

There are at most M marks. Take a further subsequence with a fixed number and cyclic labels. Lemma 8.2, with its lattice extension, separates their disk images by a fixed positive amount. A further subsequence makes every image converge to a distinct point of $\partial\mathbb{D}$. These coordinates define the limiting marked prime ends. The case of no marks requires only the domain argument. □

Theorem 8.4 (Protected exploration and marked compact exhaustion)**.** *Fix $D = B(z_0, d)$, where $z_0 \in \mathbb{C}$ and $d > 0$, $0 < \theta < 1/64$, and $0 < e_- \le e_+ < 1$. Put $R = \theta d$. For $w \in B(z_0, d/4)$ and a prescribed frontier word $\mathcal{B}$, use the protected exploration of subsection 8.1. Its allowed ellipses are those of subsection 4.3, with $e \in [e_-, e_+]$, arbitrary orientation, and $(1 + e_+)r < R/10$; the defect compares r with br for $b \in [1/2, 1]$. Let k_a and sep_a be as in subsection 8.2, with $\mathrm{sep}_a = \infty$ if $k_a < 2$. Then:*

(i) ***Exploration and completion.*** *The exploration terminates, leaves all protected cells unqueried, and has a common transcript for all allowed ellipses. Conditional on this transcript, the unrevealed cells are independent fair cells under the unforced law. The remaining domain U_a is simply connected and, for a fixed lattice constant C_{lat} and*

sufficiently small a/R, satisfies

$$B(w, R - C_{\mathrm{lat}}a) \subset U_a \subset D, \qquad \big||p - w| - R\big| \le C_{\mathrm{lat}}a$$

for each retained-edge mark p. Each mark has an access path, through its retained edge, to $B(w, R - C_{\mathrm{lat}}a)$ of diameter at most $3C_{\mathrm{lat}}a$. The completion map is a contraction in variation norm and satisfies (8.1)–(8.2). With no marks, the remaining arc-partition record is the neutral state s_{triv} defined in subsection 8.1, and its angular defect is zero; the original frontier colors and connections remain in the transcript used for completion.

(ii) ***Tip bounds.*** *There are constants $C, c > 0$, independent of the word and center, such that under the law before closing an ellipse,*

$$\mathbb{P}^{a,\mathcal{B}}(k_a > M) \le Ce^{-cM}, \qquad \limsup_{a\downarrow 0} \sup_{\mathcal{B},w} \mathbb{P}^{a,\mathcal{B}}(\mathrm{sep}_a < \delta) \le C\delta/R. \tag{8.6}$$

The first bound holds for every integer $M \ge 1$ and sufficiently small a/R; the second holds for every fixed $0 < \delta < cR$. The suprema run over all prescribed words at mesh a and all $w \in B(z_0, d/4)$.

(iii) ***Marked compactness.*** *For every fixed integer $M \ge 2$ and $0 < \delta < cR$, every sequence of remaining domains with $a \downarrow 0$, $k_a \le M$, and $\mathrm{sep}_a \ge \delta$, translated by $-w_a$, has a marked Carathéodory convergent subsequence with a fixed number and cyclic order of marks. Its limit contains $B(0, R)$ and has distinct marked prime ends. The frontier words and centers may vary along the sequence. With no marks, the conclusion is ordinary Carathéodory convergence.*

All constants may depend on the fixed θ, e_-, e_+, but not on the word, center, mesh, or allowed ellipse parameters.

Proof. The exploration invariants, termination argument, and retained-edge geometry in subsection 8.1 give the domain and access assertions in (i), including the neutral case. Lemma 8.1 proves the common-transcript, conditional-independence, and completion assertions. Equations (8.3) and (8.4) give (ii) under the unforced law. Lemma 8.3, using the lattice extension of Lemma 8.2, gives (iii) with the stated freedom to vary words and centers. □

8.4 A uniform estimate for the remaining domains

Let $\mathcal{K}^a_{M,\delta}$ consist of all triples $(U_a, \mathcal{B}_a, w)$ produced by good transcripts at mesh a, over the prescribed words and centers fixed in subsection 8.1. Thus the center and the ordered colored boundary data are part of each element.

Proposition 8.5 (Uniform bound for separated marks)**.** *Fix $M, \delta, r, R > 0$ in the ranges above, with r/R sufficiently small. Then*

$$\limsup_{a\downarrow 0} \sup_{(U_a,\mathcal{B}_a,w)\in\mathcal{K}^a_{M,\delta}} \sup_{e\in[e_-,e_+],\ b\in[1/2,1]} \|\Delta^{a,U_a,\mathcal{B}_a}_{r,b,e}(w)\|_{\mathrm{var}} \le C(r/R)^{9/4}. \tag{8.7}$$

The constant is independent of M, δ. The mesh needed to approach this upper bound may depend on M, δ, r.

Proof. 1. The conditional lattice model. Fix a realizable transcript τ. The exploration choices are functions of the colors already known, so the event $\{\mathcal{T}_a = \tau\}$ specifies only the colors actually revealed in that transcript. If J is any set of its unrevealed cells and σ is any color assignment on J, independence gives

$$\mathbb{P}^{a,\mathcal{B}}\{\omega|_J = \sigma \mid \mathcal{T}_a = \tau\} = 2^{-|J|}.$$

This remains true for a good transcript: whether it is good is already determined by τ. The boundary-edge convention in subsection 8.1 makes $U_a(\tau)$ a simply connected honeycomb subgraph with alternating fixed boundary-face colors, exactly as in [14, Sections 3.1.1–3.1.2 and 6.1.2]. Subsequent interface exploration has the same domain Markov property. The two slit banks are distinct boundary sides, not additional sampled faces. Stored exterior connections enter only the completion map $C_a(\tau)$; they impose no conditioning on the remaining link pattern.

2. A deterministic convergent sequence. Let C_0 be the constant furnished by subsection 7.4 with available interior radius $R/2$, absorbing the resulting fixed power of 2. If (8.7) with $C = C_0$ fails, choose $\eta > 0$, meshes $a_\ell \downarrow 0$, good transcript values τ_ℓ, and parameters w_ℓ, e_ℓ, b_ℓ such that

$$\|\Delta^{a_\ell, U_\ell, \mathcal{B}_\ell}_{r, b_\ell, e_\ell}(w_\ell)\|_{\mathrm{var}} > C_0(r/R)^{9/4} + \eta, \qquad (U_\ell, \mathcal{B}_\ell) = (U_{a_\ell}(\tau_\ell), \mathcal{B}_{a_\ell}(\tau_\ell)).$$

The selected domains and their conditional color laws are now deterministic. Domains with no marks give zero and can be omitted. Lemma 8.3 supplies a subsequence with a fixed even number $2m \le M$ of marks. Translate w_ℓ to 0. The domains lie in $B(0, 2d)$, contain $B(0, R - C_{\mathrm{lat}} a_\ell)$, and converge in the marked Carathéodory sense to a domain U containing $B(0, R)$. Their normalized maps f_ℓ have inverse maps converging locally uniformly in $\mathbb{D}$, and their marked disk coordinates have distinct limits. The distinctness follows from Lemma 8.2. Pass also to convergent subsequences of e_ℓ, b_ℓ.

3. Applying the verified convergence criterion. Step 1 identifies the conditional law on each remaining domain as an unconditioned member of the percolation family in Lemma 7.3. That lemma verifies hypotheses K1–K5 of Theorem 7.2 for this model family on every prescribed translated lattice sequence, including the sequence selected here. Step 2 verifies the remaining hypothesis K6. In particular, the auxiliary close inner approximations required by K5 have already been constructed on every prescribed translated mesh sequence.

Theorem 7.2 now gives joint convergence of the complete labelled curves in disk coordinates, positive limiting pattern probabilities, and convergence after conditioning on each pattern. Lemma 7.3 identifies the conditional limit as the unique global multiple SLE_6 law.

4. Interior events and the row limit. Relabel the remaining open arcs in cyclic order. Their partition space is then fixed and finite. The bound $5/e_-$ permits a further subsequence on which every mass of the angular row converges; call the limit Δ_*. Original frontier labels remain in the completion map.

Choose a common buffer radius $R_0 \in [M_0 r, 2M_0 r]$ as in Lemma 7.4, avoiding atoms of the truncated minimum distances of all limiting curves and all lattice curves in this countable sequence. Require $2M_0 r < R/128$. To check continuity despite the rough outer boundary, choose $2M_0 r < L < R/2$ and, in the translated coordinates, set

$$\chi_\ell(z) = \min\{L, |f_\ell^{-1}(z)|\}, \qquad z \in \mathbb{D}.$$

Extend χ_ℓ by L to $\partial\mathbb{D}$, and define χ analogously from the limiting map. The nonconstant parts lie in a common compact subset of $\mathbb{D}$: for large ℓ, the Schwarz lemma on $B(0, R/2) \subset U_\ell$ gives

$$|f_\ell(u)| \le 2|u|/R, \qquad |u| \le L.$$

Local uniform convergence of the inverse maps therefore yields uniform convergence $\chi_\ell \to \chi$ on $\overline{\mathbb{D}}$. The minimum of such a function along a curve is continuous for the uniform curve metric modulo reparametrization. The atom-free choice of R_0 gives convergence of the buffer-avoidance indicators and of the buffer counts.

The ellipse sizes remain positive in this mesh limit. On a compact neighborhood of these targets, f_ℓ and their derivatives converge uniformly, and the ellipses with parameters e_ℓ, b_ℓ are bracketed by arbitrarily small offsets of the limiting ellipses. The cell-contact convention contributes only an additional $O(a_\ell)$ offset. Lemma 7.4 proves the required joint hitting continuity for these offsets, including in the rough complementary components of retained limiting curves. Its bounded-convergence argument also gives convergence of the angular integral. Consequently Δ_* has decomposition (7.2), with the actual limiting pattern weights and retained marginals. The limiting joint law is disintegrated after these joint observables have been passed to the limit.

5. Uniformity of the estimate. The remainder in (7.2) is bounded before summing pairs by the probability that at least three interfaces enter the buffer. Its six-arm estimate and the interface-count moment bounds of subsection 7.3 use only annuli inside $B(0, R/2)$. Those cells retain their independent fair colors even after the transcript has been fixed. Subsection 7.4 therefore bounds the limiting pair sum and remainder by

$$\|\Delta_*\|_{\mathrm{var}} \le C_0(r/R)^{9/4}.$$

This constant is independent of the number or separation of the marks. Since the partition space is finite, coordinatewise convergence of the rows implies convergence of their variation norms, contradicting the fixed excess η.

□

Remark (Uniformity and boundary topology). The parameters M, δ select the compact family of marked domains and may affect the mesh threshold in Proposition 8.5; its limiting angular bound is independent of them. Sequential compactness proves this bound without a uniform convergence rate or a lower bound on pattern probabilities uniform over M, δ. The auxiliary close inner approximations in hypothesis K5 concern the model family, not close approximation of the actual residual domains.

Karrila's Theorem 4.2 [15, Sections 4.1–4.3] compares disk-coordinate and physical-plane limits of entire curves. Beyond marked Carathéodory convergence and one-curve crossing control, its requirements are a bounded limiting domain, uniformly bounded areas, radial limits at the marked endpoints, and close approximation of those endpoints. Close approximation includes Euclidean convergence and local access to the appropriate separating crosscuts. Those endpoint conditions would be needed for the physical-curve upgrade. Theorem 7.2 and the compact-interior argument above provide the disk-coordinate convergence used in Proposition 8.5.

8.5 Passing to the complete frontier record

Split (8.2) into good and bad transcripts. On the bad transcripts use the bound $5/e_-$ from subsection 8.1. On the good transcripts use Proposition 8.5. Equations (8.2) and (8.5) give

$$\limsup_{a\downarrow 0} \sup_{\mathcal{B},w,e,b} \|\Delta^{a,D,\mathcal{B}}_{r,b,e}(w)\|_{\mathrm{var}} \le C(r/R)^{9/4} + \frac{5}{e_-}\left(Ce^{-cM} + C\delta/R\right). \tag{8.8}$$

Every supremum uses the ranges of subsection 8.1. Keep r, R fixed, let $M \to \infty$, and then let $\delta \downarrow 0$. Since $R = \theta d$, this proves, for every sufficiently small fixed r/d,

$$\limsup_{a\downarrow 0} \sup_{\mathcal{B},w,e,b} \|\Delta^{a,D,\mathcal{B}}_{r,b,e}(w)\|_{\mathrm{var}} \le C(r/d)^{9/4}. \tag{8.9}$$

Averaging over the prescribed words with their original probabilities gives the same estimate for $\Delta^{a,D}_{r,b,e}(w)$. The complete record contains the word, so different words give disjoint sets of

output records. Any fixed exterior completion also preserves the bound by the contraction in subsection 4.1.

Order of limits. For ellipse-source limits, the mesh tends to zero at fixed positive radii and separated marked points; the radii then tend jointly to zero at arbitrary relative rates. Auxiliary cutoffs are removed at the stages specified in each proof. For the frontier estimate above, the order is

$$\text{fix } r, R; \quad \text{fix } M, \delta; \quad a \downarrow 0; \quad M \uparrow \infty,\ \delta \downarrow 0; \quad r \downarrow 0. \tag{8.10}$$

Thus the bad-transcript errors vanish before division by r^2 in the comparison of the measures Q. The proof requires no rate of convergence in the mesh. Section 9 uses this bound to compare different ellipse radii.

9 Limits as the ellipse radii tend to zero

We use the limit convention of subsection 8.5, the angular measures Q of subsection 4.3, and the variation norm of subsection 4.1.

9.1 Comparing arbitrary small radii

Fix $D = B(z_0, d)$, with $z_0 \in \mathbb{C}$ and $d > 0$. Let $w \in B(z_0, d/4)$ and $e \in [e_-, e_+] \subset (0, 1)$. Choose $r_0 = c_* d$, with $c_* > 0$ small enough for (8.9). All suprema over w, e below are taken over these ranges. These complex measures are the rows defined in subsection 4.1.

Fix $0 < r \le \epsilon \le r_0$. Choose an integer $n \ge 0$ such that $2^{-n-1}\epsilon < r \le 2^{-n}\epsilon$, and put $r_j = 2^{-j}\epsilon$. Then $r = b r_n$ for $b \in (1/2, 1]$. In the next identity abbreviate $Q_\rho = Q^{a,D}_{\rho,e}(w)$. At each fixed mesh these measures have the same record space, and

$$Q_r - Q_\epsilon = (Q_r - Q_{r_n}) + \sum_{j=0}^{n-1} (Q_{r_{j+1}} - Q_{r_j}). \tag{9.1}$$

For $0 < s \le r_0$ and $b \in [1/2, 1]$, subsection 8.1 gives $\Delta^{a,D}_{s,b,e}(w) = s^2(Q^{a,D}_{s,e}(w) - Q^{a,D}_{bs,e}(w))$. Divide (8.9) by the larger radius squared in each term. The sum is finite for fixed r, ϵ. After taking $\limsup_{a\downarrow 0} \sup_{w,e}$, the triangle inequality bounds its norm by

$$C d^{-2} (\epsilon/d)^{1/4} \sum_{j=0}^{n} 2^{-j/4} \le \frac{C}{1 - 2^{-1/4}} d^{-2} (\epsilon/d)^{1/4}. \tag{9.2}$$

Taking the supremum over r only after this mesh upper limit gives

$$\sup_{0<r\le\epsilon} \limsup_{a\downarrow 0} \sup_{w,e} \|Q^{a,D}_{r,e}(w) - Q^{a,D}_{\epsilon,e}(w)\|_{\mathrm{var}} \le C d^{-2} (\epsilon/d)^{1/4}. \tag{9.3}$$

The final comparison uses every $b \in (1/2, 1]$. Comparisons only at successive halvings would allow a periodic oscillation in $\log_2 r$.

Each law in the angular integral defining Q has mass one. Thus $\|Q^{a,D}_{r_0,e}(w)\|_{\mathrm{var}} \le e_-^{-1} r_0^{-2}$. Comparing with this reference radius in (9.3) yields

$$\sup_{0<r\le r_0} \limsup_{a\downarrow 0} \sup_{w,e} \|Q^{a,D}_{r,e}(w)\|_{\mathrm{var}} \le C d^{-2}. \tag{9.4}$$

9.2 A space for the limits

For the fixed disk D, write $S_a(D)$ for the finite complete frontier-record space of subsection 4.1. Consider families $v = (v^a)_{a>0}$ of complex measures on these spaces with

$$\|v\|_{D,*} := \limsup_{a\downarrow 0} \|v^a\|_{\mathrm{var}} < \infty. \tag{9.5}$$

Quotient these families by the subspace of zero seminorm, and let $\mathcal{V}_D$ be the Banach completion of the resulting normed space [31, Theorem 2.3-2, pp. 69–70]. We identify the quotient with its dense isometric image and keep the notation $\|\cdot\|_{D,*}$ for the extended norm. All measure differences are taken at the same mesh.

Write $Q_{r,e}(w)$ for the element represented by the family $(Q^{a,D}_{r,e}(w))_{a>0}$. For a prescribed frontier word $\mathcal{B}$, use the conditional angular rows $Q^{a,D,\mathcal{B}}_{r,e}(w)$ of subsection 4.3. For families $v = (v^{a,\mathcal{B}})_{a,\mathcal{B}}$, repeat the quotient and completion construction with

$$\|v\|^{\mathrm{unif}}_{D,*} := \limsup_{a\downarrow 0} \sup_{\mathcal{B}} \|v^{a,\mathcal{B}}\|_{\mathrm{var}}.$$

The supremum runs over all prescribed frontier words at mesh a.

Theorem 9.1 (Complete-record angular stabilization)**.** *Fix $D = B(z_0, d)$, where $z_0 \in \mathbb{C}$ and $d > 0$, $0 < e_- \le e_+ < 1$, and a protected-radius ratio $0 < \theta < 1/64$. There are constants $c_*, C > 0$, depending only on θ, e_-, e_+, with $c_* < \theta/[10(1+e_+)]$, for which the following holds. Put $r_0 = c_* d$ and use the complete-record angular rows and defects of subsection 4.3. All suprema below range over $w \in B(z_0, d/4)$, $e \in [e_-, e_+]$, and, where present, $b \in [1/2, 1]$.*

For every $0 < r \le r_0$,

$$\limsup_{a\downarrow 0} \sup_{w,e,b} \|\Delta^{a,D}_{r,b,e}(w)\|_{\mathrm{var}} \le C(r/d)^{9/4}. \tag{9.6}$$

For every $0 < \epsilon \le r_0$,

$$\sup_{0<r\le\epsilon} \limsup_{a\downarrow 0} \sup_{w,e} \|Q^{a,D}_{r,e}(w) - Q^{a,D}_{\epsilon,e}(w)\|_{\mathrm{var}} \le Cd^{-2}(\epsilon/d)^{1/4}. \tag{9.7}$$

Both estimates also hold for the conditional rows when the supremum over all frontier words $\mathcal{B}$ at mesh a is taken inside the mesh upper limit, together with the displayed suprema over w, e, b or w, e.

For each fixed e, w, $Q_{r,e}(w)$ therefore converges as $r \downarrow 0$ through arbitrary positive radii to an element $T_{D,e}(w) \in \mathcal{V}_D$, and

$$\|Q_{r,e}(w) - T_{D,e}(w)\|_{D,*} \le Cd^{-2}(r/d)^{1/4}, \qquad \|T_{D,e}(w)\|_{D,*} \le Cd^{-2}, \qquad 0 < r \le r_0. \tag{9.8}$$

The conditional families converge in the completion for $\|\cdot\|^{\mathrm{unif}}_{D,*}$ and satisfy the same bounds. The shape parameter e remains part of these local limits.

Proof. The transfer to the complete frontier record in (8.9) gives (9.6), including its conditional version. The finite telescoping sum (9.1) and bound (9.2) give (9.7), as recorded in (9.3). This argument compares every smaller radius with the reference radius. It applies unchanged with the supremum over frontier words inside the mesh upper limit.

In either completion, the comparison bound makes the family Cauchy as both radii tend to zero. Completeness gives its limit. For fixed r, let the smaller radius tend to zero in (9.7), with $\epsilon = r$, to obtain the first bound in (9.8). The reference-radius estimate (9.4) gives the second. Its proof uses only the mass-one bound for the conditional or unconditioned laws and the same radius comparison, so it applies in both norms. □

Let s range over the input records and t over a finite set of output records. A randomized exterior completion is specified by numbers $P_a(s,t) \ge 0$ with $\sum_t P_a(s,t) = 1$. It acts by

$$(v^a P_a)(t) = \sum_s v^a(s) P_a(s,t), \qquad \|v^a P_a\|_{\mathrm{var}} \le \sum_{s,t} |v^a(s)| P_a(s,t) = \|v^a\|_{\mathrm{var}}.$$

A fixed family (P_a) therefore descends to a linear contraction between the quotient spaces and extends uniquely to their Banach completions, with norm at most one [31, Theorem 2.7-11, pp. 100–101].

Subsection 9.3 treats scalar values assigned to the records, using the fixed-radius mesh-limit assumption stated there.

9.3 Joint limits for several ellipses

Fix an integer $m \ge 1$, disjoint disks $D_j = B(c_j, d_j)$, centers $w_j \in B(c_j, d_j/4)$, and parameters $e_j \in [e_-, e_+]$. Write

$$\mathbf{w} = (w_1, \dots, w_m), \qquad \boldsymbol{r} = (r_1, \dots, r_m), \qquad Q_j^a(r_j, w_j) = Q_{r_j, e_j}^{a, D_j}(w_j), \quad 0 < r_j \le c d_j.$$

The disks stay fixed when the centers move. Additional observation points, if present, are denoted $\mathbf{z} = (z_1, \dots, z_n)$, for an integer $n \ge 1$. They are integrated against a fixed smooth function $\psi(\mathbf{z})$ of compact support $\operatorname{supp}\psi = \overline{\{\mathbf{z} : \psi(\mathbf{z}) \ne 0\}}$. Require every z_i on this support to lie outside $\bigcup_j \overline{D_j}$. With no additional points, omit this integration and take $\psi = 1$.

At mesh a, let $s_j \in S_a(D_j)$ for $1 \le j \le m$. An exterior observation assigns a complex value $g_\psi^a(s_1, \dots, s_m)$ to each such record tuple, after any integration against ψ. It defines

$$\mathcal{J}_\psi^a(v_1, \dots, v_m) = \sum_{s_1, \dots, s_m} g_\psi^a(s_1, \dots, s_m) \prod_{j=1}^m v_j(s_j),$$

where v_j is a complex measure on $S_a(D_j)$. This is an m-linear functional, meaning a complex-valued map linear in each argument separately. Assume

$$|\mathcal{J}_\psi^a(v_1, \dots, v_m)| \le C_\psi \prod_{j=1}^m \|v_j\|_{\mathrm{var}}, \tag{9.9}$$

for all sufficiently small meshes, uniformly in any additional positive parameters used to approximate the exterior observation. The coefficients g_ψ^a are independent of the ellipse radii and centers. For a bounded function F of the completed records, averaging F over the exterior colors gives $|g_\psi^a| \le \sup|F|$ when no additional integration is present. The displayed bound then follows directly from the finite sum.

Keep any additional approximation parameters fixed in the mesh limit. Assume that, for every fixed positive radius tuple and every allowed center tuple, the scalar limit

$$f_{\boldsymbol{r}}(\mathbf{w}) := \lim_{a \downarrow 0} \mathcal{J}_\psi^a(Q_1^a(r_1, w_1), \dots, Q_m^a(r_m, w_m)) \tag{9.10}$$

exists. We call this the *tested correlation*. The shape parameters and ψ are kept fixed and suppressed in its notation.

For two tuples of rows $(v_1, \dots, v_m)$ and $(u_1, \dots, u_m)$, multilinearity gives

$$\mathcal{J}_\psi^a(v_1, \dots, v_m) - \mathcal{J}_\psi^a(u_1, \dots, u_m) = \sum_{j=1}^m \mathcal{J}_\psi^a(u_1, \dots, u_{j-1}, v_j - u_j, v_{j+1}, \dots, v_m). \tag{9.11}$$

Apply (9.3) to the changed row, (9.4) to the other rows, and (9.9) to each term. There are finitely many terms, so these estimates bound the mesh upper limit of their sum. For $0 < r_j \le \epsilon_j \le cd_j$ this gives

$$\sup_{\mathbf{w}} |f_{\boldsymbol{r}}(\mathbf{w}) - f_{\boldsymbol{\epsilon}}(\mathbf{w})| \le C_\psi \sum_{j=1}^{m} \epsilon_j^{1/4}, \qquad \boldsymbol{\epsilon} = (\epsilon_1, \dots, \epsilon_m), \tag{9.12}$$

where the fixed disk radii are absorbed into C_ψ.

Compare any two small radius tuples through their coordinatewise minimum. Equation (9.12) makes their pairwise differences tend to zero uniformly over the allowed centers. Hence

$$f(\mathbf{w}) := \lim_{\max_j r_j \downarrow 0} f_{\boldsymbol{r}}(\mathbf{w}), \qquad \sup_{\mathbf{w}} |f_{\boldsymbol{r}}(\mathbf{w}) - f(\mathbf{w})| \le C_\psi \sum_{j=1}^{m} r_j^{1/4}.$$

The same comparison applies when only a subset of radii changes. Thus every successive order of taking these limits exists and gives f. Sections 15–16 will verify these assumptions for the observations introduced in Section 10.

9.4 Dependence on the centers

Let $O \subset \mathbb{C}^m$ be an open set on which the hypotheses of subsection 9.3 hold locally for a common family $f_{\boldsymbol{r}}$. Fix a compact set $\mathscr{C} \subset O$ of *separated configurations*: the distances $|w_i - w_j|$, $i \ne j$, and $|w_i - z_\ell|$, for $\mathbf{z} \in \operatorname{supp} \psi$, have a common positive lower bound on $\mathscr{C}$. Omit the latter condition when there are no additional points. Write

$$|\mathbf{w} - \mathbf{w}'| := \max_j |w_j - w_j'|.$$

Near each tuple, keep one choice of the disks D_j fixed throughout a comparison. Finitely many such neighborhoods cover $\mathscr{C}$. For all sufficiently small $\delta_w > 0$, any two tuples of $\mathscr{C}$ at distance at most δ_w lie in one of these neighborhoods.

The four-arm probability α_4 defined in subsection 4.2 satisfies

$$\alpha_4(s,t) \le C_p (s/t)^p, \qquad 0 < s < t, \quad 1 < p < 5/4,$$

by [7, Theorem 4 and (9), journal p. 736]. Choose $\epsilon > 0$ small enough for every disk choice in this cover. Take $0 < r_j \le \epsilon$ and $\delta_w > 0$ small enough that $\delta_w < c\epsilon$ and the preceding neighborhood condition holds. Comparing each radius tuple with $(\epsilon, \dots, \epsilon)$ gives an error of at most $C_\psi \epsilon^{1/4}$ by (9.12). Move the centers one at a time at this fixed radius. Equation (4.13) and the four-arm bound give a row difference of at most $C_p \delta_w \epsilon^{p-3}$ after taking the mesh limsup. The other rows are bounded by (9.4). The finite cover makes the constants uniform on $\mathscr{C}$, so

$$\limsup_{\max_j r_j \downarrow 0} \sup_{\substack{\mathbf{w},\mathbf{w}' \in \mathscr{C} \\ |\mathbf{w}-\mathbf{w}'| \le \delta_w}} |f_{\boldsymbol{r}}(\mathbf{w}) - f_{\boldsymbol{r}}(\mathbf{w}')| \le C_{\mathscr{C},\psi,p} \left(\epsilon^{1/4} + \delta_w \epsilon^{p-3} \right), \quad \delta_w < c\epsilon, \quad 1 < p < 5/4. \tag{9.13}$$

Define the *modulus of continuity* of the limiting correlation on $\mathscr{C}$ by

$$\omega_{\mathscr{C},\psi}(\delta_w) := \sup_{\substack{\mathbf{w},\mathbf{w}' \in \mathscr{C} \\ |\mathbf{w}-\mathbf{w}'| \le \delta_w}} |f(\mathbf{w}) - f(\mathbf{w}')|.$$

For sufficiently small δ_w, take $p = 6/5$ and $\epsilon = \delta_w^{20/41}$. Then $\delta_w < c\epsilon$ and both terms in (9.13) are $\delta_w^{5/41}$. Consequently,

$$\omega_{\mathscr{C},\psi}(\delta_w) \le C_{\mathscr{C},\psi} \delta_w^{5/41}. \tag{9.14}$$

More generally the exponent is $(1/4)/(1/4+3-p)$, which approaches $1/8$ from below as $p \uparrow 5/4$.

Suppose a continuous function g on O has been identified after testing the centers, meaning that

$$\lim_{\max_j r_j \downarrow 0} \int_O f_{\boldsymbol{r}}(\mathbf{w})\chi(\mathbf{w})\, d^{2m}\mathbf{w} = \int_O g(\mathbf{w})\chi(\mathbf{w})\, d^{2m}\mathbf{w}$$

for every smooth χ whose support is a compact subset of O. Here $d^{2m}\mathbf{w}$ is the product of planar area measures. Uniform convergence on compact sets gives the same integral identity with f in place of $f_{\boldsymbol{r}}$. Choose nonnegative χ of integral one supported in shrinking neighborhoods of a fixed tuple. Continuity of f and g gives $f = g$ at that tuple. The same continuity extends identities from noncollinear to collinear triples.

The convergence is *locally uniform*, meaning uniform on each compact separated set $\mathscr{C}$, by (9.12) and a finite cover. Section 17 will supply the tested identities for the observations introduced later.

Part II
Density correlations

10 Finite-hole density correlations

Section 9 gives joint limits once the fixed-radius scalar limits and the bound (9.9) are known. We now establish these properties for variables obtained by assigning random signs to open clusters, in domains with finitely many holes.

Let D_0 be $\mathbb{C}$ or a bounded simply connected domain with analytic Jordan boundary. Fix an integer $m \geq 0$ and pairwise disjoint compact Jordan bodies $K_1, \ldots, K_m$ with analytic boundaries, contained in D_0. Set

$$U = D_0 \setminus \bigcup_{j=1}^{m} K_j. \tag{10.1}$$

For $m = 0$ the union is empty. Use the inner-cell approximations of subsection 4.1: sample the cells of D_0^a independently, force all cells of K_j^a closed, and close the cells outside D_0^a. This specifies our lattice approximation of U.

Conditional on the cell colors, give each open cluster C an independent sign σ_C, equal to 1 or -1 with probability $1/2$ each. Let $\mathbb{P}_a$ denote the unmodified full-plane percolation law. Write $0 \leftrightarrow \partial B(0,1)$ for an open path from the origin's cell to a cell meeting the unit circle. For a lattice vertex z, define

$$S_z = \begin{cases} \sigma_C, & z \in C \text{ open}, \\ 0, & z \text{ closed}, \end{cases} \qquad \Phi_a(z) = \pi_a^{-1} S_z, \qquad \pi_a = \mathbb{P}_a(0 \leftrightarrow \partial B(0,1)). \tag{10.2}$$

This is the cluster-sign construction of [1, Section 1.2, (1.8)–(1.10)], with each point variable normalized by π_a^{-1}. We call expected products of Φ_a the *density correlations*. Write $\mathbb{E}_U^a$ for expectation over both the cell colors and the signs in the model just defined. A fixed multiplicative normalization of Φ_a leaves the arguments unchanged.

For an integer $n \geq 0$, let

$$\mathcal{C}_n(U) = \{\mathbf{z} = (z_1, \ldots, z_n) \in U^n : z_i \neq z_j \text{ for } i \neq j\}.$$

Its elements are the marked-point configurations. Choose z_i^a as a nearest lattice vertex to z_i, resolving ties by increasing real coordinate and then imaginary coordinate. For sufficiently small a these vertices lie in the allowed region. Empty products equal one.

Uniform geometric statements concern families with a fixed bound on the numbers of marks and boundary components. Require common positive lower bounds on distances between distinct marks, between marks and boundary components, and between distinct boundary components. At fixed positive hole sizes, also require common positive radii for the boundary charts and tubular neighborhoods of subsection 4.1, with common bounds on the chart derivatives. The cited definitions specify the charts and normal neighborhoods; the holes here are analytic Jordan bodies and need not be convex. The additional uniformity bounds for boundary-collar comparisons are stated in Section 12.

We use the following convention at infinity. Write $\widehat{\mathbb{C}} = \mathbb{C} \cup \{\infty\}$. For $D_0 = \mathbb{C}$, the associated spherical domain is $U \cup \{\infty\}$; otherwise it is U. Use the coordinate z at finite points and $\zeta = 1/z$ near infinity; these coordinates are called *charts*. A conformal map of these spherical domains is a bijection whose expressions in charts are holomorphic with nonzero derivative. Lattice formulas use the planar domain in the chosen chart, with all marked points finite. Derivatives are computed in the same coordinates. Lattice connections still mean connections by finite paths: adjoining infinity adds no vertex and identifies no distinct clusters.

To specify the exterior functional, fix an integer $k \geq 1$ and bounded domains $V_1, \dots, V_k$ with pairwise disjoint closures contained in D_0. These are the *source regions*. Each hole is contained in one source region or lies outside all their closures. Define the frontier and complete records of V_j^a as in subsection 4.1, replacing D^a by V_j^a. Let $S_a(V_j)$ contain exactly the records obtainable from colorings of those cells; these are its *realizable records*.

Let ψ be smooth with compact support in $\mathcal{C}_n(U)$, with every marked point on its support a positive distance from the source regions. For a record tuple $\mathbf{s} = (s_1, \dots, s_k)$ with $s_j \in S_a(V_j)$, sample the exterior cells, retaining the fixed closed holes there, and attach the colors and connections prescribed by $\mathbf{s}$. Let $p_{\mathbf{z}}^a(\mathbf{s})$ be the probability that every z_i^a is open and every resulting open cluster contains an even number of these marks. Conditional on the completed colors, the sign average of $\prod_i S_{z_i^a}$ is the indicator of this event; see [1, (1.9)]. Averaging over the exterior colors therefore gives $p_{\mathbf{z}}^a(\mathbf{s})$. With both integrals over $\mathcal{C}_n(U)$, define

$$g_\psi^a(\mathbf{s}) = \pi_a^{-n} \int \psi(\mathbf{z}) p_{\mathbf{z}}^a(\mathbf{s})\, d^{2n}\mathbf{z}, \qquad \|\psi\|_{L^1} := \int |\psi(\mathbf{z})|\, d^{2n}\mathbf{z}.$$

The measure is the product of planar area measures, as in subsection 9.4. Use these coefficients in the k-linear functional $\mathcal{J}_\psi^a$ of subsection 9.3, with arbitrary complex measures v_j on $S_a(V_j)$. For $n = 0$, take $\psi = 1$ and omit the integrations, so $\|\psi\|_{L^1} = 1$.

For $m = 0$, the corresponding existence and covariance result is proved in [1, Theorem 1.5, (1.10)–(1.11)]. The next theorem extends that result to finitely many holes and supplies the exterior bound needed in Section 9.

For uniform completion bounds, require root disks of a common positive radius for every configuration in $\operatorname{supp}\psi$, with disjoint closures in U outside the source closures; see (15.2).

Theorem 10.1 (Density limits and completion bound)**.** *With the preceding conventions:*

(i) ***Density limits.*** *For every $n \geq 0$ and $\mathbf{z} \in \mathcal{C}_n(U)$,*

$$G_{U,n}(\mathbf{z}) = \lim_{a \downarrow 0} \mathbb{E}_U^a \prod_{i=1}^n \Phi_a(z_i^a) \tag{10.3}$$

exists and is locally bounded and locally integrable. Moreover, $G_{U,0} = 1$, and $G_{U,n} = 0$ for odd n.

(ii) ***Conformal covariance.*** *If $f : U \to U'$ is conformal between domains of the stated class and extends holomorphically across each analytic boundary component with nonzero derivative, then*

$$G_{U',n}(f\mathbf{z}) = \prod_{i=1}^{n} |f'(z_i)|^{-5/48} G_{U,n}(\mathbf{z}), \qquad f\mathbf{z} = (f(z_1), \dots, f(z_n)). \tag{10.4}$$

The same conclusions hold for the spherical domains and charts specified above.

(iii) ***Completion bound.*** *For complex rows v_j on $S_a(V_j)$ and all sufficiently small meshes,*

$$|\mathcal{J}^a_\psi(v_1, \dots, v_k)| \le C\|\psi\|_{L^1} \prod_{j=1}^{k} \|v_j\|_{\mathrm{var}}. \tag{10.5}$$

For fixed n, the constant is uniform under the root-disk condition, independently of hole sizes and shapes inside the fixed source regions; for $n = 0$, that condition is vacuous and $C = 1$ suffices.

An additional hole H of the stated class inside a source region contributes its frontier-record row ν_H; write $\nu_\varnothing$ for the row with that hole absent. Since $\|\nu_H\|_{\mathrm{var}} = 1$ and $\|\nu_H - \nu_\varnothing\|_{\mathrm{var}} \le 2$, the completion bound applies to both rows. At fixed mesh, conditioning all cells of $\bigcup_j K^a_j$ to be closed gives the same hole model, with independent signs subsequently assigned to its open clusters, by (4.9).

Sections 11–13 prove existence and local bounds. Section 14 proves covariance, and Section 15 proves the exterior bound and conditioning identity. Section 16 verifies the convention at infinity and the mesh limits of angular averages at fixed positive hole radii.

11 Published inputs and normalization at the marks

We begin the proof of Theorem 10.1 with limits in D_0, allowing an additional event determined by colors away from the marks. Each marked vertex contributes the factor π_a^{-1} defined in Section 10. The argument extends the local comparison of [1, Lemma 2.1]. We call a marked lattice vertex z_i^a a *root*.

11.1 Configurations and events at fixed positive scales

Write $\mathbb{P}^a_V$, for $V = D_0$ or U, for the law of the cell colors specified in Section 10. Write $E \leftrightarrow F$ when an open path joins cells meeting the sets E and F; for a lattice vertex, use its own cell. A specified disk or annulus confines the path, with endpoint cells allowed to meet its boundary. All other paths stay in the ambient lattice domain. A *smooth annulus* is the region between two nested, disjoint, smooth Jordan curves. A *circuit* is a simple closed path of adjacent cells; it is open or closed according to their color. A circuit in an annulus must surround its inner boundary. In this subsection all radii and separations are fixed and positive while $a \downarrow 0$.

The *quad-crossing configuration* records which quads have an open path between their designated opposite sides. Its state space and topology are defined in [10, Section 1.3, pp. 12–13]. Restriction to an open set retains the quads contained there and is continuous [10, Theorem 1.13(4)]. The accompanying collections of interface loops and their topology are defined in [23, Sections 4.1–4.2]. Their restriction retains loop excursions, meaning the maximal portions lying in that open set [23, Definition 4.4, p. 16]. Write $(\omega_{0,V}, L_{0,V})$ for

these two records of the full-plane scaling limit restricted to an open set V. In particular, this restriction records only connections that can be tested inside V; it does not identify excursions through connections made in its complement.

The domain assumptions of the two CCK results used below are different. The cluster-convergence theorem [23, Theorem 7.1, p. 31; proof, pp. 32–33] assumes a bounded simply connected domain with piecewise smooth boundary. Our bounded ambient domain D_0 satisfies those hypotheses. The restricted-configuration theorem [23, Theorem 9.5, pp. 39–40], with the restriction defined in Camia–Conijn–Kiss's Definition 4.4, allows an arbitrary domain V and gives

$$(f(\omega_{0,V}), f(L_{0,V})) \overset{\text{law}}{=} (\omega_{0,f(V)}, L_{0,f(V)}) \tag{11.1}$$

for a conformal bijection f on V. This statement concerns restrictions of the ambient configuration to an arbitrary domain; the density model with forced closed holes is constructed separately in Section 13. Lemma 14.1 below verifies that the positive-scale events used for its covariance are functions of these restricted records.

We use a *coupling* of the lattice and limiting configurations: a joint realization with the prescribed laws. Choose one in which both the loop collections and the quad-crossing records converge with probability one; see [23, Sections 4.1–4.2, Remark 4.17, and Theorem 7.1]. For each event listed below, the lattice indicator converges in probability to the limiting indicator, meaning that the two indicators disagree with probability tending to zero. Open connections between disjoint disks mean that one open cluster meets both disks. Their limiting events and continuity under changes of the disk radii are given in [1, (2.5)–(2.6) and the preceding paragraph]. For bounded D_0, convergence of these connection events with all cells outside D_0 closed follows from [23, Theorem 7.1 and its proof, pp. 31–33]; see also [1, proof of Theorem 1.4, (2.41)].

For connections confined to a fixed rectangle, disjoint open simply connected targets with piecewise smooth boundaries are treated in [23, Definition 4.5, Lemma 4.18, and Theorem 4.20]. This includes fixed conformal images of disks whose closures lie inside the map's domain. The fixed smooth annular one-arm events used here converge by [9, Lemma 2.9 and Remark 2.12]. A closed circuit separating the annular boundaries is the planar alternative to an open path between them, so its indicator also converges. A union bound gives joint convergence for any finite family of these indicators. Full-plane connections can first be confined to a large rectangle: a path leaving it requires an open arm to its boundary, whose probability tends to zero by the RSW bounds of subsection 7.3.

We also need connections after disks have been filled open. Fix finitely many disks $\mathcal{N}_i = B(x_i, t_i)$, $1 \le i \le k$, with pairwise disjoint closures contained in D_0. Let $I_i^a = \mathcal{N}_i^a$ be their inner-cell approximations, and let $I_i^{a,+}$ consist of I_i^a and all cells adjacent to it. For sufficiently small a, the sets I_i^a are connected and no two are adjacent. *Wiring a disk* means making every cell of I_i^a open. The *wired partition* groups disk labels according to open connections after this operation.

Form a finite graph on these labels, joining i and j when an open cluster of the unmodified configuration meets both $I_i^{a,+}$ and $I_j^{a,+}$. Its connected components give exactly the wired partition. Each graph edge gives a connection after filling. Conversely, any path after filling splits at its visits to the disks into paths in original open clusters. Thus two disk labels are connected precisely when a chain of graph edges joins them.

For fixed small $\epsilon > 0$ and sufficiently small a, each graph-edge event lies between the connection events for disks of radii $t_i - \epsilon$ and $t_i + \epsilon$. By the disk continuity cited above, the probability that these two events differ tends to zero as $\epsilon \downarrow 0$, after the mesh limit. The wired partition therefore converges jointly with the finite family of annular events, independently of

the one-cell contact convention.

We record the corresponding boundary comparison for fixed conformal images of disks, which will be used in Section 14. Write $\mathcal{N}_i = \varphi_i(B(x_i, t_i))$, with φ_i conformal on a neighborhood of the closed disk, and set $\mathcal{N}_i^{\pm}(\delta) = \varphi_i(B(x_i, t_i \pm \delta))$. These are nested smooth targets, and their boundaries are displaced by at most a constant times δ. Fix a scale $\rho > 0$ smaller than the target separations, their boundary-chart radii, and, in the bounded case, their distances to ∂D_0. If an original open cluster joins $\mathcal{N}_i^{+}(\delta)$ to a different target $\mathcal{N}_j$ but does not meet $\mathcal{N}_i^{-}(\delta)$, choose a cell of that cluster nearest to the inner target. It lies within $O(\delta)$ of the target boundary. The open continuation towards $\mathcal{N}_j$ and the two closed boundary paths facing $\mathcal{N}_i^{-}(\delta)$ give three arms from a ball of radius $O(\delta)$ to distance ρ, on the exterior side of the inner target. The boundary paths cannot close off before that scale while the open cluster continues to the separated target and avoids the inner target. Adjacent closed boundary cells may enter an $O(a)$ erosion of the target; using that eroded boundary for confinement absorbs this displacement into the starting scale when $a \ll \delta$. All three arms are sampled inside D_0. This is the same local separation argument as in the proof of Lemma 12.1.

Cover the displaced boundary by $O(\delta^{-1})$ such balls. The boundary charts and the half-plane three-arm bound of [23, Lemma 4.10], applied as in Section 12, bound each probability by $C(\delta/\rho)^2$ after the mesh limit. Thus, for fixed target geometry,

$$\limsup_{a \downarrow 0} \mathbb{P}^a_{D_0}\Big(\{\mathcal{N}_i^{+}(\delta) \leftrightarrow \mathcal{N}_j\} \setminus \{\mathcal{N}_i^{-}(\delta) \leftrightarrow \mathcal{N}_j\}\Big) \le C\delta. \tag{11.2}$$

The argument is local to a compact subset of D_0, so it applies in both the plane and the simply connected bounded case. A union bound over the finitely many graph edges allows all targets to be perturbed. Taking the mesh limit first and then $\delta \downarrow 0$ therefore proves target continuity and independence of the one-cell contact convention for these image neighborhoods.

For fixed $z \in \mathbb{C}$ and $t > 0$, let z^a be its lattice representative from Section 10. The one-arm normalization is [1, (2.1)]

$$\lim_{a \downarrow 0} \frac{\mathbb{P}_a(z^a \leftrightarrow \partial B(z^a, t))}{\pi_a} = t^{-5/48}. \tag{11.3}$$

The same limit holds with the circle centered at z. Indeed, $|z - z^a| \to 0$, so circles centered at z^a with radii $t - \epsilon$ and $t + \epsilon$ bound the event for every fixed $\epsilon > 0$ and all sufficiently small meshes.

11.2 Cluster signs and local arms

Fix $\mathbf{z} \in \mathcal{C}_n(U)$. When all marked vertices are open, their *marked partition* groups indices belonging to the same open cluster. Let P_n be the event that all marks are open and every block of this partition has even size. We suppress its dependence on the mesh, marks, and ambient domain. Averaging $\prod_i S_{z_i^a}$ over the independent signs gives $\mathbf{1}_{P_n}$, as in [1, (1.9)]. Hence

$$\mathbb{E}^a_U \prod_i \Phi_a(z_i^a) = \pi_a^{-n} \mathbb{P}^a_U(P_n). \tag{11.4}$$

For odd n the left side is identically zero.

Choose $d_i > 0$ so that the closed disks $\overline{B(z_i, d_i)}$ are pairwise disjoint and contained in U. Call these the *root disks*. For even $n \ge 2$, P_n requires the local arm events

$$A_i^a = \{z_i^a \leftrightarrow \partial B(z_i, d_i)\}, \qquad A^a = \bigcap_i A_i^a. \tag{11.5}$$

Here each path is stopped at its first cell meeting the outer circle. Every marked vertex must connect to another mark outside its own disk. For all sufficiently small meshes these events use disjoint sets of sampled cells, so they are independent and have their full-plane probabilities. Equation (11.3) gives

$$0 \le \pi_a^{-n}\mathbb{P}_U^a(P_n) \le \prod_i \frac{\mathbb{P}_a(A_i^a)}{\pi_a}, \qquad \limsup_{a\downarrow 0} \pi_a^{-n}\mathbb{P}_U^a(P_n) \le \prod_i d_i^{-5/48}. \tag{11.6}$$

This bound depends only on the root disks.

For a prescribed partition of $\{1,\dots,n\}$, its *exact-partition event* requires all marks to be open and their marked partition to equal that partition. The next lemma extends the local argument of [1, Lemma 2.1 and (2.14)–(2.24)] by retaining an additional event away from the root disks.

Lemma 11.1 (A fixed exterior event and the density limit)**.** *Let D_0 be the plane or a bounded simply connected domain with analytic Jordan boundary, as in Section 10. Fix $\mathbf{z} \in \mathcal{C}_n(D_0)$ and root disks as above, with $U = D_0$. Let C require a closed circuit in each of finitely many fixed smooth annuli whose closures are contained in D_0 and disjoint from the root disks. The circuit events are sampled in D_0; no interior holes are forced closed in this lemma. We suppress their mesh dependence. Then*

$$G_{D_0,n}[C](\mathbf{z}) = \lim_{a\downarrow 0} \pi_a^{-n}\mathbb{P}_{D_0}^a(P_n \cap C) \tag{11.7}$$

exists. The bracketed argument records the exterior event retained in the numerator. The same conclusion holds when P_n is replaced by an exact-partition event whose blocks all have at least two indices, or by a finite union of such events. The estimates concern intersections with C, without conditioning on C.

Proof. All ambient connection limits in this proof are taken in the plane or in the simply connected domain D_0, where the preceding subsection applies by [23, Theorem 7.1]. The circuit event is retained in the numerator throughout. For $n = 0$, the assertion is convergence of $\mathbb{P}_{D_0}^a(C)$, proved in the preceding subsection. For odd n the parity expression is zero. Consider even $n \ge 2$ and fix $0 < t < \min_i d_i/4$. Fill $B(z_i,t)^a$ open, and let W_t require every block of the resulting wired partition to have even size. It depends only on the colors outside the filled disks. Let $O_i(t)$ require an open circuit in $B(z_i,d_i/2) \setminus \overline{B(z_i,t)}$ surrounding the inner disk. Mesh dependence is again suppressed.

On $A^a \cap \bigcap_i O_i(t)$, every root reaches its surrounding open circuit. Any path from its filled small disk to another such disk also meets that circuit. Replace passages through filled cells by paths along the actual open circuits. This proves equality of the original marked partition and the wired partition. Consequently,

$$\left|\mathbb{P}_{D_0}^a(P_n \cap C \mid A^a) - \mathbb{P}_{D_0}^a(W_t \cap C \mid A^a)\right| \le \sum_i \mathbb{P}_a(O_i(t)^c \mid A_i^a). \tag{11.8}$$

Independence of the root disks removes the other arm conditions on the right. This is the circuit comparison used in [1, (2.22)–(2.24)], with the same event C retained on both sides.

An event is *increasing* if changing closed cells to open cannot destroy it. For independent cell colors, the Harris–FKG inequality states that $\mathbb{P}_a(E \cap F) \ge \mathbb{P}_a(E)\mathbb{P}_a(F)$ for increasing events E, F [8, Section 2.3, pp. 1567–1568]. Apply it to $O_i(t)$ and A_i^a. The RSW circuit bound from subsection 7.3, applied in disjoint annuli of fixed radius ratio, then gives

$$\mathbb{P}_a(O_i(t)^c \mid A_i^a) \le \mathbb{P}_a(O_i(t)^c), \qquad \lim_{t\downarrow 0} \limsup_{a\downarrow 0} \sum_i \mathbb{P}_a(O_i(t)^c) = 0. \tag{11.9}$$

Indeed, the number of these independent annuli tends to infinity as $t \downarrow 0$, and each has a uniform positive probability of an open circuit; see also [1, (2.20), (2.51)].

For $0 < \eta < t/2$, define

$$E_i^a(\eta) = \{\partial B(z_i, \eta) \leftrightarrow \partial B(z_i, d_i)\}, \qquad E^a(\eta) = \bigcap_i E_i^a(\eta),$$

with paths confined to the corresponding annuli. The coupling of [1, Lemma 2.1, (2.7)–(2.11)] compares the laws conditioned on A_i^a and on $E_i^a(\eta)$. When the coupling succeeds, the two configurations share an open circuit inside $B(z_i, t/2)$ and have identical colors outside that circuit. Apply these couplings in the disjoint root disks and use identical colors on the remainder of D_0, as in [1, (2.14)–(2.20)]. Let $c(\eta, t)$ be the $\limsup_{a\downarrow 0}$ of the probability that any local coupling fails. The cited bound gives $c(\eta, t) \to 0$ as $\eta \downarrow 0$ for fixed t. On success both W_t and C agree in the coupled configurations.

Put $q_a = \mathbb{P}^a_{D_0}(P_n \cap C \mid A^a)$ and

$$q_{a,\eta,t} = \mathbb{P}^a_{D_0}(W_t \cap C \mid E^a(\eta)). \tag{11.10}$$

For fixed η, t, the latter has a limit by the joint event convergence above. Its denominator has a positive limit by RSW and independence of the disjoint annuli. Define $b(t) = \limsup_{a\downarrow 0} \sum_i \mathbb{P}_a(O_i(t)^c)$. The circuit comparison and the coupling give

$$\limsup_{a\downarrow 0} |q_a - q_{a,\eta,t}| \le b(t) + c(\eta, t), \qquad \limsup_{a\downarrow 0} q_a - \liminf_{a\downarrow 0} q_a \le 2b(t) + 2c(\eta, t).$$

First let $\eta \downarrow 0$ at fixed t, and then let $t \downarrow 0$. Both errors vanish, so q_a converges. Since $P_n \subset A^a$,

$$\pi_a^{-n} \mathbb{P}^a_{D_0}(P_n \cap C) = q_a \prod_i \frac{\mathbb{P}_a(A_i^a)}{\pi_a}.$$

The product converges by (11.3), proving (11.7).

For an exact partition whose blocks have at least two indices, every local arm is still required. Replace P_n and W_t by the corresponding exact-partition events. The same equality of partitions and the same estimates apply, including when some blocks have odd size. Distinct exact-partition events are disjoint, so finite unions follow by addition. □

Remark 11.2. An exact-partition event need not be increasing. The comparison (11.8) uses equality of partitions on the circuit event, so it requires no monotonicity of the partition event. Related connection-and-separation events are treated in [1, proof of Theorem 1.5, pp. 2160–2165].

12 Small boundary changes at fixed hole size

We estimate how enlarging a fixed hole by a thin strip changes its complete frontier record. The estimate will let us compare the closed circuits used in the next section with deterministic boundaries.

Let K be a compact Jordan body with analytic boundary, as in Section 10. Choose a tubular radius $t_* > 0$ and boundary charts as in subsection 4.1. With n_K the outward unit normal, define

$$K^{+t} = K \cup \{x + s n_K(x) : x \in \partial K,\ 0 \le s \le t\}, \qquad 0 \le t < t_*.$$

The strip $K^{+t} \setminus K$ is its *outer collar*. Fix an analytic Jordan curve Γ surrounding K, and let V_Γ be its bounded interior. Assume $\overline{V_\Gamma} \subset D_0$ and that this closure is disjoint from every root disk and every other hole. Choose $0 < \delta_0 < t_*$ small enough that $K^{+\delta_0}$ lies strictly inside Γ and the boundary charts remain available throughout the collar.

For a closed hole $H \subset V_\Gamma$, let $S_H^{a,\Gamma}$ be the complete frontier record of V_Γ^a: the colors of its frontier cells and their open connections by paths in V_Γ^a after H^a is forced closed. Write $\nu_H^{a,\Gamma}$ for its law. The frontier, variation norm, and common-color coupling are those of subsection 4.1. All geometric choices are fixed before the mesh limit.

We also specify the record for an outer boundary. For bounded D_0 as in Section 10, set

$$D_0^{-t} = \{z \in D_0 : \operatorname{dist}(z, \partial D_0) > t\}$$

for small $t \geq 0$. Choose a fixed analytic Jordan curve Γ_0 inside D_0, enclosing the holes and root disks, and let V_{Γ_0} be its interior. The *outer record* gives the colors of cells in $D_0^a \setminus V_{\Gamma_0}^a$ adjacent to $V_{\Gamma_0}^a$, and their open connections through $D_0^a \setminus V_{\Gamma_0}^a$. Replacing D_0 by D_0^{-t} closes the additional cells outside $(D_0^{-t})^a$. Take δ_0 small enough that this change stays a positive distance from Γ_0.

Uniformity below means common upper bounds on the changing boundary lengths, common positive chart and tubular radii, common positive lower and finite upper bounds on the absolute values of chart derivatives, and a common positive distance between each changing boundary and its fixed cut. For simultaneous comparisons, the regions in which the connections are computed have a common positive distance from one another and from the root disks.

Lemma 12.1 (Small normal displacements)**.** *For $0 < \delta < \delta_0$, sample the colors once and close the selected hole in that sample. There is $C < \infty$, uniform under the stated bounds, such that*

$$\begin{aligned} \limsup_{a \downarrow 0} \mathbb{P}_a(S_{K^{+\delta}}^{a,\Gamma} \neq S_K^{a,\Gamma}) &\leq C\delta, \\ \limsup_{a \downarrow 0} \|\nu_{K^{+\delta}}^{a,\Gamma} - \nu_K^{a,\Gamma}\|_{\mathrm{var}} &\leq C\delta. \end{aligned} \tag{12.1}$$

The same bounds hold for any intermediate forced cell set J_a satisfying $K^a \subseteq J_a \subseteq (K^{+\delta})^a$. This includes $J_a = J^a$ for any closed set $K \subseteq J \subseteq K^{+\delta}$. The same assertions hold for the outer records when D_0 is replaced by $D_0^{-\delta}$, or by any allowed cell set W_a with $(D_0^{-\delta})^a \subseteq W_a \subseteq D_0^a$.

Proof. The coupled frontier colors agree. If their partitions differ, the construction of Lemma 4.1 gives two open frontier ports, a simple open path between them for the smaller hole, and a closed crosscut separating them for the larger hole. This crosscut visits the changed strip. Its portions before the first and after the last visit to $(K^{+\delta})^a$ are disjoint sampled closed paths from that strip to the frontier.

Join their attachment points to forced cells of K^a by inward normal segments with one-cell endpoint adjustments, and join the inner ends within K^a. The segments have length $O(\delta + a) = O(\delta)$ for sufficiently small a/δ. Removing redundant pieces gives a simple separating crosscut with the original frontier endpoints, as in Lemma 4.2. The open path must meet a short segment, since it cannot enter the forced cells or cross a sampled closed path. Attachments within $O(\delta)$ are handled in one enlarged box, as in Figure 2.

Before sampling, cover ∂K by at most $C \operatorname{length}(\partial K)/\delta$ boxes of diameter $C\delta$, centered at points $x_{\mathsf{B}} \in \partial K$. Enlarge them by a fixed factor. One box B then contains the normal segment met by the open path and the adjacent attachment of the closed path. Retain the open path before its first visit to B and after its last visit, reversing the first portion. Retain

the selected closed path after its last visit to B. These are two open branches and one closed branch from B to the frontier, all sampled and pairwise disjoint.

Choose $\rho_{\mathrm{loc}} > 0$ smaller than the chart and tubular radii and the distance from K to Γ. Decrease δ_0 so that every enlarged box satisfies $\mathsf{B} \subset B(x_{\mathsf{B}}, \rho_{\mathrm{loc}}/2)$. Stop each branch at its first exit from $B(x_{\mathsf{B}}, \rho_{\mathrm{loc}})$. The frontier endpoints lie outside this disk. We obtain three sampled arms on the exterior side of K^a, from scale δ to the fixed outer radius ρ_{loc}. Let A^a_{B} denote this arm event. The first and last visits to B ensure that later returns through the collar do not remove these arms.

Take $a \downarrow 0$ at fixed $\delta, \rho_{\mathrm{loc}}$, then use the boundary chart to send the exterior side to the upper half-plane. This is the comparison of subsection 4.2; the relevant arm definitions, convergence, and conformal transport are also given in [23, Definition 4.5, Lemma 4.18, and Theorem 9.5 with the following discussion]. The chart derivative bounds compare the two image scales with $\delta, \rho_{\mathrm{loc}}$. The half-plane three-arm estimate gives

$$\limsup_{a\downarrow 0} \mathbb{P}_a(A^a_{\mathsf{B}}) \le C(\delta/\rho_{\mathrm{loc}})^2;$$

see [8, Propositions 17 and 19, Section 4.6, and Theorem 24(2)]. This bound allows any order of the two open arms and one closed arm. A union bound over the deterministic boxes yields

$$\limsup_{a\downarrow 0} \mathbb{P}_a(S^{a,\Gamma}_{K^{+\delta}} \neq S^{a,\Gamma}_K) \le C \frac{\mathrm{length}(\partial K)}{\delta} \left(\frac{\delta}{\rho_{\mathrm{loc}}}\right)^2 \le C'\delta. \tag{12.2}$$

The coupling inequality of subsection 4.1 gives the variation bound.

Closing additional cells only splits open connectivity classes. If the two extreme records agree, every intermediate forced cell set therefore has that same record. This proves the assertion for J_a without any boundary regularity assumption on it.

For the outer record, the forced side is the closed exterior of D_0. The two sampled closed paths run towards the interior cut Γ_0; join their other ends through the closed exterior. All three sampled arms now lie on the interior side of ∂D_0. Boundary charts sending that side to the upper half-plane give the same estimate, with $\mathrm{length}(\partial D_0)$ in place of $\mathrm{length}(\partial K)$. The same nesting argument treats intermediate allowed cell sets. □

13 Closed circuits and finite-hole correlations

We transfer the limits of Section 11 to U by conditioning full-plane percolation on closed circuits near its boundary components. These circuits prevent open paths between the marks from entering the holes or leaving the outer boundary. To pass from the simply connected input to the domain with holes, we apply Lemma 11.1 with ambient domain $\mathbb{C}$ and use the collar estimate to compare with the forced-hole model.

Fix $D_0, U, K_1, \dots, K_m$ as in Section 10, a configuration $\mathbf{z} \in \mathcal{C}_n(U)$, and root disks as in Section 11. Choose fixed cuts Γ_j around the inner holes as in Section 12. Their enclosed regions have disjoint closures and avoid all root disks. If D_0 is bounded, choose an additional cut Γ_0 enclosing these regions and all root disks. Its outer record is the one defined in Section 12.

Take $\delta > 0$ below all the corresponding values of δ_0 from Section 12. Using the offsets defined there, choose it small enough that the annuli

$$\mathcal{A}_{j,\delta} = \mathrm{int}(K_j^{+2\delta/3}) \setminus K_j^{+\delta/3}, \qquad 1 \le j \le m,$$

lie inside their fixed cuts. In the bounded case also set

$$\mathcal{A}_{0,\delta} = D_0^{-\delta/3} \setminus \overline{D_0^{-2\delta/3}},$$

and require it to lie outside Γ_0. These are the *inner and outer collars* used below. Their closures are pairwise disjoint, lie in U, and avoid the root disks.

Under the unmodified full-plane law $\mathbb{P}_a$, let $C^a_{j,\delta}$ require a sampled closed circuit in $\mathcal{A}_{j,\delta}$ surrounding its inner boundary. For $j = 0$, this circuit surrounds all holes and root disks. When $D_0 = \mathbb{C}$, set $C^a_{0,\delta}$ equal to the certain event. Put

$$C^a_\delta = C^a_{0,\delta} \cap \bigcap_{j=1}^{m} C^a_{j,\delta}. \tag{13.1}$$

An empty intersection is the certain event. Let C_δ be the corresponding event in the limiting full-plane configuration of subsection 11.1, and let $\mathbb{P}_\mathbb{C}$ denote that configuration's law. The closed-circuit indicator convergence there gives

$$\mathbb{P}_\mathbb{C}(C_\delta) = \lim_{a \downarrow 0} \mathbb{P}_a(C^a_\delta) > 0.$$

Indeed, the RSW circuit construction of subsection 7.3 gives a positive lower bound for each fixed annulus. The disjoint annuli use independent cells for sufficiently small mesh. These lower bounds may depend on δ, which stays fixed during the mesh limit.

Lemma 13.1 (Conditional law between closed circuits)**.** *On C^a_δ, one can select one surrounding closed circuit in each collar so that, conditional on the selected circuits, the remaining cells are independent, each open with probability* $1/2$*. Here the remaining cells lie strictly outside every inner circuit and strictly inside the outer circuit when present. Let J^a_j consist of the cells on the selected inner circuit and all cells enclosed by it. For all sufficiently small a,*

$$K^a_j \subseteq J^a_j \subseteq (K^{+\delta}_j)^a. \tag{13.2}$$

If an outer circuit is present, let V^a_δ be the cells strictly inside it. Then $(D_0^{-\delta})^a \subseteq V^a_\delta \subseteq D^a_0$. In the plane case V^a_δ is the full lattice. Filling the J^a_j and the complement of V^a_δ closed preserves all open connections among the marks. For observations in the remaining region, the conditional law is thus a mixture*: first sample the circuits, then sample independent colors in that region.*

Let $\mathbb{E}^a_\mathbb{C}$ denote expectation over full-plane colors and the independent cluster signs of Section 10. Then

$$\limsup_{a \downarrow 0} \left| \mathbb{E}^a_U \prod_i \Phi_a(z^a_i) - \mathbb{E}^a_\mathbb{C} \left[\prod_i \Phi_a(z^a_i) \mid C^a_\delta \right] \right| \le C\delta. \tag{13.3}$$

The constant is uniform for bounded numbers of marks and boundary components, the geometric bounds of Section 12, and root disks with a common positive lower bound on their radii.

Proof. We use the circuit exploration in the proof of [1, Lemma 2.1], with the colors interchanged. Fix a deterministic order of the cells in each collar. For an inner collar, use the cells on its inner side that share an edge with a collar cell as open starting cells for the search only. They lie outside the random collar; their sampled colors are not changed. Reveal, in the fixed order, the unrevealed collar neighbors of the starting cells and of open cells already reached from them. Add each revealed open cell to this reached set; record a revealed closed

cell without crossing it. Stop when all such neighbors have been revealed or the reached set meets the outer boundary of the collar.

On $C^a_{j,\delta}$, a closed circuit blocks the second outcome. The revealed closed boundary contains a surrounding circuit. Select the circuit facing the starting cells, resolving contacts by the fixed cell order. The exploration reveals no cell strictly beyond it. For the outer collar, start instead from its adjacent cells on the outer side and explore inward. This selects a surrounding closed circuit without revealing cells on its inner side.

The *transcript* records the revealed cells, their colors and order, and the selected circuits. Each next revealed cell is determined by earlier revealed colors. The event specifying a transcript therefore constrains only those cells, as in subsection 8.1. A successful transcript certifies the corresponding closed-circuit event. Conditional on all successful transcripts, the cells between the selected circuits remain independent, each open with probability $1/2$. Conditioning also on C^a_δ adds no further constraint. Averaging over the transcripts compatible with given circuits proves the asserted conditional law.

The inner closed circuits separate the marks from the regions they enclose, and the outer circuit, when present, separates the marks from its exterior. Filling those regions closed therefore preserves the marked partition. The gaps of width $\delta/3$ between the collars and the deterministic extreme boundaries give the exact cell inclusions (13.2) and the stated inclusion for V^a_δ, once a is sufficiently small. Assigning independent cluster signs then gives the same sign-averaged marked products as in this filled model.

Fix the selected circuits and generate a fresh, unconditioned product configuration. Close their filled sets in this fresh sample. This realizes the conditional law between the circuits just proved. In the same sample, also form the original model in U and the deterministic models with inner holes $K_j^{+\delta}$ and outer domain $D_0^{-\delta}$. Let D^a_j be the event that the two deterministic extreme records at Γ_j differ. The index $j = 0$ is included only in the bounded case. By (13.2) and Lemma 12.1, any intermediate record can differ only on D^a_j, and

$$\limsup_{a\downarrow 0} \sum_j \mathbb{P}_a(D^a_j) \le C\delta.$$

If none of these discrepancies occurs, using the same colors in the remaining region gives the same marked partition in the two models.

Write $\mathbb{E}^a_{\mathrm{circ}}$ for expectation in the filled model with this fixed circuit collection, including its independent cluster signs. For $n = 0$ both products have expectation one, and for odd n both expectations vanish. For even $n \ge 2$, the sign average in either model is the parity indicator of (11.4). It can be nonzero only on the local arm event A^a of (11.5). Each D^a_j uses cells outside the root disks and is independent of A^a. Hence

$$\left| \mathbb{E}^a_U \prod_i \Phi_a(z^a_i) - \mathbb{E}^a_{\mathrm{circ}} \prod_i \Phi_a(z^a_i) \right| \le \left(\pi_a^{-n} \prod_i \mathbb{P}_a(A^a_i) \right) \sum_j \mathbb{P}_a(D^a_j). \tag{13.4}$$

The first factor converges to $\prod_i d_i^{-5/48}$ by (11.3). The bound is independent of the selected circuits. Averaging over their conditional distribution and then taking $\limsup_{a\downarrow 0}$ proves (13.3). □

Remark 13.2 (Dependence on the circuit probability). The comparison (13.4) is uniform for every selected circuit collection. Averaging it preserves the same bound, so (13.3) contains no factor $\mathbb{P}_a(C^a_\delta)^{-1}$. This probability is used below only at fixed positive δ, when both the conditional numerator and denominator have limits.

13.1 Existence of the finite-hole correlations

At fixed $\delta > 0$, Lemma 11.1 applies to the circuit event (13.1). The sign identity (11.4) and the positive limit of its probability give

$$M_\delta(\mathbf{z}) := \lim_{a \downarrow 0} \mathbb{E}^a_{\mathbb{C}} \left[\prod_i \Phi_a(z_i^a) \mid C_\delta^a \right] = \frac{G_{\mathbb{C},n}[C_\delta](\mathbf{z})}{\mathbb{P}_{\mathbb{C}}(C_\delta)}. \tag{13.5}$$

By (13.3), the upper and lower mesh limits of the original correlation differ by at most $2C\delta$. Letting $\delta \downarrow 0$ proves its convergence and

$$|G_{U,n}(\mathbf{z}) - M_\delta(\mathbf{z})| \le C\delta. \tag{13.6}$$

Thus the mesh limit precedes the limit of vanishing collar width.

On each compact subset of $\mathcal{C}_n(U)$, choose one common positive radius for the root disks. The bound (11.6) is then uniform over that subset and all sufficiently small meshes. It proves local boundedness and local integrability of $G_{U,n}$. It also permits passage of the limit through the integral against any smooth function with compact support in $\mathcal{C}_n(U)$, as in Section 10. The argument applies to every fixed finite number of holes.

14 Conformal covariance without filling the holes

We prove the covariance formula (10.4) using the closed-circuit events of Section 13. Let $f : U \to U'$ satisfy the hypotheses of Theorem 10.1: it is a conformal bijection extending holomorphically across each boundary component with nonzero derivative. First take both domains bounded, or both unbounded with $f(\infty) = \infty$ in the charts of Section 10. Other changes of chart are treated in Section 16.

Fix the marks and a sufficiently small collar width $\delta > 0$. Use C_δ^a and C_δ from (13.1). Define fC_δ by requiring a closed circuit separating the two boundaries of each image annulus $f(\mathcal{A}_{j,\delta})$. Write $(fC_\delta)^a$ for the corresponding event on the target lattice. The boundary extension of f places these annuli in collars of width at most $c_f\delta$, for a constant c_f independent of δ. Boundary components may be permuted.

The following lemma supplies the locality needed to use (11.1). All probabilities in its statement are full-plane probabilities.

Lemma 14.1 (Closed-circuit localization at positive scales)**.** *Fix $\delta > 0$ as above. For each mark choose nested neighborhoods*

$$z_i \in V_i \Subset W_i \Subset \mathcal{N}_i, \qquad 1 \le i \le n,$$

where $\Subset$ means that the closure of the first set is a compact subset of the second. Take these neighborhoods to be disks or conformal images of disks under maps defined on neighborhoods of their closures. Require the closures of the $\mathcal{N}_i$ to be pairwise disjoint, contained in U, and disjoint from all the collar annuli. They lie on the marked side *of each collar: outside every inner collar and inside the outer collar when present. The corresponding condition for the image annuli is the side containing the image marks, so it is preserved by f even when boundary components are permuted. Write $\boldsymbol{\mathcal{N}} = (\mathcal{N}_1, \dots, \mathcal{N}_n)$. Let $\Pi^a_{\mathbf{W}}$ be the partition of the labels after filling each W_i^a open. In the original, unmodified configuration, let*

$$E^a(\mathbf{V}, \boldsymbol{\mathcal{N}}) = \bigcap_{i=1}^n \{\partial V_i \leftrightarrow \partial \mathcal{N}_i \text{ in } \mathcal{N}_i \setminus \overline{V_i}\}.$$

For any collection $\mathcal{P}$ of partitions of $\{1,\dots,n\}$, the limit

$$\mathsf{P}_{C_\delta}(\mathbf{V},\mathbf{W};\boldsymbol{\mathcal{N}},\mathcal{P}) := \lim_{a\downarrow 0} \frac{\mathbb{P}_a(C_\delta^a \cap \{\Pi_{\mathbf{W}}^a \in \mathcal{P}\} \cap E^a(\mathbf{V},\boldsymbol{\mathcal{N}}))}{\mathbb{P}_a(E^a(\mathbf{V},\boldsymbol{\mathcal{N}}))} \tag{14.1}$$

exists, and the denominator has a strictly positive limit. The indicators of the limiting numerator and denominator events are measurable functions of $(\omega_{0,U}, L_{0,U})$ and transform by applying f to all their defining sets. Consequently,

$$\mathsf{P}_{C_\delta}(\mathbf{V},\mathbf{W};\boldsymbol{\mathcal{N}},\mathcal{P}) = \mathsf{P}_{fC_\delta}(f\mathbf{V},f\mathbf{W};f\boldsymbol{\mathcal{N}},\mathcal{P}). \tag{14.2}$$

Also $\mathbb{P}_{\mathbb{C}}(C_\delta) = \mathbb{P}_{\mathbb{C}}(fC_\delta) > 0$.

Proof. We first check the limits at fixed positive scales in the unmodified plane. As in subsection 11.1, construct a graph on the wired labels by joining i and j when an original open cluster meets the one-cell neighborhoods of both W_i^a and W_j^a. The connected components of this finite graph give $\Pi_{\mathbf{W}}^a$. Each graph-edge indicator has the full-plane connection limit from that subsection, jointly with the finitely many annular-arm and circuit indicators. Inner and outer approximations of the target neighborhoods remove the one-cell contact convention. For an image of a disk, use the images of slightly smaller and larger disks and the boundary comparison (11.2). Thus the numerator has a limit. The fixed annular-arm probabilities in the denominator have positive limits by RSW, and their disjoint cell sets give independence. This proves existence of the ratio.

We now express the limiting event in terms of the restricted records. At the lattice level, on C_δ^a every open cluster meeting one of the W_i^a stays outside every selected inner closed circuit and inside the outer closed circuit, when present. An open path leaving this region would have to cross a closed circuit. Filling the W_i^a open cannot change this conclusion, since these sets stay on the marked sides and avoid the collars. Hence, on C_δ^a, the full-plane graph has exactly the same edges as the graph whose connecting paths are required to stay in U.

For the continuum identification, use the connection event of [23, Definition 4.5 and Remark 4.6, p. 17] with ambient set $S = U$ and targets W_i, W_j. In that definition the ambient set may be arbitrary; simple connectivity is required of the two target sets. For one open arm the event is certified by a crossed quad contained in U, whose endpoint sides lie strictly inside the targets. It is Borel measurable in the restricted quad record.

The closed-circuit separation gives the same graph identification for these continuum events. To see its locality, keep δ fixed. The collar annuli have a positive distance from ∂U, and the root neighborhoods are on their marked side. A connection between target neighborhoods cannot pass to the other side of a closed annular barrier: it would give an open crossing of that annulus, which planar duality excludes on the closed-circuit event. Its connecting portion can therefore be tested on the marked side, with quad witnesses contained in U and with a positive buffer from ∂U. This remains true if each target W_i is slightly decreased or increased inside $\mathcal{N}_i$. Using such nested targets, and then removing the perturbation by the target-continuity comparison of subsection 11.1, identifies the graph with the already established full-plane graph limit on C_δ.

The circuit and conditioning-arm events are themselves tests in the fixed annuli contained in U. The graph and these annular tests therefore express the numerator event as a finite Boolean function of events measurable in the restricted records. This includes exact partitions and their complements. The denominator is measurable for the same reason. A conformal bijection takes each certifying quad, annular barrier, and labeled target to its image, and preserves the connected components of the resulting finite graph. Applying (11.1) to the

whole joint event proves (14.2). Applying it just to the circuit tests proves equality of the circuit probabilities.

In the unbounded case, we first restrict to bounded observations. Choose R_0 containing all the neighborhoods and collars, and first restrict the connecting quad witnesses to $U \cap B(0,R)$, where $R > 2R_0$. A difference from the unrestricted graph requires an original open cluster meeting a wired neighborhood to reach $\partial B(0,R)$, and hence an open arm from $B(0,R_0)$ to that circle. The full-plane arm probability tends to zero as $R \to \infty$, uniformly for sufficiently small mesh, by the RSW annular bounds of subsection 7.3; its mesh limit has the same bound. Apply (11.1) to these measurable continuum tests on the bounded domain $U \cap B(0,R)$ and then let $R \to \infty$. Since $f(\infty) = \infty$, the image domains exhaust U' and the same estimate removes their cutoff. The full-plane arm limits control the cutoff at fixed positive neighborhood and collar scales. □

Remark (Scope of the restricted-record argument). Lemma 14.1 identifies a finite connection graph on the closed-circuit event. Its indicator limits come from full-plane connection limits; its measurability in the restricted records uses Camia–Conijn–Kiss's definition of connection events [23, Definition 4.5 and Remark 4.6]. Their rectangle-confined indicator-convergence result [23, Lemma 4.18] is a separate statement. The lemma does not claim convergence of the full cluster ensemble or of unshielded connection events in a multiply connected domain. In the unbounded case, the cutoff is removed while all neighborhood and collar scales, and hence the positive denominators, remain fixed.

The cases $n = 0$ and odd n follow from $G_{U,0} = 1$ and (11.4). Take even $n \geq 2$ and set $F^a = P_n \cap C_\delta^a$, with P_n evaluated in the full plane. Let $\mathcal{N}_i \ni z_i$ be disks or their images under conformal maps defined on neighborhoods of the closed disks. Choose their closures inside the pairwise disjoint root disks, so that they also avoid the collar annuli. Let $A_i^a(\mathcal{N}_i)$ require an open path from z_i^a stopped at its first cell meeting $\partial\mathcal{N}_i$. Put $\boldsymbol{\mathcal{N}} = (\mathcal{N}_1, \dots, \mathcal{N}_n)$. Since F^a implies every local arm, independence of their disjoint cell sets gives

$$q_a(\boldsymbol{\mathcal{N}}) := \mathbb{P}_a\left(F^a \mid \bigcap_i A_i^a(\mathcal{N}_i)\right) = \frac{\mathbb{P}_a(F^a)}{\prod_i \mathbb{P}_a(A_i^a(\mathcal{N}_i))}. \tag{14.3}$$

For disks $\mathcal{N}_i = B(z_i, t_i)$, Lemma 11.1 and (11.3) give

$$q(\boldsymbol{\mathcal{N}}) := \lim_{a \downarrow 0} q_a(\boldsymbol{\mathcal{N}}) = G_{\mathbb{C},n}[C_\delta](\mathbf{z}) \prod_i t_i^{5/48}.$$

For the other neighborhoods, the proof of Lemma 11.1 again gives $q(\boldsymbol{\mathcal{N}}) = \lim_{a\downarrow 0} q_a(\boldsymbol{\mathcal{N}})$. We make the transport of this conditional probability explicit. Let $\mathcal{P}_{\text{even}}$ consist of the partitions all of whose blocks have even size. For $0 < \eta < t/2$ and sufficiently small t, abbreviate

$$\mathsf{P}_{C_\delta}(\eta, t; \boldsymbol{\mathcal{N}}) := \mathsf{P}_{C_\delta}((B(z_i,\eta))_i, (B(z_i,t))_i; \boldsymbol{\mathcal{N}}, \mathcal{P}_{\text{even}}).$$

This is the mesh limit of $\mathbb{P}_a(W_t \cap C_\delta^a \mid E^a(\eta, \boldsymbol{\mathcal{N}}))$, with W_t as in Lemma 11.1 and the confined annular arms defined in Lemma 14.1. At fixed t, the local coupling compares this test with $W_t \cap C_\delta^a$ under root conditioning, with error $c(\eta,t) \to 0$ as $\eta \downarrow 0$. The open-circuit comparison then replaces W_t by P_n with error $b(t) \to 0$. Consequently,

$$q_{C_\delta}(\boldsymbol{\mathcal{N}}) := q(\boldsymbol{\mathcal{N}}) = \lim_{t\downarrow 0} \lim_{\eta \downarrow 0} \mathsf{P}_{C_\delta}(\eta, t; \boldsymbol{\mathcal{N}}). \tag{14.4}$$

Here the mesh limit has already been taken in P, and the outer neighborhoods remain fixed.

At each fixed η, t, Lemma 14.1 transports all three parts of the ratio: the wired neighborhoods, the conditioning annuli, and the circuit event. The two inner neighborhoods on

the target side are $f(B(z_i,t))$ and $f(B(z_i,\eta))$. Since $f'(z_i)\neq 0$, constants $0<c_i<C_i<\infty$ satisfy

$$B(f(z_i),c_i r)\subset f(B(z_i,r))\subset B(f(z_i),C_i r)$$

for every sufficiently small r. The circuit-coupling argument therefore has the same vanishing errors for these image neighborhoods; this is the shape extension in [1, Lemma 2.1 and Remark 2.2]. Taking first $\eta\downarrow 0$ and then $t\downarrow 0$ in the transported ratios gives

$$q_{C_\delta}(\boldsymbol{\mathcal{N}})=q_{fC_\delta}(f\boldsymbol{\mathcal{N}}). \tag{14.5}$$

Thus conformal invariance has been used at positive scales, before conditioning is approximated at a point. For sufficiently small $\epsilon>0$, apply (14.5) with $\mathcal{N}_i=f^{-1}B(f(z_i),\epsilon)$. The disk formula on the target side gives

$$G_{\mathbb{C},n}[fC_\delta](f\mathbf{z})\,\epsilon^{5n/48}=q((f^{-1}B(f(z_i),\epsilon))_{i=1}^n).$$

Put $s_i=|f'(z_i)|>0$. Taylor expansion of f^{-1} gives a constant C, depending on f and the marks, such that

$$B(z_i,\epsilon/s_i-C\epsilon^2)\subset f^{-1}B(f(z_i),\epsilon)\subset B(z_i,\epsilon/s_i+C\epsilon^2) \tag{14.6}$$

for all sufficiently small ϵ. The numerator in (14.3) is unchanged when the neighborhoods vary. Hence the two disk conditional probabilities bound the middle one, in the same order as these inclusions. Substitute the disk formula, divide by $\epsilon^{5n/48}$, and let $\epsilon\downarrow 0$. This proves

$$G_{\mathbb{C},n}[fC_\delta](f\mathbf{z})=\prod_i|f'(z_i)|^{-5/48}G_{\mathbb{C},n}[C_\delta](\mathbf{z}). \tag{14.7}$$

This is the normalization argument of [1, (2.33)–(2.36), (2.41)–(2.45)], with the circuit event retained in the numerator. The same proof gives these derivative factors for the exact-partition events of Section 11 whose blocks all have at least two indices.

Divide (14.7) by the common positive circuit probability supplied by Lemma 14.1. The source conditional correlation tends to $G_{U,n}$ by (13.6). On the target side, the image circuits lie in collars of width $c_f\delta$. Their filled regions therefore satisfy the intermediate-set bounds of Lemma 12.1. The proof of Lemma 13.1 then gives the same comparison with $G_{U',n}$. Letting $\delta\downarrow 0$ proves (10.4).

15 Exact conditioning and the uniform completion bound

We now prove the conditioning identity and the exterior bound in Theorem 10.1. We use the model and exterior functional defined in Section 10.

Let K^a be a finite set of cells sampled in D_0^a, and let $N_a=|K^a|$ be their number. Write $\mathbb{E}^a_{D_0;K^a}$ for expectation after forcing these cells closed, leaving the other colors independent and fair, and assigning independent signs to the resulting open clusters. Exact conditioning gives

$$\mathbb{E}^a_{D_0}\left[2^{N_a}\mathbf{1}_{\{K^a\text{ closed}\}}\prod_i\Phi_a(z_i^a)\right]=\mathbb{E}^a_{D_0;K^a}\prod_i\Phi_a(z_i^a). \tag{15.1}$$

Indeed, the closing event has probability 2^{-N_a}. Conditional on it, all other sampled colors remain independent, and the conditional law of the cluster signs is exactly the law just specified.

For the fixed geometric holes of Section 10, take $K^a = \bigcup_{j=1}^m K_j^a$. The right side is then $\mathbb{E}_U^a \prod_i \Phi_a(z_i^a)$, whose mesh limit exists by Section 13. For disjoint cell sets the closing factors multiply exactly. The same identity holds with previously closed holes retained, provided K^a contains only cells that were still sampled. These identities hold before any limit is taken.

For the exterior bound, use the source regions V_j, record spaces $S_a(V_j)$, and probabilities $p_{\mathbf{z}}^a(\mathbf{s})$ of Section 10. Choose disjoint closed root disks $\overline{B(z_i, d_i)}$ in U, outside all source closures. For even $n \geq 2$, the event defining $p_{\mathbf{z}}^a(\mathbf{s})$ requires each mark to connect to another mark outside its root disk. It therefore requires all the independent local arms A_i^a from (11.5), for every record tuple $\mathbf{s}$. Thus

$$\begin{aligned} 0 \leq \pi_a^{-n} p_{\mathbf{z}}^a(\mathbf{s}) \leq C_a &:= \pi_a^{-n} \prod_i \mathbb{P}_a(A_i^a), \\ \limsup_{a \downarrow 0} C_a &\leq \prod_i d_i^{-5/48}. \end{aligned} \tag{15.2}$$

The second line is (11.3). The bound is independent of the records and of the holes inside the fixed source regions. For $n = 0$, the completion probability is one; for odd n, it is zero.

On the compact support of ψ, choose a common positive radius for all root disks. The full-plane arm probability for a disk centered at a lattice vertex is independent of that vertex. Together with the circle comparison in Section 11, this bounds C_a uniformly in the marks for all sufficiently small meshes. The finite-sum definition of $\mathcal{J}_\psi^a$ and the triangle inequality give, for arbitrary complex rows v_j,

$$\begin{aligned} |\mathcal{J}_\psi^a(v_1, \dots, v_k)| &\leq \sum_{\mathbf{s}} |g_\psi^a(\mathbf{s})| \prod_{j=1}^k |v_j(s_j)| \\ &\leq C \|\psi\|_{L^1} \prod_{j=1}^k \|v_j\|_{\mathrm{var}}. \end{aligned} \tag{15.3}$$

This proves (10.5). On a fixed compact support, $\|\psi\|_{L^1}$ is bounded by its product area times $\sup|\psi|$. The additional-hole laws ν_H and differences $\nu_H - \nu_\varnothing$ from Section 10 have variation norms one and at most two, respectively, so the same estimate applies to them.

16 Infinity and angular averages at fixed radii

This section completes the covariance proof for the spherical chart convention of Section 10. It also establishes the mesh limits of density observations averaged over ellipse orientations, at fixed positive radii.

16.1 Truncation and changes of chart

For a domain V of Section 10, write

$$G_{V,n}^a(\mathbf{z}) = \mathbb{E}_V^a \prod_{i=1}^n \Phi_a(z_i^a).$$

It remains to consider even $n \geq 2$; the other cases follow from (11.4). For $0 < s < t$, let $\alpha_1(s,t)$ be the mesh limit of the full-plane probability of an open path confined to $B(0,t) \setminus \overline{B(0,s)}$ and joining its two boundary circles. This limit exists by [9, Section 2.4, Lemma 2.9]; translation of the annulus does not change it, by subsection 11.1. The RSW bounds of subsection 7.3

give a uniform positive probability of a closed circuit in each of a family of disjoint annuli with fixed radius ratio. An open arm requires all these circuits to be absent. Independence therefore gives constants $C < \infty$ and $\kappa > 0$ such that

$$\alpha_1(s,t) \le C(s/t)^\kappa.$$

Take $D_0 = \mathbb{C}$, and choose R so that $B(0,R)$ contains all holes and closed root disks. For $L > 4R$, put $U_L = B(0,L) \setminus \bigcup_j K_j$. Its lattice model samples $B(0,L)^a$, retains the forced cells K_j^a, and closes all cells outside $B(0,L)^a$, as in Section 10. Couple it with the model in U by using the same original colors.

A changed connection between marks requires an open path reaching the newly closed cells near $\partial B(0,L)$. This path contains an open arm from radius $2R$ to radius L. If the parity indicators differ, all local root arms also occur. The annular event uses cells outside the root disks, so independence and (11.3) give

$$\limsup_{a\downarrow 0} |G^a_{U,n}(\mathbf{z}) - G^a_{U_L,n}(\mathbf{z})| \le C\alpha_1(2R,L) \longrightarrow 0 \quad (L\to\infty). \tag{16.1}$$

Here C depends only on the fixed root disks. The same bound holds for any further closing of cells that leaves every cell of $B(0,L)^a$ unchanged. Compare the large-box argument in [23, proof of Theorem 7.1, p. 32].

We also need to remove a small neighborhood of a finite point. Fix $p \in U$ distinct from the marks. After shrinking the root disks if necessary, choose $d > 0$ so that $\overline{B(p,d)} \subset U$ is disjoint from them. Let $0 < r < d/4$, and let $H \subset B(p,r)$ be an additional compact Jordan hole with analytic boundary. A changed marked connection must meet H^a and leave $B(p,d)$. The same independent-arm argument gives

$$\limsup_{a\downarrow 0} |G^a_{U,n}(\mathbf{z}) - G^a_{U\setminus H,n}(\mathbf{z})| \le C\alpha_1(2r,d) \longrightarrow 0 \quad (r\downarrow 0),$$

uniformly over such H. This comparison also holds for bounded D_0.

Now let f be a spherical conformal map as in Section 10, with source and target marks finite in the chosen charts. If a finite point p satisfies $f(p) = \infty$, delete a small closed disk about p. If the source contains infinity, also truncate it at a large circle. The remaining source domain and its image are bounded domains with analytic boundaries, so Section 14 applies. In the image, the removed regions lie either in disks shrinking to nonmarked finite points or outside disks whose radii tend to infinity. This follows from the chart expressions of f. Take the mesh limit first, then remove these auxiliary boundaries using the two estimates above. The derivative factors at the marks are unchanged, giving (10.4) under the spherical convention. This justifies the finite-path convention at infinity specified in Section 10.

16.2 Density observations averaged over orientations

Use k source disks D_j and rows $Q^a_j(r_j, w_j)$ as in subsection 9.3, with pairwise disjoint closures contained in U. Keep every $r_j > 0$ fixed, with each rotated ellipse inside its source disk. For $\boldsymbol{\phi} = (\phi_1, \dots, \phi_k) \in [0, 2\pi]^k$, set

$$U_{\boldsymbol{\phi}} = U \setminus \bigcup_{j=1}^{k} K_{r_j, e_j, \phi_j}(w_j).$$

Let ψ be as in Section 10, with its marked points outside all source closures. The definition of Q in subsection 4.3 and finite multilinearity give

$$\mathcal{J}^a_\psi(Q^a_1(r_1,w_1),\dots,Q^a_k(r_k,w_k)) = \left(\prod_{j=1}^{k}\frac{1}{2\pi e_j r_j^2}\right) \times \int_{[0,2\pi]^k} e^{-2i\sum_j \phi_j}\left[\int_{\operatorname{supp}\psi}\psi(\mathbf{z})G^a_{U_{\boldsymbol{\phi}},n}(\mathbf{z})\,d^{2n}\mathbf{z}\right]d\phi_1\cdots d\phi_k.$$

For $n=0$, omit the inner integration and take $\psi=1$, as before. By (15.1), $G^a_{U_{\boldsymbol{\phi}},n}$ is also the expectation in U of $\prod_i \Phi_a(z_i^a)$ multiplied by the closing factors for these ellipses. This identity holds before any limit.

For every fixed $\boldsymbol{\phi}$, Section 13 gives convergence of the density correlation. A common positive radius for the root disks, all outside the source disks, makes (11.6) uniform in the angles and in the marks on the support of ψ. The prefactors $(2\pi e_j r_j^2)^{-1}$ are fixed and finite. Dominated convergence therefore permits both integrations through the mesh limit and proves (9.10). Together with the bound from Section 15, this verifies both assumptions of subsection 9.3 for the density observations and completes Theorem 10.1.

Part III
The finite stress hierarchy

17 Arbitrary finite stress insertions with density spectators

Density factors observed away from the ellipse centers will be called *density spectators*. We construct joint limits of the angular ellipse variables, then identify them by an explicit recursion for their correlations.

17.1 Ellipse variables and joint limits

Work in the full-plane model of Section 10. We retain the notation of Parts I and II: n counts density marks and m counts stress sources, represented at positive radii by m elliptical holes. Fix integers $n, m \geq 0$, source centers $\mathbf{w} = (w_1, \dots, w_m)$, and density marks $\mathbf{z} = (z_1, \dots, z_n)$. Choose source disks $D_j = B(c_j, d_j)$ with pairwise disjoint closures and $w_j \in B(c_j, d_j/8)$. The density coordinates are tested against a smooth function ψ with compact support in $\mathcal{C}_n(\mathbb{C})$. Every density coordinate on its support lies outside all source closures. Fix $e_j \in [e_-, e_+] \subset (0,1)$ and radii $0 < r_j \leq cd_j$, with c small enough for Section 9. Write $\boldsymbol{r} = (r_1, \dots, r_m)$ and $Y_a = \prod_{i=1}^n \Phi_a(z_i^a)$. We suppress the fixed n and shape parameters in the notation below.

For the ellipses of subsection 4.3, let $N_a(r, e, \phi, w)$ be the number of cells in $K_{r,e,\phi}(w)^a$. Define the complex random variable

$$\tau_{a,r,e}(w) = \frac{1}{2\pi e r^2} \int_0^{2\pi} e^{-2i\phi} 2^{N_a(r,e,\phi,w)} \mathbf{1}_{\{K_{r,e,\phi}(w)^a \text{ closed}\}}\, d\phi. \tag{17.1}$$

It depends only on the colors of cells contained in $B(w, 2r)$. At fixed mesh, the integral involves finitely many cells and finitely many changes of the forced set. Equation (15.1), with no density factors, gives $\mathbb{E}^a_{\mathbb{C}} \tau_{a,r,e}(w) = 0$. Variables in disjoint source disks are independent. Consequently, at every fixed mesh and positive radii with disjoint supports,

$$\mathbb{E}^a_{\mathbb{C}}\left[\tau_{a,r_1,e_1}(w_1)\tau_{a,r_2,e_2}(w_2)\right] = \mathbb{E}^a_{\mathbb{C}}\tau_{a,r_1,e_1}(w_1)\, \mathbb{E}^a_{\mathbb{C}}\tau_{a,r_2,e_2}(w_2) = 0.$$

This exact identity gives the vanishing stress two-point function discussed in subsection 2.5; the nonzero Ward action below identifies the stress normalization.

A *distribution* is a complex-linear functional on smooth compactly supported tests. On each fixed compact support, its absolute value is bounded by a constant times the suprema of finitely many derivatives of the test. We write its value as $\langle \mathscr{F}, \psi \rangle$. A locally integrable function acts by $\langle \mathscr{F}, \psi \rangle = \int \mathscr{F}\psi$, without complex conjugation. Define the fixed-radius correlation by

$$\langle F_{m,\boldsymbol{r}}(\mathbf{w}), \psi \rangle := \lim_{a \downarrow 0} \int \psi(\mathbf{z}) \mathbb{E}^a_{\mathbb{C}} \left[\prod_{j=1}^m \tau_{a,r_j,e_j}(w_j) Y_a \right] d^{2n}\mathbf{z}.$$

The integral is over the support of ψ. Section 16 proves this limit and identifies it with $\lim_{a\downarrow 0} \mathcal{J}^a_\psi(Q^a_1, \dots, Q^a_m)$, where $Q^a_j = Q^{a,D_j}_{r_j,e_j}(w_j)$. For $n = 0$, take $\psi = 1$ and omit the integration. For $m = 0$, the correlation is $G_{\mathbb{C},n}$ from (10.3). The finite-mesh integrals are measurable in the centers and radii; their limits retain this property.

Choose root disks $B(z_i, \rho_i)$ with pairwise disjoint closures outside the source closures, and let A_i^a be the stopped arms in (11.5). The normalization used in (10.5) is

$$\pi_a^{-n} \prod_{i=1}^{n} \mathbb{P}_a(A_i^a) \longrightarrow \prod_{i=1}^{n} \rho_i^{-5/48}, \tag{17.2}$$

by (11.3); Section 15 supplies the exterior bound. For odd n the correlation is zero, and for $n = 0$ we use empty products. On fixed separated compact sets, all bounds below are uniform over ψ through $\|\psi\|_{L^1}$. Constants may depend on n, m, the disks, the separation bounds, and $[e_-, e_+]$.

Put $\boldsymbol{\epsilon} = (\epsilon_1, \dots, \epsilon_m)$. Apply (9.11), using (9.3) in the changed slot and (9.4) in the other slots. After taking the mesh limits at fixed radii, we obtain

$$|\langle F_{m,\boldsymbol{r}} - F_{m,\boldsymbol{\epsilon}}, \psi\rangle| \le C\|\psi\|_{L^1} \sum_{j=1}^{m} \epsilon_j^{1/4}, \qquad 0 < r_j \le \epsilon_j \le c d_j. \tag{17.3}$$

The fixed disk radii are absorbed into C. Comparing two radius tuples through their coordinatewise minimum proves the Cauchy property. Thus a unique joint limit F_m exists, and

$$|\langle F_{m,\boldsymbol{r}} - F_m, \psi\rangle| \le C\|\psi\|_{L^1} \sum_{j=1}^{m} r_j^{1/4}. \tag{17.4}$$

These estimates are uniform as the centers vary within the assigned disks. As in subsection 9.4, a finite cover gives uniformity on every compact set of separated centers and density supports.

Use $|\boldsymbol{w} - \boldsymbol{w}'| = \max_j |w_j - w_j'|$. The center comparison (9.13) gives, for sufficiently small $\epsilon > 0$, $1 < p < 5/4$, and $0 < \delta_w < c\epsilon$,

$$\big|\langle F_m(\boldsymbol{w}) - F_m(\boldsymbol{w}'), \psi\rangle\big| \le C_p\|\psi\|_{L^1}\big(\epsilon^{1/4} + \delta_w \epsilon^{p-3}\big), \qquad |\boldsymbol{w} - \boldsymbol{w}'| \le \delta_w. \tag{17.5}$$

Taking $p = 6/5$ and $\epsilon = \delta_w^{20/41}$ makes both terms $\delta_w^{5/41}$. The tested limit is therefore continuous in all separated center configurations, including collinear ones.

17.2 Ward recursion and transport of tests

Use $Y = \prod_{i=1}^{n} \Phi(z_i)$ as notation for the listed continuum density insertions, and write $\langle Y\rangle = G_Y := G_{\mathbb{C},n}(\mathbf{z})$. Thus the symbols $\Phi(z_i)$ are specified here through their correlations. Empty products give $Y = 1$ and $G_Y = 1$. Set $h_\Phi = 5/96$. Each density factor in (10.4) is $(f'(z_i)\overline{f'(z_i)})^{-h_\Phi}$. The exponents h_Φ in the two factors are called its holomorphic and antiholomorphic weights.

For a complex coordinate $\zeta = x + iy$, put

$$\partial_\zeta = \tfrac{1}{2}(\partial_x - i\partial_y), \qquad \partial_{\bar\zeta} = \tfrac{1}{2}(\partial_x + i\partial_y).$$

Derivatives and multiplication of distributions are defined by $\langle \partial_\zeta \mathscr{F}, \psi\rangle = -\langle \mathscr{F}, \partial_\zeta \psi\rangle$ and $\langle b\mathscr{F}, \psi\rangle = \langle \mathscr{F}, b\psi\rangle$ for smooth b. Set $H_0 = G_Y$ and define

$$\mathcal{D}_w = \sum_{i=1}^{n} \left(\frac{1}{w - z_i}\partial_{z_i} + \frac{h_\Phi}{(w - z_i)^2} \right). \tag{17.6}$$

For every integer $m \ge 1$, define recursively

$$H_m(w_1, \dots, w_m; Y) = \left[\mathcal{D}_{w_1} + \sum_{j=2}^{m} \left(\frac{1}{w_1 - w_j}\partial_{w_j} + \frac{2}{(w_1 - w_j)^2} \right) \right] H_{m-1}(w_2, \dots, w_m; Y). \tag{17.7}$$

Every derivative acts on the expression to its right. We call this the *Ward recursion*; compare the half-plane identity in [19, (4.11)]. After density testing, $\langle H_m(\mathbf{w};Y),\psi\rangle$ is holomorphic in each w_j away from the other centers and the density support. This follows inductively from the rational coefficients and their positive separation from that support.

Theorem 17.1 (Joint ellipse limits and the Ward identity)**.** *For every fixed pair of integers $n,m\ge 0$ and the separated full-plane configurations of subsection 17.1, the joint limit F_m, taken in the order specified in subsection 8.5, exists and satisfies $F_m(\mathbf{w})=H_m(\mathbf{w};Y)$ as distributions in the density coordinates. After each density test, the limit is holomorphic in the separated stress centers and convergence is locally uniform, with error (17.4) and modulus bounded by $C\|\psi\|_{L^1}\delta_w^{5/41}$. The limit is symmetric under permutations of the source labels and independent of each fixed shape parameter $e_j\in[e_-,e_+]$. No averaging in the radii or centers enters its definition.*

We denote these limiting correlations by

$$\langle T(w_1)\cdots T(w_m)Y\rangle := F_m(\mathbf{w}) = H_m(\mathbf{w};Y),$$

and call $T(w)$ a *stress insertion* in this class of correlations. Derivatives of an insertion mean derivatives of its correlations. The existence and continuity assertions were proved above; the remaining subsections prove the identification and the independence of the shape parameters.

The case $m=0$ is already known. For $m\ge 1$, temporarily replace each remaining radius r_j, $2\le j\le m$, by $r_je^{\ell_j}$ and average over the logarithmic variable. Choose nonnegative smooth functions χ_j on $\mathbb{R}$, of compact support and integral one, and integrate with $\chi_j(\ell_j)d\ell_j$. Also integrate the remaining centers against smooth tests on separated compact sets. On these bounded ranges of ℓ_j, (17.4) shows that the averaged correlations have the same limit F_m. These averages are used only in the proof.

Lemma 17.2 (Transport of tests and radius averages)**.** *Fix w_1. The remaining coordinates are*

$$x=(z_1,\dots,z_n,w_2,\dots,w_m).$$

Let $\mathscr{C}\subset\operatorname{int}\widetilde{\mathscr{C}}$ be compact sets of these coordinates, with positive distances between distinct coordinates and from w_1. For each $2\le j\le m$, choose bounded open intervals I_j and $\widetilde{I}_j$ with $\overline{I}_j\subset\widetilde{I}_j$. Tests $\Xi(x,\boldsymbol{\ell})$ have support in $\mathscr{C}\times\prod_{j=2}^m I_j$. Choose the intervals so that $\operatorname{supp}\chi_j\subset I_j$.

For an integer $k\ge 0$, set

$$\|\Xi\|_{C^k}=\max_{|\alpha|+|\beta|\le k}\sup_{x,\boldsymbol{\ell}}|\partial_x^\alpha\partial_{\boldsymbol{\ell}}^\beta\Xi(x,\boldsymbol{\ell})|.$$

Here α,β are tuples of nonnegative integers, and their absolute values are the sums of their entries. The derivatives are taken in the real coordinates, with orders specified by these entries. Let $\mathscr{F}_{\boldsymbol{\rho}}$ be distributions in x, indexed by positive $(m-1)$-tuples $\boldsymbol{\rho}$. For fixed $\boldsymbol{r}=(r_2,\dots,r_m)$, define

$$\langle\mathscr{F}_{\boldsymbol{r}},\Theta\rangle_{\mathrm{av}} := \int_{\mathbb{R}^{m-1}}\big\langle\mathscr{F}_{\boldsymbol{r}e^{\boldsymbol{\ell}}},\Theta(\cdot,\boldsymbol{\ell})\big\rangle_x\,d\boldsymbol{\ell},\qquad \boldsymbol{r}e^{\boldsymbol{\ell}}=(r_2e^{\ell_2},\dots,r_me^{\ell_m}).$$

The subscript x specifies the tested coordinates; av *denotes the integral in which the base radii $\boldsymbol{r}$ are replaced by $\boldsymbol{r}e^{\boldsymbol{\ell}}$. Assume the integrands are measurable, the integrals exist, and, for some $M_{\mathrm{test}}<\infty$, $|\langle\mathscr{F}_{\boldsymbol{r}},\Theta\rangle_{\mathrm{av}}|\le M_{\mathrm{test}}\|\Theta\|_{C^k}$ for every smooth test supported in $\widetilde{\mathscr{C}}\times\prod_j\widetilde{I}_j$. The bound M_{test} may depend on the base tuple $\boldsymbol{r}$, but not on the test. For $m=1$, omit all logarithmic variables and their integration. Products $\Xi=\xi(x)\prod_{j=2}^m\chi_j(\ell_j)$, with ξ a smooth test supported in $\mathscr{C}$, give the averages described above.*

Let g_t, for complex t near zero, be injective holomorphic maps on a fixed neighborhood of all planar points occurring as coordinates of $\widetilde{\mathscr{C}}$. Require joint smoothness in $\Re t, \Im t, z$, nonzero derivative, and $g_0(z) = z$. Define

$$\begin{aligned} X_t(x) &= (g_t(z_1), \dots, g_t(z_n), g_t(w_2), \dots, g_t(w_m)), \\ b_{t,j}(x) &= \log |g_t'(w_j)|, \qquad \boldsymbol{b}_t = (b_{t,2}, \dots, b_{t,m}), \\ W_t(x) &= \prod_{i=1}^{n} |g_t'(z_i)|^{5/48} \prod_{j=2}^{m} g_t'(w_j)^2. \end{aligned}$$

For sufficiently small $|t|$, $X_t(\mathscr{C}) \subset \widetilde{\mathscr{C}}$, and the shifted logarithmic supports stay in $\prod_j \widetilde{I}_j$. With $x = X_t^{-1}(y)$, put

$$\Xi_t(y, \boldsymbol{\eta}) = W_t(x) \, |\det D_{\mathbb{R}} X_t^{-1}(y)| \, \Xi(x, \boldsymbol{\eta} - \boldsymbol{b}_t(x)).$$

The matrix $D_{\mathbb{R}} X_t^{-1}$ is the derivative in real coordinates. Define Ξ_t on the image neighborhood and extend it by zero; its support lies strictly inside that neighborhood. Set $\Xi_+ = \partial_t \Xi_t|_{t=0}$ and $\Xi_- = \partial_{\bar{t}} \Xi_t|_{t=0}$. Then

$$\begin{aligned} \|\Xi_t - \Xi_0\|_{C^k} &\le C|t| \|\Xi\|_{C^{k+1}}, \\ \|\Xi_t - \Xi_0 - t\Xi_+ - \bar{t}\Xi_-\|_{C^k} &\le C|t|^2 \|\Xi\|_{C^{k+2}}. \end{aligned} \tag{17.8}$$

Define transport by $\langle \mathscr{P}_t \mathscr{F}_{\boldsymbol{r}}, \Xi \rangle_{\mathrm{av}} := \langle \mathscr{F}_{\boldsymbol{r}}, \Xi_t \rangle_{\mathrm{av}}$. For smooth families this transports $\mathscr{F}_{\boldsymbol{r}e^{\boldsymbol{\ell}}}(x)$ to $W_t(x) \mathscr{F}_{\boldsymbol{r}e^{\boldsymbol{\ell}+\boldsymbol{b}_t(x)}}(X_t(x))$. It satisfies

$$|\langle \mathscr{P}_t \mathscr{F}_{\boldsymbol{r}} - \mathscr{F}_{\boldsymbol{r}}, \Xi \rangle_{\mathrm{av}}| \le C M_{\mathrm{test}} |t| \|\Xi\|_{C^{k+1}}. \tag{17.9}$$

The constants depend on the fixed enlarged sets and finitely many derivatives of g_t, and are independent of the reference radii $\boldsymbol{r}$.

Proof. For a smooth family, change variables by $y = X_t(x)$ and $\boldsymbol{\eta} = \boldsymbol{\ell} + \boldsymbol{b}_t(x)$. The derivative matrix has zero upper-right block and identity lower-right block. Its inverse determinant is therefore $\det D_{\mathbb{R}} X_t^{-1}(y)$. The change-of-variables formula gives Ξ_t and hence the stated transport. Testing by Ξ_t defines the same operation for distributions.

The chain rule and differentiation of the inverse map bound the first two derivatives in t of Ξ_t, in the C^k norm, by $C\|\Xi\|_{C^{k+1}}$ and $C\|\Xi\|_{C^{k+2}}$. Taylor's formula in $\Re t, \Im t$ proves (17.8). Apply the assumed distribution bound to $\Xi_t - \Xi_0$ to obtain (17.9). Derivatives of shifted radius averages act on the smooth test. □

On fixed enlarged supports, (10.5), (9.4), and (17.4) give the required bounds with $k = 0$. Integration over the bounded sets of centers and logarithmic radii contributes only their fixed volumes. These bounds and measurability make the integrals well defined.

17.3 Mapping the first ellipse to a disk

Set $s = r_1$ and $H_s = \overline{B(w_1, s)}$. The Joukowski map used here is

$$f_t(z) = z + \frac{t}{z - w_1}, \qquad t = e_1 s^2 e^{2i\phi_1}, \qquad g_t = f_t^{-1}. \tag{17.10}$$

Its inverse g_t maps the exterior of the first ellipse onto $\mathbb{C} \setminus H_s$ and satisfies $g_t(z) - z \to 0$ at infinity. For $\theta \in [0, 2\pi)$,

$$f_t(w_1 + se^{i(\phi_1+\theta)}) = w_1 + se^{i\phi_1}\big((1 + e_1)\cos\theta + i(1 - e_1)\sin\theta\big),$$

which is the ellipse boundary of subsection 4.3. Injectivity outside H_s follows from

$$f_t(z) - f_t(\zeta) = (z-\zeta)\left(1 - \frac{t}{(z-w_1)(\zeta-w_1)}\right), \qquad |t| < s^2.$$

On compact sets separated from w_1, inversion gives

$$g_t(z) = z + \frac{t}{w_1 - z} + O(t^2), \qquad g_t'(z) = 1 + \frac{t}{(w_1-z)^2} + O(t^2), \tag{17.11}$$

uniformly with any fixed number of derivatives. Angular averages of elliptical deformations were used earlier in [19, (2.1)–(2.4)]. Here we apply (10.4) to the density correlations at fixed positive radii and angles, then compare the resulting image holes.

For $j \geq 2$, put $K_j(\phi) = K_{r_j,e_j,\phi}(w_j)$ and define the affine map

$$\lambda_j = g_t'(w_j), \qquad L_{t,j}(\zeta) = g_t(w_j) + \lambda_j(\zeta - w_j).$$

Take the radii small enough that $g_t(w_j) \in B(c_j, d_j/4)$ and both image holes lie inside the fixed disk D_j, for every angle. Taylor's formula bounds $|g_t - L_{t,j}|$ on $K_j(\phi)$ by $C|t|r_j^2$. After rescaling by r_j, the boundary parametrizations and their first two derivatives are small perturbations of those of the affine ellipse. Both holes therefore satisfy the shape bounds of subsection 4.1. Their normal displacement has a common bound δ_j over all orientations, with

$$\delta_j \leq C|t|r_j^2. \tag{17.12}$$

Write ν_H^{a,D_j} for the complete frontier-record law in D_j^a after closing H^a, as in subsection 4.1. On this common record space, define

$$Q_{j,\mathrm{aff}}^a(t) = \frac{1}{2\pi e_j r_j^2}\int_0^{2\pi} e^{-2i\phi}\nu^{a,D_j}_{L_{t,j}K_j(\phi)}\,d\phi,$$
$$E_j^a(t) = \frac{1}{2\pi e_j r_j^2}\int_0^{2\pi} e^{-2i\phi}\left(\nu^{a,D_j}_{g_tK_j(\phi)} - \nu^{a,D_j}_{L_{t,j}K_j(\phi)}\right)d\phi.$$

The true image row is $Q_{j,\mathrm{aff}}^a(t) + E_j^a(t)$. Equation (4.1) gives

$$\limsup_{a\downarrow 0}\|E_j^a(t)\|_{\mathrm{var}} \leq C|t|\frac{\alpha_4(Cr_j, d_j)}{r_j} \leq C_p|t|r_j^{p-1}, \qquad 1 < p < 5/4. \tag{17.13}$$

The last inequality uses the four-arm bound in subsection 9.4; the fixed d_j are absorbed into C_p. Changing the orientation variable in the affine row gives the exact identity

$$Q_{j,\mathrm{aff}}^a(t) = \lambda_j^2 Q^{a,D_j}_{|\lambda_j|r_j,e_j}(g_t(w_j)).$$

Since λ_j stays near one, (9.4) supplies a constant $B \geq 1$ with $\limsup_{a\downarrow 0}\|Q_{j,\mathrm{aff}}^a(t)\|_{\mathrm{var}} \leq B$, independent of the small radii and t. Each row comparison uses the same mesh and cut for both rows. Their bounds are used with the limit convention of subsection 8.5.

Expand the multilinear completion over the nonempty subsets I of error slots. By (10.5) and (17.13), the image-replacement error, divided by $|t| = e_1 s^2$, is bounded by

$$\begin{aligned} C\|\psi\|_{L^1}\sum_{\varnothing\neq I\subseteq\{2,\dots,m\}}|t|^{|I|-1}B^{m-1-|I|}\prod_{j\in I}C_p r_j^{p-1} \\ \leq C_p'\|\psi\|_{L^1}\sum_{j=2}^m r_j^{p-1}. \end{aligned} \tag{17.14}$$

For the last inequality, take all $C_p r_j^{p-1}$ and $|t|$ at most one and assign each nonempty subset to one of its members. There are finitely many subsets for fixed m. The additional disk H_s is represented by a probability row of norm one. After averaging the other centers and logarithmic radii on fixed supports, the same bound holds with $\|\psi\|_{L^1}$ replaced by a constant times $\|\Xi\|_{C^0}$.

To see the factor in the affine identity, write $\lambda_j = |\lambda_j| e^{i\theta_j}$ with $\theta_j \in \mathbb{R}$. The radius becomes $|\lambda_j| r_j$ and the orientation becomes $\phi + \theta_j$. The angular change of variable and the radius normalization contribute

$$|\lambda_j|^2 e^{2i\theta_j} = \lambda_j^2. \tag{17.15}$$

The density factors are $|g_t'(z_i)|^{5/48}$ by (10.4). These are precisely the factors in W_t of Lemma 17.2.

17.4 Removing the additional disk

Let $F^{(s)}_{m-1,\boldsymbol{r}}$ be the fixed-radius angular correlation of the remaining $m-1$ sources in $\mathbb{C} \setminus H_s$, defined as in subsection 17.1. Keep w_1, s fixed and write $\boldsymbol{r} = (r_2, \dots, r_m)$. Covariance and the image comparison above give

$$\langle F_{m,(s,\boldsymbol{r})}, \Xi \rangle_{\mathrm{av}} = \frac{1}{2\pi e_1 s^2} \int_0^{2\pi} e^{-2i\phi_1} \langle \mathscr{P}_t F^{(s)}_{m-1,\boldsymbol{r}}, \Xi \rangle_{\mathrm{av}} \, d\phi_1 + \mathcal{E}_{\mathrm{img}},$$
$$|\mathcal{E}_{\mathrm{img}}| \le C_p \|\Xi\|_{C^0} \sum_{j=2}^{m} r_j^{p-1}, \qquad 1 < p < 5/4.$$

Here $\mathcal{E}_{\mathrm{img}}$ is the error in (17.14). On the left, av averages only the remaining radii and tests $x = (z_1, \dots, z_n, w_2, \dots, w_m)$, as in Lemma 17.2. Put

$$B_{s;\boldsymbol{r}} = F^{(s)}_{m-1,\boldsymbol{r}} - F_{m-1,\boldsymbol{r}},$$

so that

$$\langle B_{s;\boldsymbol{r}}, \Xi \rangle_{\mathrm{av}} = \int \langle B_{s;\boldsymbol{r}e^{\boldsymbol{\ell}}}, \Xi(\cdot, \boldsymbol{\ell}) \rangle_x \, d\boldsymbol{\ell}.$$

Choose $d > 0$ so that $\overline{B(w_1, d)}$ avoids the other source disks and the density supports. By (4.6), the difference between the record laws with hole H_s and with no hole has variation norm at most $C\alpha_4(Cs, d)$ after taking the mesh limsup. The remaining rows satisfy (9.4). The completion estimate therefore gives, on fixed enlarged supports,

$$|\langle B_{s;\boldsymbol{r}}, \Xi \rangle_{\mathrm{av}}| \le C \|\Xi\|_{C^0} \alpha_4(Cs, d) \le C_p \|\Xi\|_{C^0} s^p, \qquad 1 < p < 5/4. \tag{17.16}$$

The bound is uniform in the remaining radii. The transport $\mathscr{P}_t$ changes only x and those radii; the disk H_s stays fixed.

Before transport, $B_{s;\boldsymbol{r}}$ does not depend on ϕ_1, so its integral against $e^{-2i\phi_1}$ is zero. Apply (17.9) with $M_{\mathrm{test}} = C_p s^p$ and $k = 0$. Since $|t| = e_1 s^2$, the normalized angular contribution of the disk difference satisfies

$$\left| \frac{1}{2\pi e_1 s^2} \int_0^{2\pi} e^{-2i\phi_1} \langle \mathscr{P}_t B_{s;\boldsymbol{r}}, \Xi \rangle_{\mathrm{av}} \, d\phi_1 \right| \le C_p \|\Xi\|_{C^1} s^p \longrightarrow 0. \tag{17.17}$$

Thus the transport difference supplies the factor $|t|$ before division by $e_1 s^2$.

For the plane term, put $\mathscr{F}_{\boldsymbol{r}} = F_{m-1,\boldsymbol{r}} - F_{m-1}$. Equation (17.4), integrated over the fixed center and logarithmic supports, gives

$$|\langle \mathscr{F}_{\boldsymbol{r}}, \Xi \rangle_{\mathrm{av}}| \le C \|\Xi\|_{C^0} \sum_{j=2}^{m} r_j^{1/4}.$$

The same cancellation and transport estimate yield

$$\left|\frac{1}{2\pi e_1 s^2}\int_0^{2\pi} e^{-2i\phi_1}\langle \mathscr{P}_t \mathscr{F}_{\boldsymbol{r}}, \Xi\rangle_{\mathrm{av}}\, d\phi_1\right| \le C\|\Xi\|_{C^1}\sum_{j=2}^{m} r_j^{1/4}. \tag{17.18}$$

All transformed tests stay in the fixed enlarged supports. The estimates differentiate these tests, not the finite-radius correlations.

17.5 Ward identification by induction

A direct argument for one stress insertion. Fix a smooth density test ψ with separated compact support and let w vary in a compact set separated from that support. On fixed enlarged density supports, put

$$\|\psi\|_{C^k} = \max_{|\alpha|\le k}\sup|\partial^\alpha \psi|,$$

where derivatives are in the real density coordinates. Write $G = G_{\mathbb{C},n}$, $H_s = \overline{B(w,s)}$, and $G_s = G_{\mathbb{C}\setminus H_s,n}$. The fixed-radius mesh limit defining $F_{1,s}$ is proved for density observations in subsection 16.2, which verifies (9.10) in this case. With $t = es^2e^{2i\phi}$ and the maps in (17.10), covariance gives the exact identity

$$\langle F_{1,s}(w),\psi\rangle = \frac{1}{2\pi e s^2}\int_0^{2\pi} e^{-2i\phi}\langle G_s,\psi_t\rangle\, d\phi,$$

where ψ_t is the transported density test of Lemma 17.2 with $m = 1$. There are no remaining source coordinates or logarithmic radius variables. The change-of-variables calculation in that lemma gives

$$\psi_t = \psi + t\psi_+ + \bar t\psi_- + \mathcal{E}_t^{\psi}, \qquad \|\mathcal{E}_t^{\psi}\|_{C^0} \le C|t|^2\|\psi\|_{C^2},$$

and explicitly

$$\psi_+ = \sum_{i=1}^{n}\left[-\frac{\partial_{z_i}\psi}{w-z_i} + \frac{h_\Phi - 1}{(w-z_i)^2}\psi\right].$$

The uniform local bound (11.6) controls G_s on these supports. The normalized angular integral sends $1, t, \bar t$ to $0, 1, 0$, respectively, and hence

$$\langle F_{1,s}(w),\psi\rangle = \langle G_s,\psi_+\rangle + O(s^2\|\psi\|_{C^2}).$$

Choose a common $d > 0$ with $\overline{B(w,d)}$ separated from all density supports. The elementary hole-influence bound (4.6), followed by the completion bound (10.5) with this single probability-row difference, gives

$$|\langle G_s - G,\eta\rangle| \le C\|\eta\|_{L^1}\alpha_4(Cs,d)$$

for tests η on the enlarged supports. Integration by parts in the density coordinates gives $\langle G,\psi_+\rangle = \langle \mathcal{D}_w G,\psi\rangle$. Consequently,

$$|\langle F_{1,s}(w) - \mathcal{D}_w G,\psi\rangle| \le C\left[\alpha_4(Cs,d)\|\psi\|_{C^1} + s^2\|\psi\|_{C^2}\right].$$

The four-arm estimate $\alpha_4(Cs,d) \le C_p(s/d)^p$, for each fixed $0 < p < 5/4$, from [7, Theorem 4 and (9)], makes this tend to zero, uniformly in the separated center w and in $e \in [e_-, e_+]$. This proves the single-insertion limit and its Ward identity directly. The expression $\mathcal{D}_w G$ is holomorphic in w after density testing and contains no shape parameter. This argument uses Part II, the elementary four-arm hole-influence estimate, and smooth transport of the test; its error involves derivatives of ψ. The stronger L^1-uniform bounds (17.4) and (17.5), including their case $m = 1$, are supplied by Part I.

Induction for several stress insertions. For $m \geq 2$, suppose $F_{m-1} = H_{m-1}$, with the single-insertion case established above. The limit H_{m-1} is independent of the remaining radii, so the logarithmic radius shifts in $\mathscr{P}_t$ have no effect on it. Equation (17.11) gives the coefficient $(w_1 - z)^{-1}$ for the change of a coordinate z. The multiplier derivatives are

$$\partial_t |g_t'(z_i)|^{5/48}\Big|_{t=0} = \frac{h_\Phi}{(w_1 - z_i)^2}, \qquad \partial_t g_t'(w_j)^2\Big|_{t=0} = \frac{2}{(w_1 - w_j)^2}.$$

Hence the coefficient of t in the tested transport of H_{m-1} is

$$\left[\mathcal{D}_{w_1} + \sum_{j=2}^{m}\left(\frac{1}{w_1 - w_j}\partial_{w_j} + \frac{2}{(w_1 - w_j)^2}\right)\right] H_{m-1}(w_2, \dots, w_m; Y). \tag{17.19}$$

The normalized angular integral sends $1, t, \bar{t}$ to $0, 1, 0$, respectively. By (17.8), after division by $e_1 s^2$ the tested remainder is bounded by $C\|\Xi\|_{C^2} s^2$.

Combining (17.14), (17.17), (17.18), and (17.19) gives $F_m = H_m$ after the temporary radius and center integrations. Every error vanishes in the joint radius limit. By (17.4), the radius averages have the same limit as the original correlations. Equality against all center tests gives equality at every separated fixed center tuple: the density-tested F_m is continuous by (17.5), and H_m is holomorphic there. This completes the induction.

The resulting H_m contains no shape parameter e_j, so the limit is independent of these parameters. Symmetry follows from the symmetric product of disjoint lattice variables and uniqueness of the joint limit. For $n = 0$, $H_0 = 1$ and the recursion gives $H_m = 0$ for $m \geq 1$, in agreement with their finite-mesh zero means and independence. This proves Theorem 17.1.

18 Conclusion and further questions

In percolation terms, we place small closed ellipses away from two marked sites and ask whether an open path still joins the sites. Rotating an ellipse changes the paths it blocks. Equation (A.4) takes the cosine and sine components at twice each orientation angle, with the required normalizations. These weighted connection probabilities give a percolation interpretation of repeated stress insertions.

The estimate (8.9) applies to the complete frontier record of subsection 4.1. It retains the boundary colors and the connections between open frontier cells. The Cauchy estimate (9.3) yields the completed local row (9.8), for each fixed shape parameter. Theorem 10.1 supplies density correlations in the domains of Section 10, with conformal covariance and the completion bound (10.5).

Theorem 17.1 constructs correlations of every fixed finite collection of stress insertions T and density insertions Φ. These are distributions in the density coordinates. All marked points stay separated on the test supports. After density testing, convergence is locally uniform in the stress centers. The limits are symmetric in the stress insertions, independent of the fixed ellipse shape parameters, and satisfy the Ward recursion (17.7).

Appendix A derives the sequential collision identity (A.11) from the same recursion. Subtracting its poles defines $:TT:$ in Proposition A.1. The contour modes satisfy (A.14), with central charge $c = 0$, inside the tested correlations specified in Section 17. The stress response with two densities is nonzero by (A.6), although correlations containing only separated stress insertions vanish by (A.10). Complex conjugation gives the corresponding statements with angular weight $e^{2i\phi}$.

The present bounds keep distinct marked points apart; in particular, (11.6) is not uniform as density points collide. Further work must control simultaneous collisions and establish

compatible subtraction rules when points are grouped in different orders. These statements must remain valid with other insertions present in the same correlations; see [1, discussion after (2.72)]. Mixed Ward identities, involving both angular weights, also remain to be identified. Extending the stress action to other percolation observables requires their joint construction and completion bounds. A further problem is to construct the bulk logarithmic stress partner t jointly with T and recover the coupling b from their mixed correlations, as discussed in subsection 2.5.

A Examples and consequences of the Ward identities

This appendix records explicit examples and algebraic consequences of the Ward recursion (17.7). Throughout, n denotes the number of density insertions and m the number of stress insertions, as in Section 17. The construction and proof of the joint limit are given in that section.

A.1 The first three stress responses

As distributions in the density coordinates, the first two cases of (17.7) are

$$H_1(w;Y) = \mathcal{D}_w G_Y, \tag{A.1}$$

$$H_2(w_1,w_2;Y) = \left[\mathcal{D}_{w_1} + \frac{1}{w_1-w_2}\partial_{w_2} + \frac{2}{(w_1-w_2)^2}\right]\mathcal{D}_{w_2} G_Y. \tag{A.2}$$

For the third, use the density test ψ and Y_a from subsection 17.1. The identity is

$$\begin{aligned}\lim_{r_1,r_2,r_3\downarrow 0}\lim_{a\downarrow 0}&\left\langle \mathbb{E}^a_{\mathbb{C}}\left[\prod_{j=1}^{3}\tau_{a,r_j,e_j}(w_j)Y_a\right],\psi\right\rangle \\ &= \left\langle\left[\mathcal{D}_{w_1} + \sum_{j=2}^{3}\left(\frac{1}{w_1-w_j}\partial_{w_j} + \frac{2}{(w_1-w_j)^2}\right)\right] H_2(w_2,w_3;Y),\psi\right\rangle.\end{aligned} \tag{A.3}$$

The recursion determines these correlations once G_Y is given. For four density points, define their complex cross-ratio by

$$x = \frac{(z_1-z_2)(z_3-z_4)}{(z_1-z_3)(z_2-z_4)}.$$

A *Möbius map* has the form $M(\zeta) = (A\zeta+B)/(C\zeta+D)$, with $A,B,C,D\in\mathbb{C}$ and $AD-BC\neq 0$. Covariance under these maps alone does not determine the dependence of a four-density correlation on $x,\bar{x}$. The Ward recursion differentiates that dependence; compare [5, Section 7.1, (7.1)–(7.4), p. 24].

A.2 A connection observed through one, two, and three rotating ellipses

For distinct density marks u,v, fix $m\geq 1$ disjoint holes $\boldsymbol{K} = (K_1,\dots,K_m)$ avoiding both marks. Define

$$p^a_{\boldsymbol{K}}(u,v) = \mathbb{P}_a\{\text{there is an open path from } u^a \text{ to } v^a \text{ avoiding } \bigcup_j K^a_j\}.$$

The event depends only on the colors outside the forced cell sets. For $K_j = K_{r_j,e_j,\phi_j}(w_j)$, exact conditioning and the two-root case of (11.4) give

$$\mathbb{E}^a_{\mathbb{C}}\left[\prod_{j=1}^{m}\tau_{a,r_j,e_j}(w_j)\Phi_a(u^a)\Phi_a(v^a)\right] = \pi_a^{-2}\left(\prod_{j=1}^{m}\frac{1}{2\pi e_j r_j^2}\right)\int_{[0,2\pi]^m} e^{-2i\sum_j \phi_j} p^a_{\boldsymbol{K}}(u,v)\,d\phi_1\cdots d\phi_m. \tag{A.4}$$

Here the closing factors are removed by (15.1) before either limit. Theorem 17.1 gives the density-tested limit of this complex angular average of nonnegative probabilities.

For a pair of density insertions put

$$G(u,v) = G_{\mathbb{C},2}(u,v) = C_\Phi|u-v|^{-4h}, \qquad h = h_\Phi = \frac{5}{96}, \qquad C_\Phi = G_{\mathbb{C},2}(0,1) > 0.$$

This two-point formula follows from [1, (1.3), (1.9)]. Its constant cancels from the ratios below. For $1 \le i,j \le m$, with $i \ne j$ in d_{ij}, define

$$a_i = \frac{u-v}{(w_i-u)(w_i-v)}, \qquad d_{ij} = w_i - w_j, \qquad \mathcal{W}_m = \frac{H_m(w_1,\dots,w_m;\Phi(u)\Phi(v))}{G(u,v)}. \tag{A.5}$$

All points in this subsection are distinct, and the displayed expressions are smooth there. Set $\mathcal{W}_0 = 1$. Testing in u, v remains understood for statements about the lattice limits. The formulas below follow from (17.7).

One stress insertion gives

$$\mathcal{W}_1 = ha_1^2. \tag{A.6}$$

Indeed, $\partial_u \log G = -2h/(u-v)$ and $\partial_v \log G = 2h/(u-v)$; inserting these derivatives into (17.6) and combining fractions gives (A.6).

Applying (17.7) once more gives

$$\mathcal{W}_2 = h^2 a_1^2 a_2^2 + \frac{2h\,a_1 a_2}{d_{12}^2}. \tag{A.7}$$

The first term is the product of the individual normalized responses. The second records how the two local deformations interact and diverges when w_1 approaches w_2.

A third application of (17.7) gives the fully symmetric expression

$$\mathcal{W}_3 = h^3 a_1^2 a_2^2 a_3^2 + 2h^2 \sum_{\mathrm{cyc}(i,j,k)} \frac{a_i a_j a_k^2}{d_{ij}^2} + 2h \sum_{\mathrm{cyc}(i,j,k)} \frac{a_i a_j}{d_{ik}^2 d_{jk}^2}, \tag{A.8}$$

where the cyclic triples are $(1,2,3),(2,3,1),(3,1,2)$. There are three types of terms: a product of individual responses, pair interactions accompanied by the response at the third center, and terms coupling all three centers. The formula also shows that the result is independent of the order in which the Ward recursion is applied. Collinear configurations are included whenever the marked points remain distinct.

To check the coefficients, for $J \subseteq \{2,\dots,m\}$ let

$$\mathcal{A}_{1;J} = \frac{1}{w_1-u}\partial_u + \frac{1}{w_1-v}\partial_v + \sum_{j\in J}\left(\frac{1}{d_{1j}}\partial_{w_j} + \frac{2}{d_{1j}^2}\right).$$

Then the normalized Ward recursion reads $\mathcal{W}_m = (ha_1^2 + \mathcal{A}_{1;\{2,\dots,m\}})\mathcal{W}_{m-1}$, where the response on the right is evaluated at $w_2, \dots, w_m$. Direct differentiation and combination of fractions give

$$\mathcal{A}_{1;\{2\}}(a_2^2) = \frac{2a_1a_2}{d_{12}^2}. \tag{A.9}$$

This proves (A.7). The product rule and the same partial-fraction calculation give (A.8) from the next recursion step.

Correlations with no density insertions are called *vacuum correlations*. Finite-lattice independence, or (17.7) with $H_0 = 1$, gives

$$\langle T(w_1) \cdots T(w_m) \rangle = 0, \qquad m \geq 1, \tag{A.10}$$

for pairwise distinct centers. The lattice variables have zero mean and depend on disjoint cell sets. This agrees with $H_m = 0$ for $m \geq 1$ when $H_0 = 1$, while (A.6) gives a nonzero correlation with two densities.

A.3 Sequential stress collisions and local contour operations

Starting with the limiting correlations at distinct centers, we now let two stress centers approach each other. Fix $k \geq 0$ and additional centers $\boldsymbol{u} = (u_1, \dots, u_k)$. Require $z, v, u_1, \dots, u_k$ to be pairwise distinct and outside the density supports. The recursion gives

$$\begin{aligned} H_{k+2}(v, z, \boldsymbol{u}; Y) = {} & \frac{2H_{k+1}(z, \boldsymbol{u}; Y)}{(v-z)^2} + \frac{\partial_z H_{k+1}(z, \boldsymbol{u}; Y)}{v - z} \\ & + \left[\mathcal{D}_v + \sum_{j=1}^{k} \left(\frac{1}{v - u_j} \partial_{u_j} + \frac{2}{(v-u_j)^2} \right) \right] H_{k+1}(z, \boldsymbol{u}; Y). \end{aligned} \tag{A.11}$$

After density testing, the last line is holomorphic in v near z. The *central charge* c is the coefficient specified by a term $\frac{c}{2}(v-z)^{-4} H_k(\boldsymbol{u}; Y)$ in this expansion. Such a term is absent here, so $c = 0$. The two remaining singular coefficients agree with the standard stress coefficients [24, Section 5.4, (5.121), p. 135].

Proposition A.1 (Sequential normal-ordered square)**.** *For these limiting correlations with $v \neq z$, subtract the double and simple poles displayed in (A.11), then let $v \to z$. This defines an insertion $:TT:(z)$ in correlations with every finite product of additional stress and density insertions at distinct points. Its correlation is the last line of (A.11) evaluated at $v = z$. This subtraction and limit are the* normal ordering *used here.*

Proof. The subtracted expression is holomorphic near z, so its limit is independent of direction and uniform on every smaller disk avoiding the other insertions. □

With only density spectators, this identity reads

$$\langle :TT:(z) Y \rangle = \mathcal{D}_z \langle T(z) Y \rangle, \tag{A.12}$$

where $\mathcal{D}_z$ differentiates only the density coordinates. The limit is sequential, since the constants in the earlier estimates may depend on the distances between distinct stress centers.

Let $\mathcal{X}$ be a finite product of stress insertions T and density insertions at points distinct from z. Let $\mathcal{O}(z)$ be an insertion whose correlations with such products have been defined

above. Choose a counterclockwise circle Γ enclosing z and excluding all other insertion points and their density test supports. For $q \in \mathbb{Z}$, define the *contour mode* L_q by

$$\langle (L_q\mathcal{O})(z)\mathcal{X}\rangle = \frac{1}{2\pi i}\oint_\Gamma (\zeta - z)^{q+1}\langle T(\zeta)\mathcal{O}(z)\mathcal{X}\rangle\, d\zeta. \tag{A.13}$$

If the coordinate z itself is density-tested, choose a fixed circle enclosing its whole test support. For repeated operations, use nested circles: L_pL_q places the p-circle outside the q-circle. All identities involving these modes are understood inside the tested correlations. The mode definition is the convention of [24, Section 6.2.1, (6.21), p. 155]; the nested-contour convention is explained in [24, Section 6.1.2, (6.15)–(6.18), pp. 154–155]. The contours stay fixed and separated in the limiting procedure of subsection 8.5. Local uniform convergence in Theorem 17.1 permits these integrations.

For integers p, q, define $[L_p, L_q] = L_pL_q - L_qL_p$. For $f(\zeta) = (\zeta - z)^{p+1}$ and $g(\zeta) = (\zeta - z)^{q+1}$, the difference between the two contour orders is computed from (A.11). The inner contour gives $2f'g\,T + fg\,\partial T$. Integration by parts on the remaining contour replaces this by $(f'g - fg')T$. Since $f'g - fg' = (p - q)(\zeta - z)^{p+q+1}$, we obtain

$$[L_p, L_q] = (p - q)L_{p+q}. \tag{A.14}$$

This is the usual contour calculation [24, Section 6.2.1, (6.24)–(6.25), pp. 156–157], now valid with every such product $\mathcal{X}$.

Define the identity insertion $\mathbf{1}$ to leave every correlation unchanged. With no insertion at z, the correlation containing $T(\zeta)$ is holomorphic near z. Thus $L_q\mathbf{1} = 0$ for $q \geq -1$ by Cauchy's theorem. The same contour definition gives

$$T = L_{-2}\mathbf{1}, \qquad :TT:= L_{-2}^2\mathbf{1}, \qquad \partial_z^2 T = 2L_{-4}\mathbf{1}.$$

Now define

$$\Lambda(z) =: TT:(z) - \frac{3}{10}\partial_z^2 T(z). \tag{A.15}$$

From (A.14),

$$L_1L_{-2}^2\mathbf{1} = 3L_{-3}\mathbf{1}, \qquad L_1L_{-4}\mathbf{1} = 5L_{-3}\mathbf{1}.$$

Consequently $L_1\Lambda = 0$ and $L_0\Lambda = 4\Lambda$. Translation of the contour also gives $L_{-1}\Lambda = \partial_z\Lambda$.

An insertion is called *quasiprimary of holomorphic weight four* if it contributes the factor $M'(z)^{-4}$ under a Möbius map M of all insertion coordinates. Each additional $T(w)$ contributes $M'(w)^{-2}$, and each density at q contributes $|M'(q)|^{-5/48}$. Changes of density coordinates are interpreted through the test transport of Lemma 17.2. The three mode relations above give this covariance for Λ in the present tested correlations. They correspond to the infinitesimal maps $\zeta \mapsto \zeta + t$, $\zeta \mapsto e^t\zeta$, and $\zeta \mapsto \zeta/(1 - t\zeta)$. The identities for the other insertions follow from density covariance and the Ward recursion; integrating these variations gives the stated transformation law.[4] All coordinates and test supports are taken away from the pole of M.

For a normalization check, use $G(u, v)$ and $h = 5/96$ from subsection A.2. The preceding formulas give

$$\frac{\langle T(z)\Phi(u)\Phi(v)\rangle}{G(u,v)} = h\frac{(u-v)^2}{(z-u)^2(z-v)^2}, \tag{A.16}$$

$$\frac{\langle \Lambda(z)\Phi(u)\Phi(v)\rangle}{G(u,v)} = h\left(h + \frac{1}{5}\right)\frac{(u-v)^4}{(z-u)^4(z-v)^4}. \tag{A.17}$$

[4] For this definition and its relation to the three global generators, see P. Ginsparg, *Applied Conformal Field Theory*, arXiv:hep-th/9108028, Sections 1.3 and 3.5, (1.12)–(1.13) and (3.21)–(3.22).

For the second identity, call the rational function in (A.16) $\mathcal{W}_1(z)$. Using $\partial_u \log G = -2h/(u-v)$ and $\partial_v \log G = 2h/(u-v)$, apply (A.12) to $\mathcal{W}_1 G$ and subtract $(3/10)G\partial_z^2\mathcal{W}_1$. Combining the fractions gives (A.17). At $h = 5/96$, its coefficient is $121/9216$. Both coefficients are determined by the density weight and the Ward recursion.

B Checks on normalization and on the order of limits

The following calculations clarify the conditioning, time parameters, and normalization used above.

B.1 Exact conditioning in an adaptive exploration

Use the independent cell colors of subsection 4.1 at a fixed mesh. Let K be a finite deterministic set of sampled cells, and let $|K|$ be its number of cells. An adaptive exploration chooses its next unrevealed cell using only earlier choices and revealed colors. Auxiliary random variables independent of all cell colors are also allowed; their values are included in the history. Write $\mathbb{E}$ for expectation over the colors and auxiliary variables.

For $n \geq 0$, let J_n be the set queried by step n. Let $\mathcal{F}_n$ be the collection of events determined by the ordered choices, revealed colors, and auxiliary variables. For a random variable X with $\mathbb{E}|X| < \infty$, the conditional expectation $\mathbb{E}[X \mid \mathcal{F}_n]$ is a function of these data whose integral on every event in $\mathcal{F}_n$ equals that of X. Equalities of conditional expectations hold with probability one. We have

$$\mathbb{E}[2^{|K|}\mathbf{1}_{\{K \text{ closed}\}} \mid \mathcal{F}_n] = 2^{|K\cap J_n|}\mathbf{1}_{\{\text{every queried cell in } K \text{ is closed}\}}. \tag{B.1}$$

At each step the query rule uses no unrevealed color. By induction, all unqueried colors remain independent and fair conditional on the history. If a queried cell in K is open, both sides vanish. Otherwise, the remaining $|K \setminus J_n|$ cells are all closed with conditional probability $2^{-|K\setminus J_n|}$, which proves the identity.

When $J_n \cap K = \varnothing$, the right side is one. Thus an exploration that avoids K has the same history law before and after K is forced closed. This is the property used in Lemma 8.1.

B.2 Why a bounded random clock error is not enough

A bounded change of observation time can destroy an angular cancellation. Let B_t be a standard real Brownian motion started at zero, as in subsection 5.1, and put $\Theta_t = \sqrt{3/8}\, B_t$. Independently choose a nonnegative random time ζ with

$$\mathbb{P}(\zeta > t) = e^{-5t/4}, \qquad t \geq 0.$$

This defines the exponential lifetime of rate $5/4$. Here $\mathbb{P}$ and $\mathbb{E}$ refer to the joint law of these variables. At deterministic times,

$$\mathbb{E}[\mathbf{1}_{\{t<\zeta\}}e^{2i\Theta_t}] = e^{-5t/4}e^{-3t/4} = e^{-2t}. \tag{B.2}$$

Fix $\delta_t > 0$. For $L \geq 0$, set

$$A_L = \{\cos(2\Theta_L) \geq 0\}, \qquad \tau_L = \begin{cases} L, & \text{on } A_L, \\ L + \delta_t, & \text{on } A_L^c. \end{cases}$$

Thus $L \le \tau_L \le L+\delta_t$. This is a *stopping time*: whether $\tau_L \le t$ is determined by the Brownian observations up to time t. Conditioning at L and using independent Brownian increments gives

$$e^{5L/4}\mathbb{E}[\mathbf{1}_{\{\tau_L<\zeta\}}e^{2i\Theta_{\tau_L}}] = \mathbb{E}\Big[e^{2i\Theta_L}\big(\mathbf{1}_{A_L} + e^{-2\delta_t}\mathbf{1}_{A_L^c}\big)\Big].$$

The extra factor $e^{-2\delta_t}$ includes both survival and angular averaging during the additional wait.

For $L > 0$, reducing $2\Theta_L$ to $[0, 2\pi)$ gives the probability law $\varrho_L(\theta)d\theta$, where

$$\varrho_L(\theta) = \frac{1}{\sqrt{3\pi L}} \sum_{k\in\mathbb{Z}} \exp\left[-\frac{(\theta+2\pi k)^2}{3L}\right].$$

Riemann sums for the Gaussian integral give $\varrho_L(\theta) \to (2\pi)^{-1}$ uniformly in θ as $L \to \infty$. The integrals of $e^{i\theta}$ under this uniform law over $\cos\theta \ge 0$ and $\cos\theta < 0$ are $1/\pi$ and $-1/\pi$. Consequently,

$$\lim_{L\to\infty} e^{5L/4}\mathbb{E}[\mathbf{1}_{\{\tau_L<\zeta\}}e^{2i\Theta_{\tau_L}}] = \frac{1-e^{-2\delta_t}}{\pi} > 0. \tag{B.3}$$

Thus the bounded change of observation time does not preserve the e^{-2L} decay. Equation (6.8) retains the actual image of the ellipse under the map F_t of (6.6) at the deterministic time $t = \log(\epsilon/r)$, with $0 < r \le \epsilon$ as in subsection 6.2.

B.3 A positive normalization test for the one-stress response

Use C_Φ and $G(u,v)$ from Appendix A.2. For this check, define $\widehat{\Phi} = C_\Phi^{-1/2}\Phi$: correlations with two hatted factors are C_Φ^{-1} times the original correlations. Hence

$$\widehat{G}(u,v) := \langle\widehat{\Phi}(u)\widehat{\Phi}(v)\rangle = |u-v|^{-5/24}.$$

For pairwise distinct w, u, v, (A.6) gives

$$\langle T(w)\widehat{\Phi}(u)\widehat{\Phi}(v)\rangle = \frac{5}{96}\frac{(u-v)^2}{(w-u)^2(w-v)^2}|u-v|^{-5/24}. \tag{B.4}$$

This smooth function represents the density-tested limit of Theorem 17.1.

At $(w,u,v) = (2,0,1)$, its value is $5/384 > 0$. With $w = 2$ fixed, nonzero nonnegative smooth tests supported sufficiently near $(u,v) = (0,1)$ therefore give a positive real part. The stress insertion has a nonzero correlation with two densities, although its vacuum correlation is zero by (A.10).

C Close inner approximations on prescribed lattices

We verify the model-family approximation property in K5, which is Karrila's Assumption 5.4. The marked convergence and close-approximation conventions are those of [14, Sections 3.2.3–3.2.4, pp. 13–14, and Assumption 5.4, p. 26].

Lemma C.1 (Close inner approximations)**.** *Let V be a bounded simply connected domain, let $u \in V$, and fix $2m$ distinct marked prime ends, $m \ge 1$, whose radial limits exist. For every prescribed sequence of translated honeycomb lattices $\Gamma_\nu = b_\nu + a_\nu\mathbb{H}$, with $a_\nu \to 0$, there are admissible marked percolation graphs on these lattices whose domains Ω_ν lie in V for all sufficiently large ν. Their boundary marks are distinct and have the prescribed cyclic order. The domains converge to V in the marked Carathéodory sense of subsection 7.1, and the marked endpoints approximate the prescribed prime ends closely in the sense of K5. The Euclidean radial limits of distinct prime ends may coincide.*

Proof. Let V be any bounded simply connected domain, let $g : \mathbb{D} \to V$ satisfy $g(0) = u$ and $g'(0) > 0$, and let $\zeta_1, \dots, \zeta_{2m} \in \partial\mathbb{D}$ represent the marked prime ends in cyclic order. Assume that their radial limits

$$p_j = \lim_{s\uparrow 1} g(s\zeta_j)$$

exist. The prime ends are distinct at this stage; the Euclidean points p_j need not be distinct. Fix any prescribed sequence of translated honeycomb lattices $\Gamma_\nu = b_\nu + a_\nu\mathbb{H}$, where $\mathbb{H}$ is the unit honeycomb lattice and $a_\nu \to 0$. We construct admissible marked graphs on every lattice sufficiently far along this sequence.

(a) Compact cores and lattice domains. Choose $R_0 < \frac{1}{4}\min_j |p_j - u|$, put $r_k = 2^{-k}R_0$, and choose $s_k \uparrow 1$ so that, simultaneously for all marks,

$$g([s_k, 1)\zeta_j) \subset B(p_j, r_k/4). \tag{C.1}$$

Set

$$t_k = \frac{1+s_k}{2}, \qquad v_k = \frac{1+t_k}{2}, \qquad K_k = g(\overline{s_k\mathbb{D}}), \quad U_k = g(t_k\mathbb{D}), \quad q_{k,j} = g(s_k\zeta_j).$$

The boundary of U_k is an analytic Jordan curve, $K_k \Subset U_k$, and $g(v_k\zeta_j) \notin \overline{U}_k$.

For fixed k, we construct the inner approximation as follows. Let d_a be the diameter of a mesh-a hexagon. For a small enough the inner parallel set

$$U_k^{-2d_a} = \{z \in U_k : \operatorname{dist}(z, \partial U_k) > 2d_a\}$$

is connected: a compact analytic Jordan curve has a tubular neighborhood with a unique normal coordinate, and its sufficiently small inner parallel curves are again Jordan curves. Take the union of all closed hexagons meeting $U_k^{-2d_a}$, and fill its bounded complementary components. Before filling, every selected hexagon is contained in U_k, at distance at least d_a from its boundary. The selected hexagons are connected through shared edges, since they meet the connected open set $U_k^{-2d_a}$ and any two honeycomb faces meeting at a vertex also share an edge. Filling cannot leave U_k, because its exterior is connected to infinity and disjoint from the selected hexagons. The resulting finite union has one simple honeycomb boundary cycle: at any vertex of a union of honeycomb faces there are either zero or two boundary edges, and filling removes all inner boundary cycles. Denote its interior by $\Omega_{k,a}$. Thus

$$U_k^{-2d_a} \subset \Omega_{k,a}, \qquad \overline{\Omega}_{k,a} \subset U_k.$$

For all sufficiently small a, this domain contains a neighborhood of K_k. These assertions hold uniformly in the translation of the lattice.

(b) Marked incoming edges and admissible colors. Choose a common lattice vertex u^a near u. Approximate each radial arc $g([0, v_k]\zeta_j)$ by a honeycomb edge walk starting at u^a and ending outside $\overline{U}_k$. Such walks can be chosen within $C_{\mathbb{H}}a$ of the arcs: follow the finite chain of hexagons crossed by each arc and connect along their edges, doing this separately before and after $q_{k,j}$ with a common intermediate vertex near that point. An arbitrarily small perturbation handles an arc passing through a lattice vertex or along an edge. The initial part lies inside $\Omega_{k,a}$, since the domain contains a fixed neighborhood of K_k. Stop at the first boundary vertex $p_j^{k,a}$ of $\Omega_{k,a}$. The final edge $e_j^{k,a}$ joins an interior vertex to a boundary vertex, as required in [14, Section 3.1.1, p. 11]. Connecting $q_{k,j}$ to the intermediate vertex and retaining the terminal part of the walk gives a path whose interior lies in

$$\Omega_{k,a} \cap B(p_j, r_k/2).$$

Here and below only the marked endpoint of such an access path lies on the domain boundary.

At fixed k, the terminal radial segments are pairwise disjoint compact arcs, even when some p_j coincide. Choose disjoint tracking neighborhoods for these segments. The marks are then distinct and retain their cyclic order. To see the latter directly, erase loops and trim each access path at its last intersection with ∂K_k. Its initial point lies on a small arc around $q_{k,j}$, and the resulting disjoint arcs cross the region between K_k and $\partial\Omega_{k,a}$. The Jordan separation theorem forces their terminal points to have the same cyclic order.

We next verify the alternating face prescription. The union of the stopped walks is connected and meets $\partial\Omega_{k,a}$ only at the marked vertices. Take a spanning tree of this union, retaining the terminal edges, and prune its unmarked leaves. The resulting embedded tree has precisely the $2m$ marked boundary vertices as leaves and otherwise lies in $\Omega_{k,a}$. Cutting a Jordan domain along such a tree gives $2m$ components, each incident to one boundary arc between consecutive marks: start with a path between two boundary leaves, then add branches, each of which splits one component in two. Every open hexagonal face of the domain is connected and disjoint from the tree, which uses lattice edges, so it lies in a single component. Assign alternating colors to these components and fix only the boundary faces to their component's color. This is consistent even if a boundary face touches the boundary more than once. Across a marked incoming edge the two incident faces have opposite colors; at any other boundary vertex the interior faces have the same color. All remaining faces are independent fair cells. Hence the measures in [14, Section 6.1.2, p. 45] are defined on these marked graphs.

(c) The diagonal on the prescribed lattice sequence. The mesh thresholds can be chosen from finitely many positive geometric clearances. At stage k these are the tubular radius of ∂U_k, $\operatorname{dist}(K_k, \partial U_k)$, the distances of the finitely many $g(v_k\zeta_j)$ from $\overline{U}_k$, the widths and separations of the terminal tracking neighborhoods, their clearances from ∂K_k outside the chosen small ordered arcs, and $r_k/8$. Let $c_k > 0$ be their minimum. Enlarge the fixed lattice constant $C_{\mathbb{H}}$ to include the face-diameter bound and, starting with any $\delta_0 > 0$, take

$$\delta_k = \min\{\delta_{k-1}/2,\ c_k/(10C_{\mathbb{H}})\}.$$

Every construction above then works for every $a < \delta_k$, independently of the lattice translation. Choose strictly increasing integers $N_k \geq k$ such that $a_\nu < \delta_k$ for every $\nu \geq N_k$, and set

$$k(\nu) = \max\{k : N_k \leq \nu\}, \qquad \Omega_\nu = \Omega_{k(\nu),a_\nu}, \qquad e_j^{(\nu)} = e_j^{k(\nu),a_\nu}. \tag{C.2}$$

For the finitely many indices $\nu < N_1$, choose arbitrary admissible marked graphs. This defines an approximation on the entire given sequence, and $k(\nu) \to \infty$.

For all later indices, $K_{k(\nu)} \subset \Omega_\nu \subset V$; hence every compact subset of V is eventually contained in Ω_ν, and these domains converge to V in the kernel sense. Write $p_j^{(\nu)}$ for the boundary endpoint of $e_j^{(\nu)}$. The following local access property is stronger than Euclidean endpoint convergence: for every fixed ℓ and every $\nu \geq N_\ell$ there is a path

$$q_{\ell,j} \longleftrightarrow p_j^{(\nu)} \quad \text{with interior in } \Omega_\nu \cap B(p_j, r_\ell). \tag{C.3}$$

Indeed, first follow the radial segment from $q_{\ell,j}$ to $q_{k(\nu),j}$, which lies in $K_{k(\nu)} \cap B(p_j, r_\ell/4)$, and then use the terminal access path from (b). In particular $p_j^{(\nu)} \to p_j$. The associated lattice graphs lie inside V, and uniform boundedness follows from boundedness of V.

(d) Convergence of the marked conformal coordinates. We verify marked convergence by a length–area estimate. Let $f_\nu : \Omega_\nu \to \mathbb{D}$ and $f = g^{-1} : V \to \mathbb{D}$ be normalized at u. Kernel

convergence gives $f_\nu \to f$ locally uniformly in V; see [14, Section 3.2.3, p. 13]. The maps f_ν extend continuously to the polygonal boundaries. For a regular radius $r_\ell < t < R_0$, let

$$L_{\nu,j}(t) = \int_{\Omega_\nu \cap \partial B(p_j,t)} |f'_\nu(z)|\,|dz|,$$

the total length of the images of all the circle arcs. Cauchy–Schwarz on each circle and the conformal area formula give

$$\int_{r_\ell}^{R_0} L_{\nu,j}(t)^2\,\frac{dt}{t} \le 2\pi \int_{\Omega_\nu} |f'_\nu(z)|^2\,dA(z) = 2\pi^2. \tag{C.4}$$

Consequently, we can choose a radius $t = t_{\nu,\ell,j}$, avoiding boundary vertices and tangencies, such that

$$L_{\nu,j}(t) \le \eta_\ell := \left(\frac{2\pi^2}{\log(R_0/r_\ell)}\right)^{1/2}.$$

The intersection of this circle with Ω_ν is a finite collection of disjoint crosscuts. There is no whole-circle component: its center p_j is outside Ω_ν, whereas a simply connected domain containing a circle contains its interior. Cutting a Jordan domain along finitely many disjoint crosscuts gives a tree of complementary components. Since u is outside the circle, and the path in (C.3) lies inside the smaller ball, one of these crosscuts separates both $q_{\ell,j}$ and $p_j^{(\nu)}$ from u. Its image has length at most η_ℓ. A disk crosscut of length $h < 1$ cuts off, on the side not containing 0, a component of diameter at most $2h$: the crosscut and the shorter unit-circle arc joining its endpoints lie in the closed ball of radius h about either endpoint; that convex ball also contains their Jordan interior and excludes 0. Thus, for ℓ large and $\nu \ge N_\ell$,

$$|f_\nu(p_j^{(\nu)}) - f_\nu(q_{\ell,j})| \le 2\eta_\ell.$$

Taking $\nu \to \infty$ at fixed ℓ, and then $\ell \to \infty$, yields

$$\limsup_{\nu\to\infty} |f_\nu(p_j^{(\nu)}) - \zeta_j| \le 2\eta_\ell + (1 - s_\ell) \longrightarrow 0. \tag{C.5}$$

This proves marked Carathéodory convergence, with the individual prime-end labels preserved.

(e) The separating-crosscut condition. Fix a mark j and any $0 < r < |p_j - u|$. In the notation of [14, Section 3.2.4, p. 14], let S_r be the innermost component of $\partial B(p_j, r) \cap V$ separating that prime end from u, and fix $w_r \in S_r$. The component of $V \cap B(p_j, r)$ approached by the terminal radial arc is incident to S_r; otherwise another circle crosscut would separate S_r from that prime end, contrary to the innermost choice. Choose ℓ large enough that $r_\ell < r$ and $q_{\ell,j}$ belongs to this component. There is a fixed path from $q_{\ell,j}$ to w_r lying in $V \cap B(p_j, r)$ except for its endpoint on the circle: use a short segment into the component at w_r, then a path inside the component. Its image, including w_r, is compact in V, so it lies in Ω_ν for all sufficiently large ν. Concatenate it with (C.3). This connects $p_j^{(\nu)}$ to the specified point w_r within $\Omega_\nu \cap B(p_j, r)$, with the two boundary endpoints understood in the usual closure sense. This proves the condition for every fixed radius and every permitted reference point, without a further diagonal choice over the radii.

If repeated prime ends are allowed in the indexing of Karrila's Assumption 5.4, the same construction applies after separating equal disk marks at each stage into distinct, cyclically ordered marks $\zeta_{j,k} \to \zeta_j$, before choosing δ_k. Uniform continuity of g on $\overline{v_k\mathbb{D}}$ allows these perturbations to be chosen so small that the perturbed terminal segments and the short connecting arcs at radius s_k remain within $r_k/8$ of the original segments. The short connecting arcs lie in K_k and join the original $q_{k,j}$ to the perturbed access paths. Thus (C.3) and the

subsequent arguments are unchanged. This also verifies the approximation requirement with repeated limiting marks, completing the verification of the model-family assertion recorded in [14, proof of Proposition 6.2, p. 46]. □

D Geometry of an inner-cell disk

This appendix supplies the initial-domain fact used in the exploration invariants of subsection 8.1.

Lemma D.1 (The lattice disk)**.** *Let $D = B(z_0, d)$ and use the inner-cell approximation of subsection 4.1 on a triangular lattice of mesh a. For sufficiently small a/d, the cells contained in D form a nonempty edge-connected set. Their union has no holes and its boundary is one simple cycle of honeycomb edges. The mesh restriction is uniform over translations of the lattice and the center z_0.*

Proof. Write x for a cell center relative to z_0 and $h_1, \dots, h_6$ for its vertex offsets, and put $M(x) = \max_i |x + h_i|^2$. A decrease of M preserves containment of the cell in D. Among the six neighboring-center displacements, choose v making angle at most $\pi/6$ with $-x$. Then

$$M(x+v) - M(x) \le 2x \cdot v + |v|^2 + 2|v| \max_i |h_i| \le -ca|x| + Ca^2,$$

with constants depending only on the cell geometry. Outside a fixed $O(a)$ neighborhood of z_0, both $M(x)$ and $|x|$ decrease under this move. Successive contained cells therefore reach the core of hexagons meeting a fixed $O(a)$-radius disk about z_0. For sufficiently small a/d, every core cell is contained in D. The core is edge-connected: follow a path in this disk through the cells it meets, and use the fact that any two honeycomb faces incident to the same vertex share an edge. This also proves nonemptiness and connects every contained cell to the core.

Every excluded hexagon contains a point outside D, and an outward radial ray supplies a chain of excluded hexagons to infinity. The same incidence rule handles passages through vertices. There is consequently no bounded complementary component. At a honeycomb vertex, either zero or two edges separate the contained and excluded cells, so the boundary is a disjoint union of simple cycles. Connectedness and the absence of holes leave exactly one such cycle. All constants are independent of the lattice translation and z_0. □

E Use of generative AI

The research programme was conceived by the author before generative AI was used in this project. ChatGPT 6 (OpenAI) was used extensively in proposing and developing proof strategies, mathematical arguments and calculations, and in drafting and revising the manuscript. The author takes responsibility for the content of the manuscript.

References

[1] F. Camia, *Conformal covariance of connection probabilities and fields in 2D critical percolation*, Comm. Pure Appl. Math. **77** (2024), 2138–2176. DOI: 10.1002/cpa.22171.

[2] F. Camia and C. M. Newman, *Two-dimensional critical percolation: the full scaling limit*, Comm. Math. Phys. **268** (2006), 1–38. DOI: 10.1007/s00220-006-0086-1.

[3] F. Camia and Y. Feng, *The percolation energy field and its logarithmic partner*, arXiv:2508.16047v2 (1 June 2026).

[4] F. Camia and Y. Feng, *Conformally covariant probabilities, operator product expansions, and logarithmic correlations in two-dimensional critical percolation*, arXiv:2407.04246v2 (2025).

[5] F. Camia, V. F. Foit, A. Gandolfi and M. Kleban, *Scalar conformal primary fields in the Brownian loop soup*, Comm. Math. Phys. **400** (2023), 977–1018. DOI: 10.1007/s00220-022-04611-7; arXiv:2109.12116v2.

[6] F. Camia, V. F. Foit, A. Gandolfi and M. Kleban, *The Brownian loop soup stress-energy tensor*, J. High Energy Phys. **11** (2022), 009. DOI: 10.1007/JHEP11(2022)009; arXiv:2112.00074v1.

[7] S. Smirnov and W. Werner, *Critical exponents for two-dimensional percolation*, Math. Res. Lett. **8** (2001), 729–744; arXiv:math/0109120v2.

[8] P. Nolin, *Near-critical percolation in two dimensions*, Electron. J. Probab. **13** (2008), 1562–1623, paper no. 55. DOI: 10.1214/EJP.v13-565.

[9] C. Garban, G. Pete and O. Schramm, *Pivotal, cluster, and interface measures for critical planar percolation*, J. Amer. Math. Soc. **26** (2013), 939–1024; arXiv:1008.1378v5.

[10] O. Schramm and S. Smirnov, *On the scaling limits of planar percolation*, with an appendix by C. Garban, Ann. Probab. **39** (2011), 1768–1814; arXiv:1101.5820. DOI: 10.1214/11-AOP659.

[11] D. Zhan, *Two-curve Green's function for 2-SLE: the interior case*, Comm. Math. Phys. **375** (2020), 1–40; arXiv:1806.09663v2.

[12] D. Zhan, *Existence and uniqueness of nonsimple multiple SLE*, J. Stat. Phys. **191** (2024), article 101; arXiv:2308.13886v1.

[13] V. Beffara, E. Peltola and H. Wu, *On the uniqueness of global multiple SLEs*, Ann. Probab. **49** (2021), 400–434; arXiv:1801.07699v2.

[14] A. Karrila, *Multiple SLE type scaling limits: from local to global*, arXiv:1903.10354v1 (2019).

[15] A. M. Karrila, *Limits of conformal images and conformal images of limits for planar random curves*, Enseign. Math. **70** (2024), no. 3/4, 385–423. DOI: 10.4171/LEM/1066.

[16] S. Sheffield and D. B. Wilson, *Schramm's proof of Watts' formula*, Ann. Probab. **39** (2011), 1844–1863; arXiv:1003.3271v4.

[17] D. J. Fernández C. and R. Reyes, *Spectral manipulation of the trigonometric Rosen–Morse potential through supersymmetry*, arXiv:2107.00232v2 (2021).

[18] K.-J. Engel and R. Nagel, *One-Parameter Semigroups for Linear Evolution Equations*, Graduate Texts in Mathematics 194, Springer, 2000.

[19] B. Doyon, V. Riva and J. Cardy, *Identification of the stress-energy tensor through conformal restriction in SLE and related processes*, Comm. Math. Phys. **268** (2006), 687–716; arXiv:math-ph/0511054v2.

[20] B. Doyon, *Conformal loop ensembles and the stress-energy tensor*, Lett. Math. Phys. **103** (2013), 233–284. DOI: 10.1007/s11005-012-0594-1; arXiv:1209.1560v1.

[21] D. Chelkak, A. Glazman and S. Smirnov, *Discrete stress-energy tensor in the loop $O(n)$ model*, arXiv:1604.06339v4 (2025).

[22] G. Baverez and A. Jego, *The CFT of SLE loop measures and the Kontsevich–Suhov conjecture*, arXiv:2407.09080v3 (31 July 2026).

[23] F. Camia, R. P. Conijn and D. Kiss, *Conformal measure ensembles for percolation and the FK-Ising model*, in *Sojourns in Probability Theory and Statistical Physics–II*, Springer Proceedings in Mathematics & Statistics **299** (2019), 44–89. DOI: 10.1007/978-981-15-0298-9_2; arXiv:1507.01371v3.

[24] P. Di Francesco, P. Mathieu and D. Sénéchal, *Conformal Field Theory*, Graduate Texts in Contemporary Physics, first edition, Springer, New York (1997). DOI: 10.1007/978-1-4612-2256-9.

[25] A. Kupiainen and J. Oikarinen, *Stress-Energy in Liouville Conformal Field Theory*, J. Stat. Phys. **180** (2020), 1128–1166. DOI: 10.1007/s10955-020-02601-4; arXiv:1911.05359v3.

[26] F. Camia and Y. Feng, *Logarithmic correlation functions in 2D critical percolation*, J. High Energy Phys. **08** (2024), 103. DOI: 10.1007/JHEP08(2024)103; arXiv:2403.18576v2.

[27] R. Vasseur, A. M. Gainutdinov, J. L. Jacobsen and H. Saleur, *The puzzle of bulk conformal field theories at central charge $c = 0$*, Phys. Rev. Lett. **108** (2012), 161602. DOI: 10.1103/PhysRevLett.108.161602; arXiv:1110.1327v2.

[28] T. Kato, *Perturbation Theory for Linear Operators*, corrected printing of the second edition, Springer, Berlin, 1980.

[29] E. B. Davies, *A review of Hardy inequalities*, in *The Maz'ya Anniversary Collection*, Vol. 2, Operator Theory: Advances and Applications **110**, Birkhäuser, Basel, 1999, pp. 55–67. DOI: 10.1007/978-3-0348-8672-7_5; arXiv:math/9809159v1.

[30] H. Brezis, *Functional Analysis, Sobolev Spaces and Partial Differential Equations*, Universitext, Springer, New York, 2011. DOI: 10.1007/978-0-387-70914-7.

[31] E. Kreyszig, *Introductory Functional Analysis with Applications*, John Wiley & Sons, New York, 1978.